A study on cost-effective and colorless wavelength-division-multiplexed passive optical networks

Xiong, Fei

2013

Xiong, F. (2013). A study on cost-effective and colorless wavelength-division-multiplexed passive optical networks. Doctoral thesis, Nanyang Technological University, Singapore.

https://hdl.handle.net/10356/61047

https://doi.org/10.32657/10356/61047

NANYANG TECHNOLOGICAL UNIVERSITY

A Study on Cost-Effective and Colorless Wavelength-Division-Multiplexed Passive Optical Networks

XIONG FEI

SCHOOL OF ELECTRICAL AND ELECTRONIC ENGINEERING

A THESIS PRESENTED TO THE NANYANG TECHNOLOGICAL UNIVERSITY
IN FULFILLMENT OF THE REQUIREMENT FOR THE DEGREE OF
DOCTOR OF PHILOSOPHY

2013

Abstract

To meet the explosive demand of high-speed Internet access, future-proofing infrastructure for access networks which are capable of being fully scalable in capacity to each subscriber is vital. Wavelength-division-multiplexed passive optical network (WDM-PON) is considered as the ultimate solution for next-generation access networks thanks to the unlimited bandwidth guaranteed by a dedicated wavelength (or a pair of wavelength) for each subscriber. However, some challenging issues are still blocking the way of mass deployment of WDM-PON systems. This dissertation is devoted to developing some enabling solutions for these challenging issues in WDM-PON technologies, including 1) implementation of cost-effective colorless optical network units (ONUs) and 2) delivery of broadcast service over WDM-PON architectures.

The primary concern in WDM-PON implementation is the cost-efficiency of ONUs. Self-seeding of reflective semiconductor optical amplifiers (RSOAs) has been demonstrated as a cost-effective method to realize colorless ONUs in WDM-PONs. This dissertation first provides an in-depth study of the transmission performance of self-seeded RSOA-based WDM-PONs. The impact of various system parameters on the system performance are investigated through experiments. The bit rate of a self-seeded RSOA is increased by boosting the seeding power as well as employing electronic equalization. A low-cost colorless WDM-PON system is proposed where 5-Gb/s downstream transmission is enabled using self-seeded RSOAs and 1.25-Gb/s upstream transmission is achieved using remote-seeded RSOAs.

Another work dedicated to develop low-cost colorless ONUs is to utilize a multimode-injected Fabry-Perot laser diode (FP-LD) as the remote seeding light in carrier-distributed WDM-PON architectures. The feasibility of the proposed scheme is demonstrated by the improved transmission performance when compared to the system in which an amplified spontaneous emission source is adopted as the remote seeding light.

The latter part of the dissertation discusses two new techniques to enable broadcast service over WDM-PON architectures. One of the broadcast-capable WDM-PONs is based on polarization multiplexing technique. The downstream unicast and broadcast data are carried by two orthogonally polarized optical beams. Not only does this technique support broadcast services without allocating additional wavelength channels and using high-frequency subcarrier multiplexing, but it also depolarizes the seeding light to FP-LDs for upstream transmission. However, active polarization tracking is required to demultiplex the two polarization-multiplexed signals at each ONU, which may hinder the real deployment of such a system.

To improve the cost-effectiveness, another broadcast-capable WDM-PON based on offset polarization multiplexing is proposed and demonstrated. In this WDM-PON architecture, the downstream differential phase-shift keying (DPSK)-formatted unicast and broadcast signals are offset polarization-multiplexed at the central office and demultiplexed and detected at the ONUs without resorting to any polarization tracking. Meanwhile, the offset polarization-multiplexed downstream signals could also facilitate the external injection of polarization-sensitive FP-LDs for colorless operation. Successful transmissions of 10-Gb/s downstream unicast and broadcast DPSK signals as well as 2.5-

Gb/s upstream signal over a 20-km standard single-mode fiber are experimentally demonstrated.

Acknowledgement

The four-year life as a Ph.D. candidate in Nanyang Technological University is flying away faster than I could ever imagine. I owe thanks to many people who have made my journey smooth, intriguing and fruitful.

I would like to express my most sincere gratitude to my supervisor, Professor Zhong Wen-De. Being a serious and diligent researcher, he sets a good example for me to follow. His constant guidance and support have led me to overcome difficulties one after another. I am deeply indebted to Assistant Professor Kim Hoon in National University of Singapore. The experience and insight he has being sharing with me is a great treasure. I benefit a lot from the inspiring talks with him.

I'm grateful to Dr. Fu Songnian, Dr. Zhou Junqiang, Dr. Zhang Yixin, and Mr. Li Ruoming who have helped me solve elusive problems in my experiments. Special thanks go to all the professors, staffs and students in our research center—OPTIMUS (formerly NTRC)—including Professor Shum Ping, Mr. Poh Khoon Yong, Mr. Chong Lui Tat, Dr. Ouyang Chunmei, Dr. Wu Xuan, Ms. Liu Huanhuan, Dr. Jiang Meng, Ms. Cui Ying, to name a few. Together, we've created a friendly and relaxing environment. I have benefited from their support and consideration and enjoyed their company and care. Without them, I won't have so many pleasant memories to recall.

Lastly, to my dearest parents, I am so proud of having parents like you. For the endless love and trust you have dedicated to me, I hope I don't let you down.

Table of Contents

List of Abbreviations

APD	Avalanche Photodiode
APON/ATM-PON	Asynchronous Transfer Mode PON
ASE	Amplified Spontaneous Emission
ASK	Amplitude Shift Keying
AWG	Arrayed Waveguide Grating
BER	Bit Error Rate
BLS	Broadband Light Source
BPF	Band-Pass Filter
BPON	Broadband PON
BS	Base Station
CATV	Community Antenna Television
CO	Central Office
CW	Continuous Wave
CWDM	Coarse WDM
DCF	Dispersion Compensation Fiber
DEMUX	Demultiplexer
DFB	Distributed Feedback
DFE	Decision Feedback Equalizer
DI	Delay Interferometer
DMT	Discrete Multi-Tone
DOP	Degree of Polarization
DPSK	Differential Phase Shift Keying
DSB	Double-Sideband
DSL	Digital Subscriber Line
EAM	Electro-Absorption Modulator
EDFA	Erbium-Doped Fiber Amplifier
E/O	Electro/Optical
EPON	Ethernet PON
ER	Extinction Ratio
FEC	Forward-Error Correction
FFE	Feed-Forward Equalizer

FP-LD	Fabry-Perot Laser Diode
FR	Faraday Rotator
FRM	Faraday Rotator Mirror
FSAN	Full Service Access Network
FSK	Frequency Shift Keying
FSR	Free Spectral Range
FTTX	Fiber To The X
GPON	Gigabit PON
ICT	Information and Communications Technology
IPTV	Internet Protocol Television
IRZ	Inverse Return-to-Zero
ISI	Inter-Symbol Interference
ITU	International Telecommunication Union
LED	Light Emitting Diode
LPF	Low-Pass Filter
MI	Multimode-Injected
MLSE	Maximum-Likelihood Sequence Estimation
MMW	Millimeter-Wave
MPN	Mode Partition Noise
MUX	Multiplexer
MZM	Mach-Zehnder Modulator
NRZ	Non-Return-to-Zero
OCS	Optical Carrier Suppressed
ODL	Optical Delay Line
OFDM	Orthogonal Frequency Division Multiplexing
OLT	Optical Line Terminal
ONU	Optical Network Unit
OOK	On-Off Keying
OSA	Optical Spectrum Analyzer
OSSBM	Optical Single-Sideband Modulator
PAM	Pulse Amplitude Modulation
PBC	Polarization Beam Combiner
PBS	Polarization Beam Splitter
PC	Polarization Controller

PDG	Polarization Dependent Gain
PDL	Polarization Dependent Loss
PDλ	Polarization-Dependent Wavelength Shift
PM	Power Meter
PMF	Polarization-Maintaining Fiber
PolMUX	Polarization Multiplexing
PON	Passive Optical Network
PRBS	Pseudo-Random Binary Sequence
PSK	Phase Shift Keying
QAM	Quadrature Amplitude Modulation
QPSK	Quadrature Phase Shift Keying
RBS	Rayleigh Backscattering
RF	Ratio Frequency
RIN	Relative Intensity Noise
RM	Reflection Module
RN	Remote Node
RoF	Radio-over-Fiber
RSOA	Reflective Semiconductor Optical Amplifier
RZ	Return-to-Zero
SCM	Subcarrier Multiplexing
SLD	Superluminescent Diode
SMSR	Side-Mode Suppression Ratio
SNR	Signal-to-Noise Ratio
SOA	Semiconductor Optical Amplifier
SOP	State of Polarization
SS	Spectrum-Sliced
SSB	Single Sideband
SSMF	Standard Single Mode Fiber
TDM	Time Division Multiplexing
TDMA	Time Division Multiple Access
TE	Transverse-Electric
TEC	Thermo-Electric Cooling
TM	Transverse-Magnetic
TO	Transistor Outlook
VOA	Variable Optical Attenuator
VoD	Video-On-Demand

WDM-PON	Wavelength-Division-Multiplexed PON
WRC	Weak-Resonant-Cavity
XGM	Cross Gain Modulation

List of Figures

List of Tables

CHAPTER 1

Introduction

The purpose of this dissertation is to provide potential solutions for addressing two technical issues in wavelength-division-multiplexed passive optical network (WDM-PON) systems, including 1) the implementation of cost-effective colorless optical network units (ONUs) and 2) broadcast service delivery over WDM-PON architectures. This chapter introduces the background and motivation for the studies elaborated in this dissertation. It also includes the research contributions and the organization of this dissertation.

1.1 Background and motivation

This section introduces bandwidth drivers in access networks and the corresponding evolution of access network solutions. It explains why WDM-PON is regarded as the ultimate solution for next-generation access networks and summarizes the ongoing research aspects in WDM-PON technologies.

1.1.1 Bandwidth drivers in access networks

The access network, also known as the "first-mile network", connects the service provider central offices (COs) to businesses and residential subscribers. The bandwidth demand in the access network has been increasing rapidly over the past several years [1]. Communication and Internet services being offered to residential homes have undergone rapid expansion in the last two decades. Customers are no longer only interested in voice telephony, broadcast television, and radio; they are also increasingly asking for always-

on fast Internet communication, video-based multimedia, fast peer-to-peer file transfer, high definition multimedia on-line gaming, etc. Service providers have been facing an increased bandwidth demand not only for their Internet protocol television (IPTV), high-definition TV, video on demand (VoD) and mobile broadband services, but also due to the growing success of Over-The-Top Internet applications like YouTube [2, 3].With the advent of these bandwidth-consuming applications, the bandwidth demand has been growing at roughly 50-60% annually and is expected to reach several gigabits per second per subscriber by the year of 2020 [4]. Fig. 1.1 illustrates the downstream and upstream bandwidth requirements of several killer applications and the transmission capacities of some access solutions.

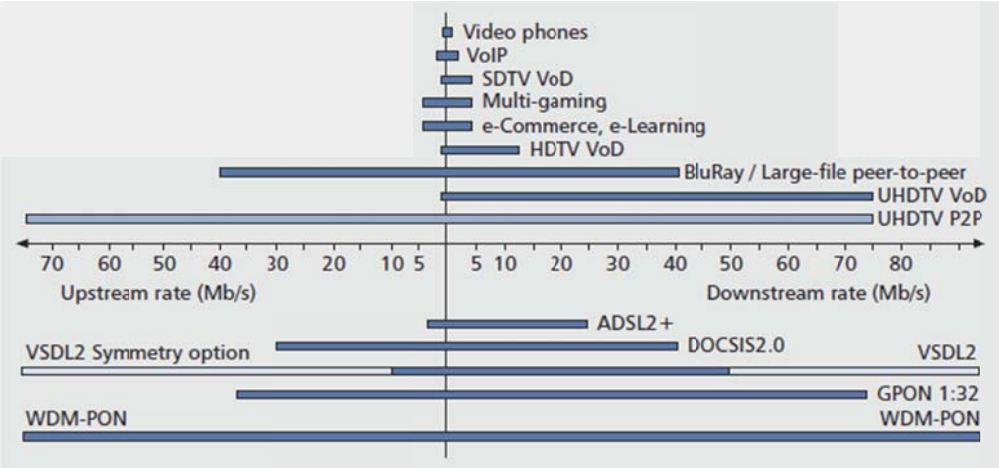

Fig. 1.1. Downstream and upstream bandwidth requirements and capabilities of different (near-future) services and solutions [5].

The predominant broadband access solutions deployed today are the community antenna television (CATV) and digital subscriber line (DSL) based networks [1, 2]. However, both of these technologies have limitations because they are based on infrastructure that was originally built for carrying analog TV and voice signals, respectively. The coaxial cable CATV networks are having a hard time to keep up with

the traffic demands. DSL techniques and cable modem techniques are evolving into higher speeds but at the cost of a shorter reach.

The unique properties of optical fibers, low loss and extremely wide bandwidth, make it the ideal candidate to meet the capacity challenges for now and the foreseeable future. Single-mode fiber has already been adopted in the core and metropolitan networks, and is increasingly penetrating the access domain as well. There is a common understanding that the various Fiber-to-the-X (FTTX, where X can mean home, curb, cabinet, or building) will overcome the bandwidth limitation of today's copper-based and hybrid fiber access solutions [6]. FTTH is seen as the ultimate and most future-proof access solution leading to the next generation optical access network.

Basically, three architectures can be deployed for fiber access networks. They are point-to-point architecture, active star architecture, and passive star architecture, also known as passive optical network (PON). A PON is a point-to-multipoint optical network, where an optical line terminal (OLT) at the central office is connected to many ONUs through remote nodes by one or multiple 1×N optical power splitters or wavelength multiplexer/demultiplexers. The network between the OLT and the ONUs is passive because no power supply is required.

1.1.2 PON evolution: from TDM-PON to WDM-PON

Since a common feeder fiber is shared among all ONUs in a PON architecture, accurate multiple access techniques are needed to avoid collisions among the traffic streams generated by different ONUs. The most traditional multiple access technology is time division multiple access (TDMA) and TDMA-based optical access networks have been deployed widely. In a typical time-division-multiplexed (TDM) PON, all ONUs use the

same wavelength for downstream or upstream transmission. A passive power splitter resides at the remote node to divide or combine the downstream or upstream signals. For the downlink, the downstream data from the OLT is broadcast to all ONUs but each ONU is only allowed to access the data intended for itself, as illustrated in Fig. 1.2. For the uplink, ONUs are dynamically assigned to time slots to transmit individual data.

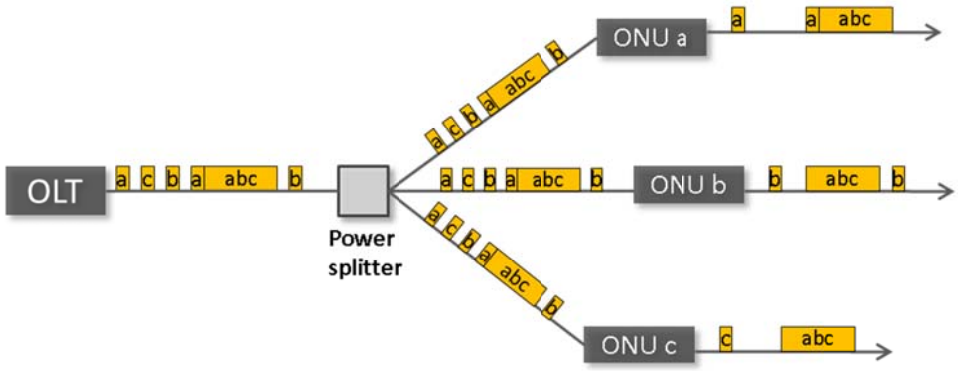

Fig. 1.2. Downstream operation of a TDM-PON.

The three major TDM-PON standards are asynchronous transfer mode (ATM) PON (also termed as APON or BPON), Ethernet PON (EPON), and Gigabit PON (GPON) [2, 7-9]. Table 1.1 summaries the commercial deployments for major phases in the TDM-PON evolution. The corresponding downstream and upstream line rates are also listed here.

- APON/BPON (ITU-T G.983 [10])
  - The first PON standard and established in the early 90's of last century
  - Based on ATM
  - Mainly developed in Germany
  - Typical data rate: 155 or 622 Mb/s in downstream direction and 155 Mb/s in upstream direction
- EPON (IEEE 802.3ah [11])
  - Completed in 2004 and broadly deployed in Japan and Korea

- Based on Ethernet protocol
- Typical data rate: 1.25 Gb/s in both downstream and upstream direction

➢ GPON (ITU-T G.984 [12])

- Widely deployed in parts of the U.S. and Europe
- Can carry ATM as well as Ethernet traffic in any mixed mode
- Typical data rate: 2.5 Gb/s in downstream direction and 1.25 Gb/s in upstream direction

➢ 10G-EPON (IEEE 802.3av [13])

- Ratified in 2009
- Support two configurations: symmetric, 10 Gb/s in both direction; asymmetric, 10 Gb/s in downstream direction and 1 Gb/s in upstream direction

➢ XG-PON (10G-PON, ITU-T G.987 [14])

- Completed part of the standard in 2010
- Support two configurations: symmetric (XG-PON2), 10 Gb/s in both direction; asymmetric (XG-PON1), 10 Gb/s in downstream direction and 2.5 Gb/s in upstream direction

Table 1.1. Commercial deployments of TDM-PON [15].

PON type	Commercial Deployment	Year	Line rate (Mb/s)	
			Down	Up
Narrowband	Deutsche Telekom OPAL	1995	29	29
Narrowband	NTT Pi PON	1997	49	49
ATM PON	NTT	2001	155	155
BPON	NTT West	2003	622	155
EPON	NTT East	2004	1000	1000
GPON	Verizon FiOS	2007	2488	1244
10G PON (IEEE)	t.b.d.	2012	10000	1000
10G PON (ITU-T)	t.b.d.	2013	9953	2488

Although the 10G-EPON and XG-PON guarantee 10 Gb/s transmission capacity for both the downlink and uplink, most agree that TDM-PONs cannot cope with the requirements of future network evolution with respect to the aggregated bandwidth and the allowable power budget. The power budget limits both the PON splitting ratio and the distance between OLT and ONUs. Then what is the succeeding technology? An installed fiber plant can be efficiently upgraded to higher capacity by introducing multiple

wavelength channels in the same fiber infrastructure. Given this, one of the most attractive candidates for future optical access next to 10G-EPON and XG-PON is WDM-PON.

As shown in Fig. 1.3, a WDM-PON is a physically shared system, but a logically unshared system, in which each ONU is connected to the OLT by a specific wavelength (or a pair of wavelength) in a point-to-point fashion. Fig. 1.4 summarizes the data rate for each subscriber supported by various PON technologies. The exclusive ownership of a pair of wavelength channels for each ONU enables incomparable transmission capacity for subscribers in a WDM-PON system.

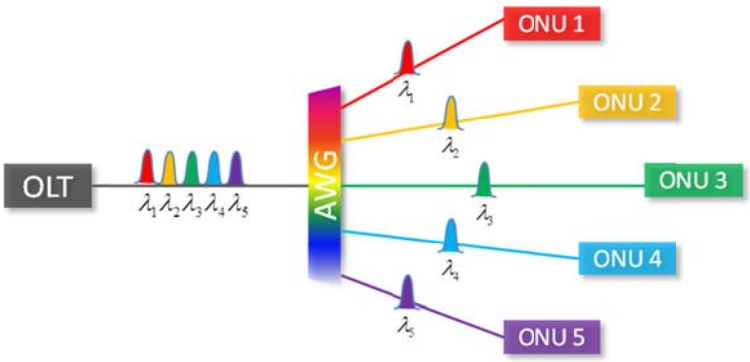

Fig. 1.3. Schematic of a WDM-PON system.

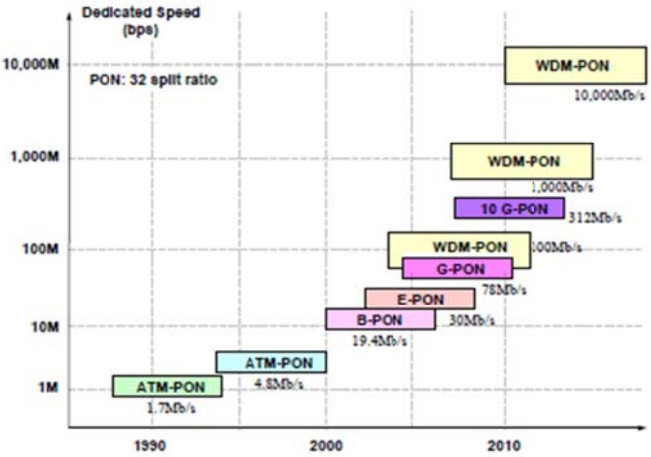

Fig. 1.4. History of PON development [16].

Although various architectures for WDM-PONs have been proposed as early as the mid-1990s, WDM-PONs have not been widely deployed throughout the world. To the knowledge of the author, only Korea Telecom has deployed an early implementation of a WDM-PON which delivers 100 Mb/s symmetric bandwidth to each subscriber in 2005 [17].The lack of further installations is mostly attributed to low cost-efficiency and lack of international standardization. This situation is expected to change once the International Telecommunication Union (ITU) or IEEE provides relevant standards. Increased deployment enabled by standardization will in turn lead to decreased WDM-PON cost. Recently the Full Service Access Network (FSAN) is working on white paper for NG-PON2 where various kinds of WDM-PON technologies including external seeding, tunable laser, and wavelength reuse are considered as candidate technologies.

Current TDM-PON architectures are economically feasible and are being deployed rapidly around the world [7, 15]. However, they are bandwidth-limited and cannot meet the continuously increasing bandwidth demands of subscribers. WDM-PONs can be combined with additional TDMA techniques, in particular those already used by the EPON and GPON standards [18, 19]. This leads to hybrid WDM/TDM PONs (TWDM-PON) which provide a smooth migration from current TDM-PONs to future WDM-PONs.

A TWDM-PON combines the flexibility of TDM-PON with the increased overall capacity of WDM technology. The advantages of a TWDM-PON over a pure WDM-PON are its high fan out, easy migration from the existing network deployment, and ability to provide higher peak data rates [20, 21]. The TWDM-PON variants can be generally classified into three categories: 1) wavelength selected TWDM-PON with

power splitters at the remote node; 2) wavelength split TWDM-PON with an arrayed waveguide grating (AWG) at the remote node; and 3) wavelength switched TWDM-PON with wavelength selective switches at the remote node.

The wavelength selected TWDM-PON offers the highest flexibility in terms of bandwidth utilization but has a high insertion loss and poor security since the power splitter broadcasts all wavelengths to all users. The poor power budget restricts its overall reach. The wavelength split TWDM-PON combines wavelength splitters and power splitters in the remote node. It has a fixed wavelength allocation and thus reduced flexibility. The advantages of this architecture are the improved data security and power budget. The wavelength switched TWDM-PON employs wavelength selective switches in the remote node. One wavelength selective switch feeds wavelengths to multiple AWGs so that the architecture has a higher fan out. Due to the switching functionality, it improves the data security without compromising flexibility.

1.1.3 WDM-PON research and road ahead

WDM-PONs have received tremendous attention from research groups all over the world. Fig. 1.5 shows the statistic data about the number of publications with the topic of WDM-PONs in each year from the Web of Knowledge [22]. The concept of WDM-PON architecture first appeared in the mid-1990s [23]. The relevant research works have increased remarkably from the beginning of the 21th century and hit the peak between 2008 and 2011. They cover a wide range of aspects in WDM-PON technologies including devices, architectures, services, and protocols.

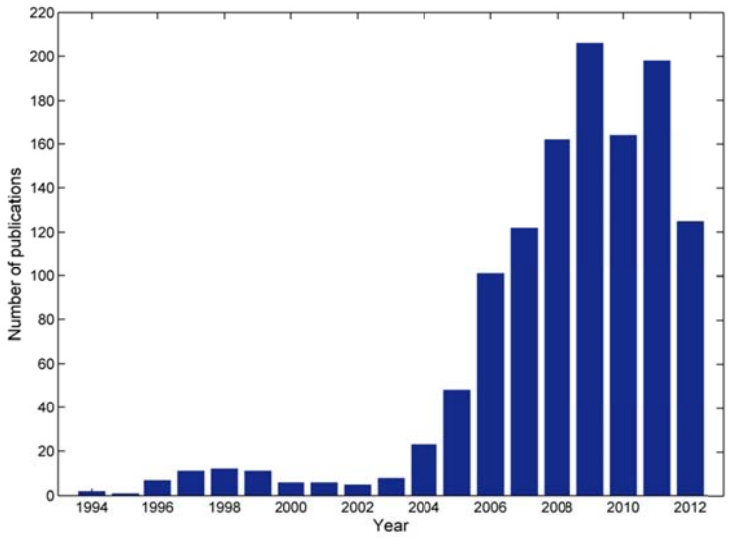

Fig. 1.5. Research development in WDM-PON technologies (statistics from the Web of Knowledge).

The benefits of WDM-PONs are manifold. Besides the incomparable bandwidth guaranteed for each subscriber, WDM-PONs also feature the following advantages over TDM-PONs thanks to the logical point-to-point connection through dedicated wavelength channels:

- High security and privacy
- Protocol and line-rate transparency (enabling separate services and/or separate service providers)
- Flexible upgradability
- Easy management and reduced complexity (no point-to-multi-point access control)

However, many challenges and technical issues are still blocking the way to wide real deployment of WDM-PON systems [8, 24]. Some argue that the bandwidth provided by a WDM-PON is too large for a single user and there is a lack of an available market requiring high bandwidth. However, the ever-increasing bandwidth demand resulted from the emergence of various bandwidth-consuming applications and services would

eventually prove the necessity of WDM-PON technology. A lack of suitable network protocols and software to support the architecture would be no longer a problem as long as WDM-PON gets standardized. It is predicted that the standardization of WDM-PON will eventually come up around 2020 when the bandwidth demand per subscriber is expected to reach 1 Gb/s [25].

The key bottleneck in developing practical WDM-PON systems is the costs of upgrading existing access networks to support WDM-PON technologies. These costs not only include the obvious capital expenditure including land and buildings, network infrastructure, installation, software, customer premise equipment and project management cost, but also the hidden operational expenditure including renting, energy consumption, failure reparation, network operation, marketing, pricing, billing and service provisioning cost [26].

The point-to-point connection through dedicated wavelengths in WDM-PON systems requires that each ONU operates on a specific wavelength, which is in turn decided by the particular port of the wavelength multiplexer (located in the remote node) the ONU is connected to. An obvious solution is to use wavelength-specific light sources, e.g. DFB lasers, in ONUs. The laser diode usually comes with a thermo-electric cooler for stable operation as a WDM source. In addition, a wavelength locker, which helps the laser diode to lock exactly to its assigned wavelength, is needed [27]. Although a wavelength-specific DFB laser can support high-speed modulation, it is regarded as a costly way to implement a WDM-PON because a number of DFB laser diodes would be required and moreover each of them should be managed separately. To keep in the inventory all different wavelength lasers needed for each channel of a WDM-PON and to

install ONUs with different wavelength lasers at different homes is costly and not easy to maintain. End users would welcome unlimited bandwidth but they would be reluctant to pay much more than what they are paying for current DSL and TDM-PON technologies. An important factor that will reduce the cost of WDM-PON to meet the needs of FTTH as well as those of the enterprise will be the introduction of standard and colorless ONUs.

Colorless (also termed as color-free or wavelength-independent) operation of ONUs in WDM-PONs is considered to be the key to reduce the installation and maintenance cost significantly since in a colorless WDM-PON identical light sources are adopted in ONUs and the wavelength assignment can be controlled by the OLT or the remote node (RN). A colorless ONU can be realized by employing light sources which could cover a wide spectrum range. Tunable lasers have superior performance in terms of data rate and transmission distance but are too expensive to be adopted in cost-sensitive ONUs. Low-cost broadband light sources such as light-emitting diodes (LEDs), amplified spontaneous emission (ASE) from erbium-doped fiber amplifiers (EDFAs) are economically feasible to be utilized as the light sources at ONUs of WDM-PONs [28-30].

A more advanced scheme for colorless operation is carrier distribution in which the upstream carriers are generated in the OLT and distributed to corresponding ONUs through the logical point-to-point architecture [31-33]. Fabry-Perot laser diodes (FP-LDs) and reflective semiconductor optical amplifiers (RSOAs) are considered as promising candidates employed at ONUs of the carrier-distributed WDM-PONs. The fact that a FP-LD and a RSOA can act as an optical amplifier and at the same time as a modulator makes them a cost-effective solution. In addition to external seeding/injection, the RSOA

and FP-LD could also be self-seeded/injected [34, 35]. This scheme further reduces the cost by eliminating the remote seeding light.

The use of standard colorless ONUs will result in higher production volumes that will translate into significant cost reduction for manufacturers. More importantly, it reduces the inventory management cost [36, 37]. This standardization will also reduce the complexity and cost of deployment, maintenance, and sparing, helping further decrease operation expenditure [38].

Another challenging issue in WDM-PON is the delivery of broadcast/multicast services. Unlike the point-to-multi-point TDM-PON in which downstream data is broadcast to all attached ONUs, the logical point-to-point WDM-PON architecture is not well suited for broadcast service delivery. Special techniques are needed to enable broadcast/multicast service delivery over conventional WDM-PON architectures.

Other research aspects in WDM-PON technologies include WDM radio-over-fiber (RoF) PON in which wired and wireless services are converged in WDM-PON systems, long-reach WDM-PON which merges the access and metro networks, fiber fault protection with the capacity of detecting and localizing the fiber failures without delay, and energy-saving issue in WDM-PONs.

1.2 Research contributions

The research work presented in this dissertation puts an effort in making WDM-PON a viable technology for the next-generation access network by addressing two major technical issues in WDM-PON systems, low-cost colorless ONUs and broadcast service delivery. The major contributions include:

- In-depth experimental investigation and analysis on transmission performance of a colorless WDM-PON based on directly modulated self-seeded RSOAs are carried out. The impact of several important system parameters on upstream transmission performance are characterized and investigated through experiments. The findings in this work provide a better understanding of the mechanism and limitations of the directly modulated self-seeded RSOAs. Hence, they serve as a guide on designing WDM-PON systems using self-seeded RSOAs. (Chapter 3)

- The transmission capacity of a directly modulated self-seeded RSOA, which is primarily limited by the modulation bandwidth of the RSOA itself, is enhanced by increasing the seeding power through inserting an optical amplifier in the self-seeding cavity. And it is further increased by electronic equalization after detection. A low-cost colorless WDM-PON system based on self-seeded RSOAs for downstream transmission and remote-seeded RSOAs for upstream transmission is demonstrated and its transmission performance is investigated. This scheme serves as an alternative solution for future low-cost WDM-PON systems. (Chapter 3)

- A multimode-injected FP-LD is proposed as the remote seeding light in carrier-distributed WDM-PON systems. By feeding ASE spectrum slices into a common FP-LD used as a noise suppressor in the OLT instead of seeding them into FP-LDs in corresponding ONUs directly, the noise of the remote seeding light is suppressed. Improved transmission performance of a WDM-PON based on FP-

LDs injection-locked by a spectrum-sliced multimode-injected FP-LD is observed. (Chapter 4)

- Polarization multiplexing technique is exploited to enable broadcast service delivery over WDM-PON architectures. Although automatic polarization tracking is required in each ONU to demultiplex the downstream unicast and broadcast data, the polarization-multiplexed downstream signals facilitate the external injection of polarization-sensitive FP-LDs for upstream remodulation. Transmission performance of the proposed WDM-PON system is investigated in detail. The work provides an alternative solution for broadcast-capable WDM-PONs. (Chapter 5)

- Another broadcast-enabling scheme for WDM-PON systems based on offset polarization multiplexing is proposed and demonstrated. This new scheme not only preserves the advantages of the previous proposed broadcast-enabling scheme based on polarization multiplexing but also brings improved cost-efficiency. More specifically, the technique eliminates the necessity of automatic polarization tracking in each ONU by employing two separate differential phase shift keying (DPSK) receivers for downstream unicast and broadcast signals detection. Meanwhile, the offset polarization-multiplexed downstream signals could also facilitate the external injection of polarization-sensitive FP-LDs for colorless upstream transmission. (Chapter 6)

1.3 Thesis organization

The rest of this dissertation consists of six chapters.

Chapter 2 reviews the progress of several research aspects in WDM-PON technologies. Various proposed schemes for colorless operation of ONUs and broadcast service delivery over WDM-PON architectures are reviewed in detail. Development in other research directions including WDM-RoF-PONs, long reach WDM-PONs, fiber fault protection, and energy saving in WDM-PONs are briefly discussed.

Chapter 3 focuses on low-cost colorless WDM-PONs based on self-seeded RSOAs. Firstly, the impact of various system parameters on the transmission performance is experimentally investigated. Secondly, the data rate of a directly modulated self-seeded RSOA is enhanced by increasing the seeding power and electronic equalization. Lastly, a low-cost full-duplex bidirectional colorless WDM-PON based on bit-rate-enhanced self-seeded and remote-seeded RSOAs is demonstrated.

Chapter 4 explores another type of prevalent low-cost light sources, FP-LDs, for colorless WDM-PONs. A theoretical mode of injection-locked FP-LDs is introduced, based on which the steady and dynamic characteristics of the free-running and injection-locked FP-LDs are simulated. A multimode-injected FP-LD is proposed as the remote seeding light in carrier-distributed WDM-PONs. The feasibility is demonstrated by comparing its transmission performance to that based on a spectrum-sliced ASE through simulation.

Chapter 5 introduces a broadcast-capable WDM-PON system using polarization multiplexing technique. Experimental demonstration of successful transmission of 10 Gb/s downstream unicast and broadcast signals with low extinction ratio as well as 2.5

Gb/s upstream signal with forward error correction (FEC) confirms the feasibility of the proposed architecture. The impact of polarization dependence, injection-locking range, and signal extinction ratio on the transmission performance are investigated detailedly.

Chapter 6 discusses another WDM-PON architecture with broadcast capability utilizing offset polarization multiplexing technique. Successful transmissions of 10-Gb/s downstream unicast and broadcast DPSK signals as well as 2.5-Gb/s upstream on-off keying (OOK) signal over a 20-km standard single-mode fiber are experimentally demonstrated. The robustness of the proposed scheme against polarization fluctuation along the link, relative bit delay between the unicast and broadcast signals, frequency deviation of the downstream signals from the delay interferometer (DI), and imperfection of the DI is investigated.

Chapter 7 draws conclusions on the research work presented in this dissertation and also discusses some future research work in the area of WDM-PON technologies.

CHAPTER 2

A Review on the Development of WDM-PON Technologies

As a promising candidate for the next-generation optical access network, WDM-PON has attracted remarkable research attention for more than ten years. Researchers around the world have made significant efforts to develop viable WDM-PON technologies in various aspects. This chapter gives a detailed review on those topics which are related to the author's work, including colorless light sources for ONU and broadcast/multicast service delivery over WDM-PON architectures. Other topics in WDM-PON technologies are also briefly summarized in this chapter.

2.1 Colorless operation of ONUs

In the WDM-PON system, each ONU is virtually point-to-point connected to the OLT by assigning a specific wavelength for downstream/upstream transmission. This could be realized by adopting wavelength-specific optical light sources, e.g. an array of distributed feedback (DFB) lasers in the OLT and one wavelength-specific DFB laser in each ONU. However, this brings about the cost issue. Firstly, the cost of the wavelength-specific DFB lasers is still high; secondly, such WDM-PON management induces high operating and inventory costs. In order to reduce cost and complexity, service providers would strongly prefer all ONUs to be identical, so that any ONU can be connected to any port of the arrayed waveguide grating (AWG) in the remote node. In other words, there should

be one light source that can be operated over the entire wavelength range covering all ONUs. Finally, the ONU light source must be inexpensive [39].

Colorless operation of ONUs in WDM-PONs will significantly reduce the high costs of installation, operation and maintenance of WDM-PON systems. Hence, developing reliable wavelength-independent light sources used as colorless transmitters in ONUs is the prerequisite of the wide deployment of WDM-PON systems. Tunable lasers followed by external modulators are considered to provide the best performance in terms of data rate and transmission reach but are regarded to be too expensive to be used for cost-sensitive optical access networks [40]. Several techniques are proposed and investigated to achieve colorless operation of ONUs with low-cost light sources such as RSOAs and FP-LDs. Each of them is introduced and discussed in detail in this section. A summative evaluation of the techniques enabling colorless ONUs is given in Table 3.2.

2.1.1 Spectrum-sliced broadband light sources

Spectrum-slicing of broadband light sources (BLS) has been proposed as a potential technique which could meet the requirement of cost-effective colorless light sources for WDM-PON systems. The broadband light sources could be LEDs, superluminescent diodes (SLD), FP-LDs, and ASE sources such as EDFA or SOA/RSOA [28, 39, 41, 42]. As Fig. 2.1 shows, with a BLS such as an LED, some fraction of the emitted light will match the optical passbands of the AWG in the RN. The exact wavelengths that pass through the AWG will depend on the AWG port to which the LED is attached. Identical LEDs could be applied to all ONUs and hence colorless operation is achieved. Spectrum slicing is attractive because LEDs are simple sources compared to widely tunable single frequency lasers.

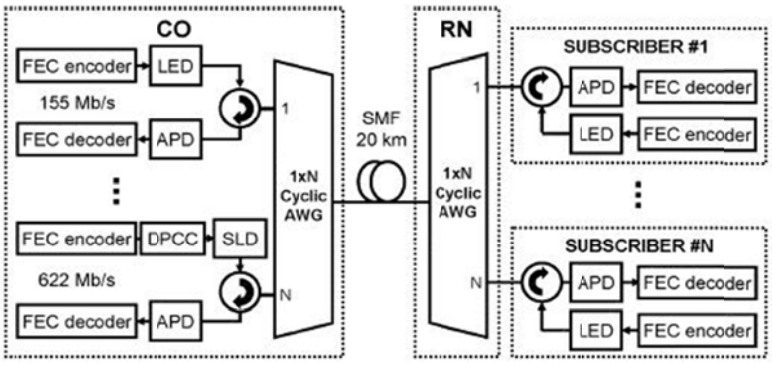

Fig. 2.1. LEDs used as colorless light sources in ONUs [28].

The broadband light sources used in spectrum-sliced WDM-PON applications need to fulfill the following requirements. First, it shall have broad bandwidth to accommodate more end users; secondly, it has high power spectral density to relax the power budget of the spectrum-sliced signal [29]. The power margin could be increased by employing high-power BLS. Reference [29] demonstrated a ~130 nm broadband erbium fiber ASE-based continuous-wave (CW) supercontinuum source with 500 mW output power. Error-free transmission of 622-Mb/s spectrum-sliced signals over 25-km single-mode fiber (SMF) was achieved.

The spectrum-sliced ASE sources suffer from the spontaneous-spontaneous beat noise due to the inherent incoherence. The signal-to-noise ratio (SNR) of an ASE source at the receiver is given by (2.1) when the electrical noise is neglected.

$$SNR \approx \frac{B_o}{B_e} \tag{2.1}$$

where B_o is the optical bandwidth of the spectrum-sliced source and B_e is the electrical bandwidth of the signal. It is necessary to increase the optical bandwidth and/or decrease the electrical bandwidth, i.e., the bit rate, to improve the SNR, which in turn determines

the transmission capacity of the WDM-PON system using the proposed light source [42]. Transmission of up to 1.7-Gb/s data was demonstrated when the 3-dB bandwidth of the spectrum slice equaled to 1.3 nm. However, large B_o makes high-speed optical signals vulnerable to fiber dispersion. The maximum dispersion-uncompensated transmission distance is inversely proportional to the square of the data rate if B_o increases with B_e to keep the SNR unchanged. Moreover, this approach also makes the incoherent light signal sensitive to optical filtering [43].

Recently, H. Kim *et al*. reported a 10-Gb/s WDM-PON using an ultranarrow spectrum-sliced incoherent light source. A wideband ASE generated by an EDFA was spectrum-sliced by an ultranarrow fiber Fabry-Perot filter with a 3-dB bandwidth of 0.006 nm. The spectrum-sliced light was intensity-smoothed by using a gain-saturated RSOA. Due to the ultranarrow linewidth of the source, an uncorrected bit-error rate (BER) better than 3×10^{-3} after transmission over 20-km SSMF was achieved. Fig. 2.2 shows the experimental setup in which the proposed ultranarrow spectrum-sliced source was externally modulated with downstream data through an electro-absorption modulator (EAM).

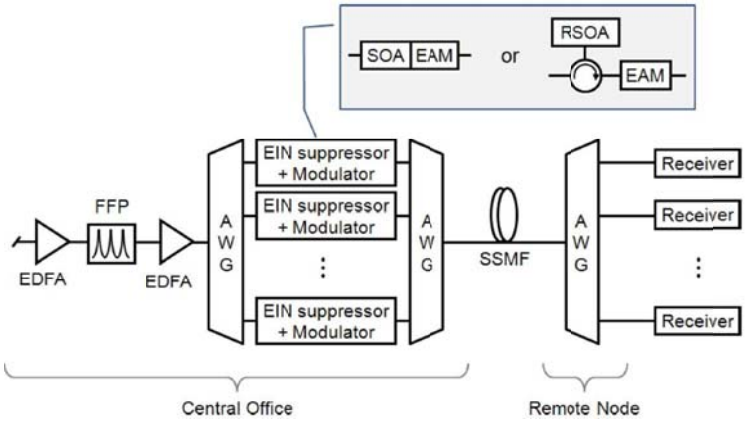

Fig. 2.2. Schematic of a downstream WDM-PON system based on the ultranarrow spectrum-sliced incoherent light source [43].

As shown in Fig. 2.2, the broadband light source could replace an array of DFB lasers in the OLT as the downstream carriers since its broad spectrum could cover many transmission channels. The cost induced by the special techniques to improve the data rate and power margin for each channel would be justified since it is shared among all the end users. However, if it is employed as a colorless light source for upstream transmission, a BLS is required in each ONU and any cost induced by improving the BLS performance shall be covered by one end user, which makes the spectrum-sliced BLS technique less attractive to upstream operation than it is to downstream operation. In fact, researchers have already come up with solutions in which the BLS could be shared among end users for upstream transmission and meanwhile the colorless operation of ONUs could be satisfied. In the next subsection, this technique–carrier distribution–is discussed.

2.1.2 Carrier distribution

Colorless ONUs mean that all the ONUs connected to one WDM-PON are identical and they can be operated over the entire wavelength range of this network. Inventory cost is significantly reduced since each ONU can be connected to any port of the wavelength MUX/DEMUX in the RN. No record about the operating wavelength of each specific ONU needs to be made, and the end user would not need to concern about the operation wavelength of their installed ONUs. The wavelength assignment for uplink should be decided by the OLT in the central office or the RN. Like all the downstream transmitters are allocated in the OLT uniformly, if the upstream optical carriers could be also placed in the central office and distributed to the corresponding ONUs by the wavelength multiplexer in the RN, then the ONUs would be color-free.

2.1.2.1 System structure

Fig. 2.3 illustrates the schematic of a carrier-distributed WDM-PON system. The upstream carrier module located in the OLT could be an array of DFB lasers, a multi-wavelength light source, or an incoherent BLS. If DFB lasers or a multi-wavelength light source is employed, the wavelength and channel spacing should match the AWG in the RN. When the upstream optical carriers are transmitted to the RN, they will be routed to different ports according to the AWG and distributed to the corresponding ONUs attached to the AWG. If the upstream carrier module is a BLS, some fractions of the emitted light which match the optical passbands of the AWG in the RN are routed to the attached ONUs.

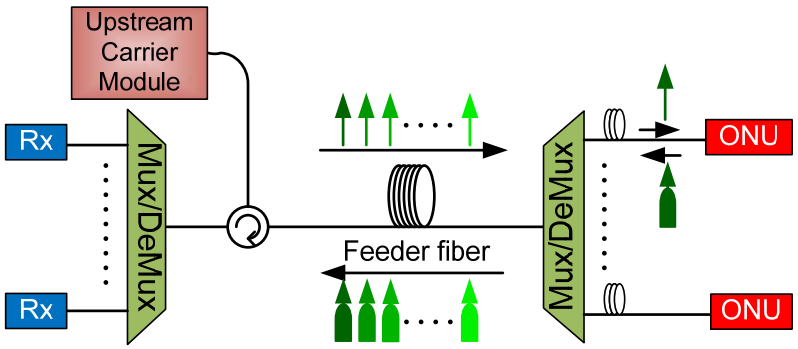

Fig. 2.3. Schematic of a carrier-distributed WDM-PON.

In the ONU, a loopback configuration is needed for upstream transmission. Several configurations for the ONUs in a carrier-distributed WDM-PON are shown in Fig. 2.4. The upstream optical carrier will be first encoded by an external modulator driven by upstream data and then looped back through a circulator as Fig. 2.4 (a) shows. The transmission reach is limited by the power of the upstream optical carrier since it would undergo twice of the link loss from the OLT to ONUs. The power insufficiency could be

alleviated by providing optical gain in the ONU [31]. As shown in Fig. 2.4 (b), the SOA after the modulator would boost the power of the upstream signal. Transmission capacity will be limited if a BLS is employed as the upstream optical carriers as discussed in Section 2.1.1. Coherent CW lasers are usually employed as the distributed upstream carriers for high-speed operation. For data modulation, a polarization-insensitive optical modulator such as an electro-absorption modulator is preferred [32]. Moreover, a monolithic integrated device consisting of an EAM and a SOA could support data rate as high as 40 Gb/s with relative low cost and high compactness [33].

Since the functions of an ONU in a carrier-distributed WDM-PON system include modulation and amplification, the most cost-effective choice for such an ONU would be RSOAs. The front facet of the RSOA is anti-reflection coated. The upstream optical carrier could be fed into the RSOA with negligible power loss. This seeding light is amplified while traveling in the RSOA until it hits the rear facet of the RSOA. Most of the seeding light is reflected since the rear facet is high-reflection coated. At the same time, the amplified optical carrier is encoded with upstream data by electrically driving the bias current of the RSOA, as shown in Fig. 2.4 (c). RSOAs would be promising candidates for wavelength-independent ONUs in WDM-PONs as long as its main drawback, limited electrical bandwidth, is overcome.

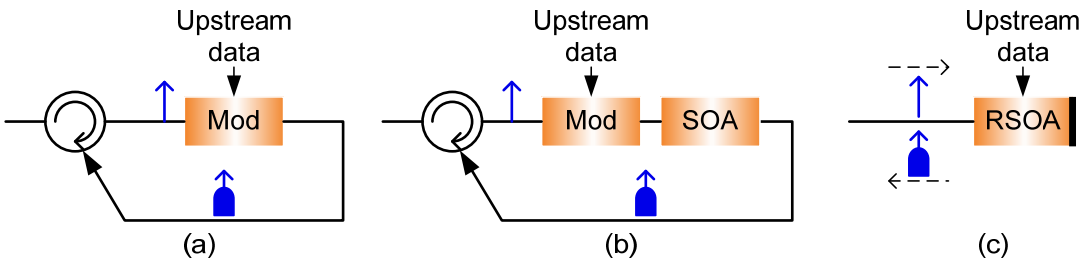

Fig. 2.4. Different configurations of ONUs in a carrier-distributed WDM-PON system.

2.1.2.2 High-speed operation of RSOAs

The typical 1~2-GHz electrical bandwidth has become the primary drawback of a RSOA and hinders its deployment in high-speed WDM-PON applications. Exhaustive studies have been carried out to demonstrate 10-Gb/s or higher operation of RSOAs for WDM-PON system. Various proposed techniques will be summarized in this part. Some works employ more than one technique to achieve high-speed operation of RSOAs.

A fundamental method is to increase the modulation bandwidth of a RSOA by improving the device and/or package design. The modulation speed of a RSOA is limited by carrier lifetime. By increasing the RSOA length to 850 μm, 3-GHz modulation bandwidth was obtained. Transmission over a 2-km SMF at 10 Gb/s below the FEC limit without any electronic processing was demonstrated in [44]. The chirp generated by high-speed direct modulation of the RSOA becomes a limiting factor. However, chirp reduction in RSOAs has been demonstrated using multi-electrode devices [45]. In [46], a butterfly-packaged RSOA was developed to minimize the electrical parasitics. As a result, the modulation bandwidth of RSOA was improved from 2.2 to 3.2 GHz. Error-free transmission of 25.78-Gb/s signal obtained from a directly modulated RSOA was demonstrated by electrical equalization in conjunction with the use of FEC. A compressively strained multi-quantum-well RSOA was designed and an electro/optical (E/O) bandwidth of approximately 4 GHz was achieved. Up to 10.7-Gb/s data rate was demonstrated [47].

Another attractive method to increase the data rate supported by directly modulated RSOAs would be electronic equalization. The frequency response of a RSOA has a

smooth roll-off with no relaxation oscillation peak while its modulation has a good linearity. These properties are almost ideal for the electronic equalization using the decision feedback equalizer (DFE) that consists of feedforward and feedback filters. A RSOA with 2.2-GHz modulation bandwidth was operated at 10 Gb/s by using the electronic equalizer consisting of half-symbol-spaced DFE (17, 3), i.e., 17-tap feedforward equalizer (FFE) and 3-tap DFE. The maximum reach could be extended to greater than 20 km with the help of FEC code [48]. The same authors extended their study by increasing the data rate to 25.78 Gb/s with a butterfly-packaged RSOA whose modulation bandwidth was around 3.2 GHz [49]. In [50], error-free transmission of 20-Gb/s over 20 km SMF was achieved for a WDM-PON based on a 1-GHz RSOA by using partial-response maximum likelihood equalizer together with optical filter detuning and FEC. Ref. [51] demonstrated a 10-Gb/s extended-reach WDM-PON with low-bandwidth RSOA using a conventional maximum-likelihood sequence estimation (MLSE) receiver. The MLSE helped to recover from the inter-symbol interference (ISI) and Rayleigh backscattering (RBS) allowing the signal from a directly modulated RSOA to reach up to 19-km bidirectional fiber and 125-km unidirectional fiber with a BER = 10^{-3}. In addition to post-equalization, pre-equalization was also demonstrated for improving the data rate of directly modulated RSOAs [52].

Besides equalization in electrical domain, the signal distortion due to chirp generated by direct modulation and chromatic dispersion can also be smoothed in the optical domain by detuned optical filtering. The positive chirp factor of RSOAs varies the frequency of the signal during direct modulation. The frequency is blue-shifted at the leading edge and red-shifted at the trailing edge. Thus reducing (blue-shifting) the center

wavelength of the optical bandpass filter (BPF) placed before the photodiode causes more attenuation for the trailing edge than the leading edge. The phase modulation generated by the chirp of the RSOA would be transformed into constructive amplitude modulation [53-56]. Detuned optical filtering is usually applied together with electrical equalization for high-speed operation of RSOAs. Error-free symmetrical 10-Gb/s full-duplex bidirectional transmission over 25-km SMF by modulating a strongly bandwidth-limited RSOA was experimentally demonstrated. The optimal filter position was 0.16 nm blue-shifted with respect to the central wavelength of the transmitted signal and the detected signal was post-processed with DFE (5, 2) [53, 54]. By using duobinary partial response equalization and detuned optical filtering techniques, a WDM-PON system operating at 10 Gb/s with only 1-GHz-bandwidth RSOA over 10-km transmission was achieved [55]. Ref. [56] proposed an improved detuned filtering approach based on the use of a single narrow-bandwidth AWG detuned in respect to the WDM grid. The narrow-bandwidth AWG acted both as a WDM demultiplexer and a detuned optical filter. 10-Gb/s operation of a RSOA with < 1 GHz bandwidth was investigated and error-free transmission was obtained after a 20-km SMF without the use of electronic equalization.

H. Kim proposed and demonstrated 10-Gb/s operation of the RSOA using an optical delay interferometer (DI) [57-59], where the DI acts as an optical equalizer as well as a vestigial sideband filter. As shown in Fig. 2.5, a DI having a 25-GHz free-spectral range (FSR) was employed before the photodetector. The transmission null of the DI was red-shifted by 3 GHz to the central frequency of the RSOA output. Transmission of 10-Gb/s directly modulated RSOA signals over 20-km SSMF in a carrier-distributed WDM-PON system was demonstrated [58]. The use of the 25-GHz DI

could be shared among multiple WDM channels. The author further improved the receiver sensitivity and lowered the error floor by adopting a dual-detector receiver [59].

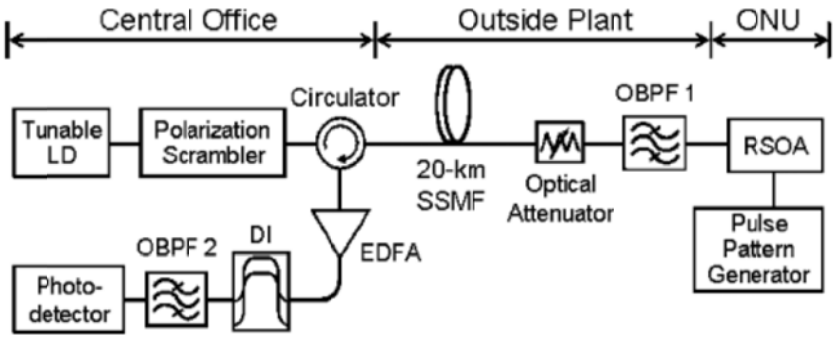

Fig. 2.5. 10-Gb/s operation of a RSOA using an optical delay interferometer [58].

Bandwidth-efficient modulation formats such as duobinary, 4-ary pulse amplitude modulation (PAM), and quadrature phase shift keying (QPSK) are adopted to achieve high-speed operation of direct modulation of bandwidth-limited RSOAs [52, 60-64]. Duobinary has been demonstrated as an alternative to non-return-to-zero (NRZ) due to its reduced bandwidth requirement with external modulators as well as directly modulated sources. A passive microstrip RLC pre-equalizer was optimized for the combination of the RSOA and the electrical filter to match the required frequency response to generate duobinary signal. 10-Gb/s transmission by direct modulation of a RSOA has been achieved with duobinary encoding [52]. The 11-Gb/s 4-ary PAM signal generated by an arbitrary waveform generator was directly modulated onto a 2.2-GHz RSOA and error-free transmission over 20-km SMF was fulfilled with electronic equalization at the receiver [60]. Since both the amplitude and phase of the RSOA output vary with the modulation current, QPSK signal can be generated by directly modulating the RSOA with a proper 4-level electrical signal. Ref. [61] has successfully demonstrated the transmission of 10-Gb/s optical QPSK signal over 80-km long link in the WDM-PON

implemented by using directly modulated RSOAs and digital coherent receivers together with the electronic phase equalization techniques. The data rate was further increased to 40-Gb/s by utilizing the QPSK format and the offset polarization division multiplexing technique in which two RSOAs was directly modulated with two 20-Gb/s QPSK signals separately [62]. 8-phase shift keying (PSK) optical signal generation technique by directly modulating RSOA using sophisticated optimization process of the instantaneous injection/depletion current was proposed in [63]. By compensating the patterning effect through optimizing the instantaneous injection/depleting current according to all the symbol patterns, 10.5-Gb/s 8-PSK signal by directly modulating a RSOA with a bandwidth of only 0.9 GHz was demonstrated. Discrete Multi-Tone (DMT) modulation allows maximizing the capacity of a communication system by measuring the available SNR of the link and then performing optimal bit and power loading on each subcarrier. This technique results in advantages in systems where the transmitter is bandwidth-limited. In case of RSOAs, DMT could significantly increase the transmission capacity compared to the NRZ modulation format. 25-Gb/s transmission by using a DMT modulated 1-GHz RSOA in combination with optical detuned filtering was demonstrated [64].

2.1.2.3 Backreflection in carrier-distributed WDM-PONs

The major technical issue for a single-fiber carrier-distributed (or loopback) WDM-PON which supports bidirectional transmission of the same wavelength is SNR degradation by the backreflection-induced crosstalk in the fiber link. The backreflection would include RBS and discrete Fresnel reflection induced by reflection points such as splices and connectors. The discrete Fresnel reflection could be minimized by using angled

connectors and splices. However, RBS is inevitable as it is the intrinsic property of optical fibers. Numerous research studies have been carried out to reduce the RBS-induced performance degradation in carrier-distributed systems.

Fig. 2.6 illustrates the two types of Rayleigh backscattering in a carrier-distributed system. Reflection-I, defined as carrier-generated RB (Carrier-RB), is the backreflection of the upstream carrier sent from CO to ONU. It causes intensity noise as it interferes with the upstream signal. Reflection-II, defined as signal-generated RB (Signal-RB), is the backreflection of the modulated upstream signal sent from ONU to CO. After reflection, Signal-RB proceeds toward ONU together with the distributed upstream carrier. It is modulated again at the ONU and sent to the OLT where it interferes with the upstream signal [65].

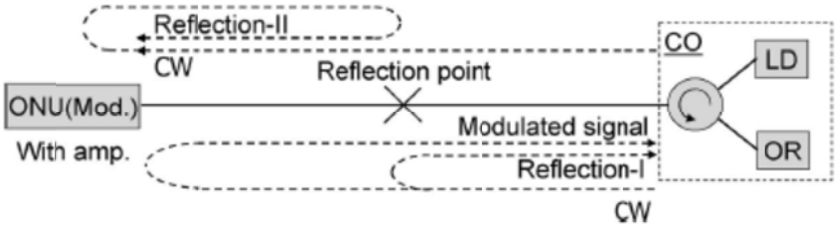

Fig. 2.6. Two types of reflections in carrier-distributed system [65].

The intraband crosstalk induced by backreflection noise is dominated by the signal-crosstalk beat noise. It has been demonstrated that incoherent spectrum-sliced light sources used as the distributed carriers are less sensitive to intraband crosstalk than the laser sources with higher coherency. This is mainly because the optical bandwidth of the spectrum-sliced light sources is much broader than the receiver's electrical bandwidth which blocks a large portion of beat components [66]. However, the data rate is limited when a spectrum-sliced BLS is adopted as the distributed upstream carriers.

For coherent CW distributed carriers, the interferometric crosstalk could be reduced by broadening the optical spectrum, i.e., decreasing the coherent time, of the CW carrier or the modulated upstream signal. This can be done by external phase modulation of the CW carrier or by bias dithering of RSOA in the ONU [67, 68]. Single-tone bias dithering of a RSOA with a frequency outside the data bandwidth will move the noise from baseband to higher harmonics out of the receiver bandwidth. Reduction of reflection-induced crosstalk in a link employing RSOAs achieved by applying bias dithering at RSOAs and phase modulation at the carrier source gave 6 dB and 7 dB improvement in power penalty, respectively [69].

The interferometric crosstalk could be also mitigated by reducing the spectra overlap between the modulated signal and the backreflection noise so that most of the electrical beat frequency will fall outside the receiver bandwidth. This could be realized by employing techniques such as line coding and subcarrier multiplexing (SCM). The purpose of line coding applied to the upstream transmitter, e.g. RSOAs, is to spectrum-shape the power spectral density and up-shift the signal spectrum compared with the NRZ signal. A system demonstration of 6-dB enhanced tolerance to backreflection for WDM-PON based on 8B10B coding and high-pass electrical filtering was reported in [70]. Two correlative level codes, dicode and modified duobinary, were implemented to reduce the RB-induced interferometric crosstalk. At 10 Gb/s, the minimal allowable optical signal-to-RB ratio at the BER of 10^{-4} was reduced to16.5 dB by dicode coding, which was 4.3 dB better than the uncoded transmission. Experiments also demonstrated that 10 Gb/s and 20 Gb/s uplink could reach up to 70 km and 35 km using dicode and modified duobinary signaling, respectively [71].

By applying SCM, the upstream signal would be shifted away from the backreflection noise and therefore the RB-induced power penalty could be eliminated. The SCM could be applied at ONU or RN where the distributed carrier was externally modulated with a subcarrier frequency. The upstream data was encoded onto the resulted subcarrier and transmitted back to the OLT. Since there was no overlap between the upstream signal and the backreflection noise, the high-frequency beat noise could be removed by the low-pass filter (LPF) at the receiver [72, 73].

2.1.3 Injection-locked FP-LDs

To achieve colorless operation of ONUs in WDM-PONs, another cost-effective method is based on injection-locked FP-LDs. External seeding light required for injection-locking the FP-LDs in ONUs are distributed from the OLT. Compared to the carrier-distributed WDM-PONs introduced in the previous subsection, in which the ONU based on a RSOA or an EAM-SOA acts simply as a modulator and an amplifier, the ONU based on a FP-LD will work as a directly-modulated laser subject to the injection-locking mechanism.

A free-running FP-LD exhibits multiple longitudinal modes decided by the length of the Fabry-Perot (FP) cavity and the refractive index of the gain media. Strong mode partition noise (MPN) will be exhibited if any longitudinal mode is filtered out. The large relative intensity noise (RIN) makes the spectrum-sliced free-running FP-LD unsuitable to be transmission carrier [74]. However, if an external light source is fed into a free-running FP-LD, the cavity mode located near the injection wavelength can be injection-locked and enhanced in intensity while other cavity modes are suppressed. When the side-mode suppression ratio (SMSR) is greater than 30 dB, the FP-LD is supposed to lead quasi-single-mode operation.

2.1.3.1 External seeding sources

The external seeding light can be incoherent spectrum-sliced ASE sources or coherent CW lasers. The advantages of incoherent spectrum-sliced ASE sources are low cost and more importantly it is unpolarized which is a desirable feature when working with polarization-dependent devices, e.g. polarization-dependent FP-LDs. However, the data rate of a spectrum-sliced ASE injection-locked FP-LD is limited by the RIN of the spectrum-sliced ASE seeding source. Although the total power of an ASE source is relatively stable, the RIN of any spectrum-sliced narrow-band spectrum is quite large. This intensity noise will be transferred to the injection-locked mode of the FP-LD and degrade the output performance of the injection-locked FP-LD [75]. The SNR of the directly modulated spectrum-sliced ASE injection-locked FP-LD would be determined by the ratio of optical bandwidth to electrical bandwidth, which is similar to a spectrum-sliced ASE source used as a carrier as described by (2.1). The self-filtering effect and the additional phase noise of an injection-locked FP-LD would limit the system performance for high-capacity (beyond 1.25 Gb/s) long-reach WDM-PONs [76, 77]. Return-to-zero (RZ) modulation was utilized to improve the system dispersion tolerance and 1.25-Gb/s signal over 45 km of SSMF based on incoherent light injection-locked FP-LD was demonstrated [78]. With a noise suppressor after the external seeding light, the data rate of a spectrum-sliced ASE injection-locked FP-LD was increased up to 2.5 Gb/s in [79].

To improve the transmission capacity of injection-locked FP-LDs, coherent CW light is used as the external seeding source. For coherent seeding light, the required seeding power is smaller than that of incoherent seeding light. Thanks to the low RIN in the coherent seeding light, the data rate of directly-modulated coherent light injection-

locked FP-LD has been increased to 10 Gb/s [80]. However, the injection-locking range to achieve 10-Gb/s operation was very tight. The detuning ranges between the CW seeding light and the targeted longitudinal mode was about 0.029 nm (3.6 GHz) to guarantee the BER smaller than 10^{-9}. Moreover, the fact that low-cost FP-LDs are polarization-sensitive makes the polarized laser source unsuitable for the role of external seeding source [81].

An external seeding source whose performance is between the incoherent spectrum-sliced ASE and the coherent CW laser would be a spectrum-sliced FP-LD. Although the large MPN exhibited in a spectrum-sliced FP-LD makes it unsuitable for being an optical carrier, a spectrum-sliced FP-LD (master FP-LD) could be used as the external seeding source to injection-locked another FP-LD (slave FP-LD). Simultaneous transmission of four channel 2.5-Gb/s over 25 km SMF was demonstrated with injection-locked FP-LDs by another spectrum-sliced FP-LD [82].

A multimode-injected FP-LD is proposed and used as the external seeding light for a carrier-distributed WDM-PON [83]. The multimode-injected FP-LD performs as a noise suppressor to reduce the RIN of the injected ASE spectrum slices. It is verified by simulation that based on the proposed remote seeding light the transmission performance of the injection-locked FP-LD for upstream transmission is improved. The details of the simulation architecture and results will be introduced in Section 4.4.

2.1.3.2 Technical issues in injection-locked FP-LDs

Since the external seeding sources are distributed from the OLT, a colorless WDM-PON based on injection-locked FP-LDs would also suffer RBS-induced performance degradation. Similar to external-seeded RSOAs, the RBS-induced penalty could be

reduced as the linewidth of the seeding light increases. A FP-LD injection-locked by a spectrum-sliced ASE source would show high robustness on the backreflection, while a coherent seeding light results in high backreflection-induced penalty [84]. Some techniques reviewed in Section 2.1.2.3, which are applied to mitigate the backreflection-induced penalty in carrier-distributed WDM-PONs with RSOAs, are also applicable to injection-locked FP-LDs.

In practical systems, the wavelengths of both the seeding light source and the FP-LD fluctuate with the temperature and bias current. Even with a temperature controller, the central wavelength may still fluctuate slightly and randomly. So a large injection-locking range would be desirable for real implementation. By reducing the reflectivity of the front facet to a relative low value, e.g. 1%, the FP-LD would exhibit weak resonance and hence weak-mode lasing. The weak-resonant-cavity (WRC) FP-LD has a wider injection-locking range compared to conventional FP-LDs [85]. The WRC FP-LD could enable a nearly uncooled operation of injection-locking, i.e., the external seeding light would no longer need to be carefully aligned to the longitudinal mode. Even the external seeding light aligned with the valleys of a free-running FP-LD could injection-lock the corresponding WRC FP-LD. This operation is similar to an external-seeded RSOA in which no wavelength alignment is required [86, 87].

For a conventional polarization-sensitive FP-LD, injection-locking by a coherent source strongly depends on the polarization state of the injected light. For example, if the FP-LD favors the transverse-electric (TE) mode, the FP-LD makes light by lasing on the TE mode when the FP-LD is driven over a threshold current. On the other hand, the transverse-magnetic (TM) mode in the FP-LD shows only absorption nulls instead of

lasing, due to the very small TM gain inside the FP resonator [88]. When the seeding light is linear-polarized and it is aligned to the TE mode of the FP-LD, the FP-LD will be injection-locked at the longitudinal mode located closest to the seeding light at the shorter wavelength side; when the seeding light is aligned to the TM mode of the FP-LD, it is absorbed by the FP-LD instead of injection-locking the FP-LD. To tackle this, a two section FP-LD was designed by using a polarization-insensitive gain material as the active section and a strained InGaAsP material as the birefringence compensating section. As a result, the optical emission spectrum shows superimposed TE and TM modes after the proper amount of electrical currents are injected into both sections. In this case, TE and/or TM mode will be locked to the incoming signal whatever its polarization state [89].

2.1.4 Wavelength remodulation

All the schemes discussed so far for fulfilling colorless operation of ONUs require separate wavelength channels for upstream and downstream transmission. To increase spectral efficiency, carrier reuse or downstream wavelength remodulation, has been proposed. In such a scheme, the downstream signal is divided into two portions in the ONU. One portion is detected by the downstream receiver and the other portion is fed into a RSOA or a FP-LD where it is encoded with upstream data and transmitted back to the OLT. Fig. 2.7 depicts the typical configuration of the ONU in a wavelength-remodulated WDM-PON. Since each ONU requires only one wavelength channel for simultaneous upstream and downstream transmission, the number of end users served by one WDM-PON can be doubled and the implementation cost can be shared by more end users.

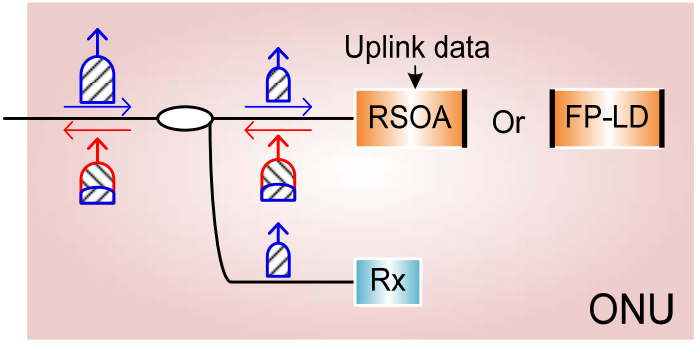

Fig. 2.7. The typical configuration of ONUs in a wavelength-remodulated WDM-PON.

Similar to carrier-distributed WDM-PONs, bidirectional WDM-PONs with remodulation scheme suffer backreflection-induced performance degradation. Moreover, the performance of wavelength-remodulated WDM-PONs is also degraded by remodulation crosstalk, i.e., the residue downstream modulation on the upstream signal. Some techniques proposed to mitigate the remodulation crosstalk-induce penalty are reviewed here.

The NRZ format is preferred for both downstream and upstream transmission due to its simple implementation. However, the extinction ratio (ER) of downstream signal shall be compromised to facilitate upstream remodulation. In the case of using a FP-LD for upstream remodulation, the downstream ER should be carefully controlled to guarantee the power at spaces (binary “0”s) is well above the injection-locking threshold. The data rate of downlink is usually higher than that of uplink and the injection-locked FP-LD would function as a high-pass filter to remove most of the downstream modulation in the low-frequency region [90]. If an RSOA is employed as the upstream transmitter, it should be operated in the saturation region to suppress the power fluctuation resulted from downstream modulation in the seeding light. If the RSOA is operated in the unsaturated region, the performance of the upstream signal could be

seriously degraded by the thick '1-level' induced by power fluctuation in the seeding light [91]. Similarly, the downstream ER should be optimized to keep some residual power during its space bits for remodulation with upstream data. A too low downstream ER results in an unacceptable high penalty for its detection, while a too high downstream ER degrades the upstream performance.

To alleviate the constraint on the downstream ER, several modulation schemes for downlink were proposed, including inverse-return-to-zero (IRZ) and spectrum-shaping coding such as Manchester coding, miller coding, and dicode [92-95]. The Manchester-encoded signal had a negligible amount of low-frequency components. Thus, the residual downstream signal superimposed on the upstream signal could be washed out by the limited bandwidth of the upstream receiver. However, Manchester coding needs to double electrical receiver bandwidth which increases the cost of ONUs [93]. The Miller signal follows the similar scheme as Manchester signal since they both belong to 1B/2B coding. The frequency spectrum of this signal contains less energy in low frequency than a conventional NRZ signal and less energy in high frequency than Manchester signal. It not only preserves the advantages of Manchester coding but also features an added advantage of reduced bandwidth as most of the power resides within the range of 0.5 times the bit rate [95]. An alternative modulation format for downstream signal in wavelength-remodulated WDM-PONs is DPSK due to its constant-intensity nature. The DPSK-formatted downstream signal can be appropriately controlled to substantially suppress the crosstalk between the upstream and the downstream data [96]. However, the phase-to-intensity conversion would still introduce crosstalk to upstream signal.

Subcarrier modulation technique is also applied to wavelength-remodulated WDM-PONs to reduce remodulation crosstalk [97, 98]. In [97], the downstream data was transmitted at the subcarrier frequency and detected at baseband. In the upstream, the optical signal was remodulated at baseband. There was no significant penalty due to the crosstalk from the downstream signal. Since the downstream and upstream data are modulated and transmitted at subcarriers frequency and baseband respectively, the crosstalk in this scheme is expected to be lower than the scheme where both downlink and uplink data are modulated on the baseband.

The remodulation crosstalk could be also cancelled by employing feed-forward cancellation circuitry adapted to the RSOA or FP-LD in the ONU [99]. As Fig. 2.8 shows, a 50/50 coupler split detection and remodulation branch, whereby the latter held a fiber delay line to cope for the slower propagation of the electronic cancellation signal that originates at the avalanche photodiode (APD). The relation between gain and bias current required an inverted data signal for the cancellation. The cancellation circuit itself consisted of an electrical delay for fine tuning of the path lengths, a derivative filter, and RF amplifiers. A passive combiner was taken to add the upstream data to the cancellation signal.

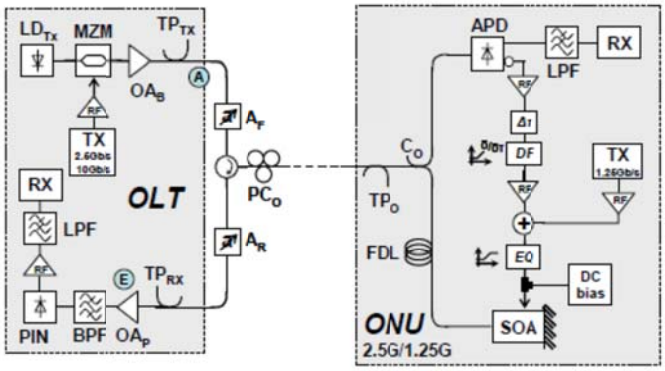

Fig. 2.8. Schematic of a wavelength-remodulated WDM-PON with feed-forward downstream cancellation circuitry [99].

2.1.5 Self-seeding of FP-LDs or RSOAs

The carrier-distributed WDM-PONs and wavelength-remodulated WDM-PONs suffer from backreflection-induced power penalty. The backreflection noise could be reduced or eliminated by allocating the distributed carrier sources at the RN, however the RN would be no long passive. Self-seeding technique can remove the need of remote seeding light and therefore avoid the crosstalk induced by backreflection noise and at the same time achieve colorless operation of ONUs. Fig. 2.9 illustrates the schematic of a WDM-PON architecture with self-seeding technique and two feasible configurations of the reflection module (RM) located at the RN.

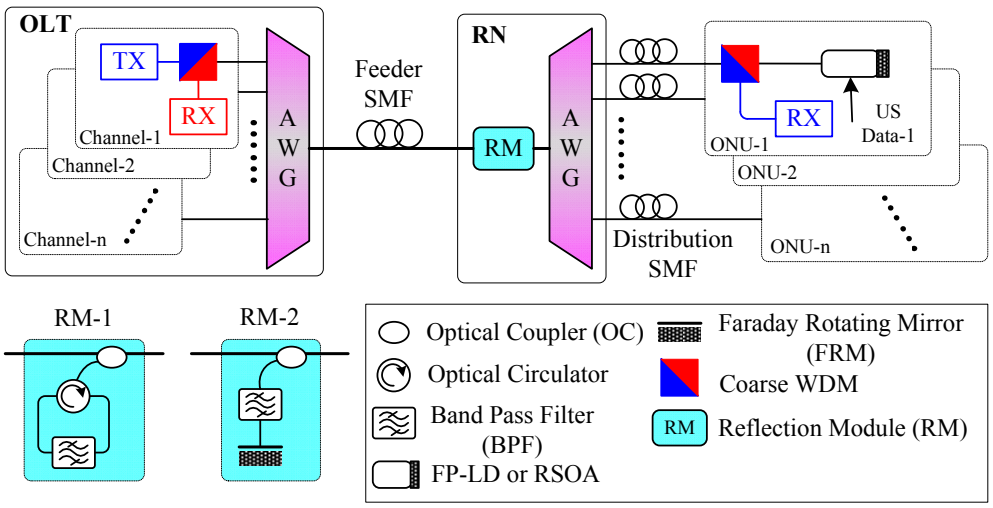

Fig. 2.9. Schematic of a colorless WDM-PON architecture based on self-seeding technique.

The self-seeding cavity is formed by the rear facet of the FP-LD or RSOA and the RM in the RN. The downstream and upstream wavelength channels for each ONU are located at different wavebands which are separated by one or multiple FSRs of the cyclic AWG. They could be separated by the coarse wavelength division multiplexers (CWDMs) in each ONU and the OLT. Not only does the AWG in the RN multiplex the upstream wavelength channels and demultiplex the downstream wavelength channels, but each

channel of the AWG is also utilized as a filter in the self-seeding cavity to determine the lasing wavelength. The output of the upstream transmitter, i.e., FP-LD or RSOA, is spectrum-sliced by one AWG channel within the cavity and then looped back to feed the same transmitter. The light is reflected back and forth between the RM in the RN and the FP-LD or RSOA in the corresponding ONU.

2.1.5.1 Self-injected FP-LDs

Self-injection of FP-LDs has been widely studied as a method to generate tunable single-frequency fiber Fabry-Perot lasers [100-102]. When a FP-LD is utilized as the upstream transmitter in a self-seeded WDM-PON, one of the free-running longitudinal modes of the FP-LD should be aligned with the central wavelength of the AWG channel to which the ONU is attached.

In [34], the self-injected FP-LD was directly modulated at 2.5 Gb/s and error-free transmission over 85-km SMF was achieved. Due to the large polarization dependent gain (PDG) of FP-LDs, the polarization of the seeding light should be carefully adjusted to align with the favored polarization mode of the FP-LD. Ref. [103] proposed stable 1.25-Gb/s self-seeding operation of a directly modulated FP-LD without polarization control. The polarization independence of the self-seeding operation was fulfilled by adopting a 90° Faraday rotator mirror (FRM) as the RM and placing an in-line non-reciprocal 45° Faraday rotator (FR) at the output of the FP-LD. In a later work, the same authors demonstrated uncooled and polarization independent operation of self-seeded FP-LDs [104]. The uncooled operation in the temperature range of 0–60 °C was realized by utilizing an automatic power control circuit which would keep the FP-LD output power constant over temperature variations. However, about 2-dB periodic oscillation of the

receiver sensitivity was observed and this was attributed to the fact that the wavelength offset between the FP-LD longitudinal mode and the central wavelength of the AWG channel changes with temperature.

2.1.5.2 Self-seeded RSOAs

Compared to a self-seeded RSOA, a self-injected FP-LD shows narrower emission linewidth, resulting in improved resilience to chromatic dispersion. However, a self-seeded FP-LD could not tolerate a large wavelength offset between the longitudinal mode of the FP-LD and the AWG channel whereas a self-seeded RSOA does not require wavelength alignment.

Self-seeded RSOAs directly modulated at 1.25 Gb/s with a reflection module same to RM-1 in Fig. 2.9 was demonstrated with negligible transmission and crosstalk penalties after traversing 21-km SMF [35]. The polarization-independent RSOAs are preferred since the need for controlling the polarization of the seeding light could be eliminated. For a RSOA with a small PDG of 1~2 dB, the system instability induced by the polarization dependence of self-seeding operation could be overcome by employing a 90° FRM as the RM in the RN [105, 106]. In [107], stable performance of a self-seeded RSOA was observed when the operating wavelength was tuned from 1530 nm to 1595 nm. The signal sensitivities were similar and almost no power penalty was induced. The data rate of self-seeded RSOA was increased to 2.5 Gb/s by using a low-PDG RSOA with the E/O bandwidth > 2 GHz [108]. A similar self-seeding configuration applied to polarization-sensitive FP-LDs was exploited to work with high-PDG RSOAs. With the proposed technique, the polarization at the RSOA input was stable and aligned with the high gain transverse mode of the RSOA. Since the RSOA had a large E/O bandwidth of

approximately 4 GHz, the bit rate of the directly modulated self-seeded RSOA was enhanced to 10 Gb/s. The FEC threshold was met with the help of post-electronic equalization [45].

Although these research works provide valuable knowledge of the feasibility of utilizing self-seeded RSOAs as colorless transmitters in WDM-PON systems, these investigations are not comprehensive enough to give an in-depth understanding of the characteristics of the directly modulated self-seeded RSOA-based transmission systems. The influences of several system parameters on the transmission performance remain unexplored, including the signal extinction ratio, the stable seeding power to the self-seeded RSOA, the pattern length dependency, the bandwidth and shape factor of the wavelength multiplexer within the self-seeding cavity, and the length of the self-seeding cavity. These issues will be addressed in detail in Section 3.1.

2.2 Broadcast/multicast delivery over WDM-PONs

Along with the growing bandwidth requirement of each end user, the demand for the flexibility and variety of services over a certain network is ever-increasing. Therefore, providing both unicast and broadcast/multicast services simultaneously is highly desirable for viable access network architectures. Fig. 2.10 illustrates the concepts of unicast, broadcast, and multicast deliveries over a WDM-PON architecture. Unicast in a WDM-PON refers to a point-to-point transmission through a dedicated wavelength channel. Broadcast is the term used to describe communication where a piece of information is sent from one point to all connected points. Multicast is the term used to describe communication where a piece of information is sent from one or more points to a set of other points. Compared to broadcast, multicast is more attractive as it allows

flexible control of the multicast traffic for individual subscribers [109].The multicast service is delivered to a subset of subscribers and can be selectively enabled or disabled by the OLT.

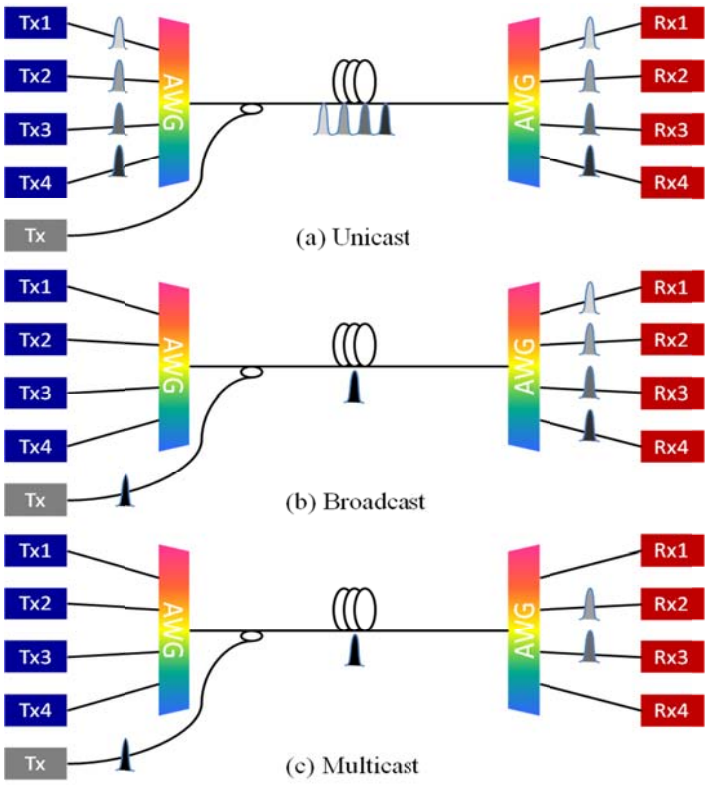

Fig. 2.10. (a) Unicast, (b) broadcast, and (c) multicast delivery over a WDM-PON architecture.

It is straightforward to deliver broadcast service over TDM-PONs due to its point-to-multipoint topology. However, the logical point-to-point topology of WDM-PONs hinders direct and simple delivery of broadcast/multicast services. In order to meet the ever-increasing demand of broadcast/multicast services, e.g. video-on-demand and high-definition television distribution services, several approaches have been proposed to deliver broadcast or multicast services over WDM-PON architectures.

One obvious method would be employing additional light source to deliver broadcast/multicast services [110-113]. In [110], a broadband incoherent light source was modulated with broadcast data and distributed to individual ONU after being spectrum-sliced by the wavelength demultiplexer at the remote node. However, the incoherent light source suffered low SNR due to large RIN. An ASE-injected FP-LD and mutually-injected FP-LDs have been proposed to act as the BLS for broadcast delivery [111, 112]. By ASE injection, the noise characteristic of FP-LD was improved and the bit rate supported by spectrum-sliced ASE-injected FP-LD was increased to 622 Mb/s. By reducing the external cavity length between the two mutually-injected FP-LDs, the FSR was increased to 6.1 GHz. A Manchester modulation format was used to locate signal spectrum within the low-noise region between two noise peaks. 10-Gb/s NRZ broadcast signal transmission with the FEC was demonstrated. The drawback of employing a BLS or multi-wavelength light source for broadcast delivery is that it requires a dedicated wavelength channel for transmitting broadcast data to each ONU. In [113], only one wavelength channel was employed to deliver broadcast signal to all end users by utilizing an AWG and a power splitter in the RN. However, a high-power broadcast signal is required to compensate for power loss induced by the large splitting ratio.

Subcarrier multiplexing technique was utilized to support broadcast/multicast capability, whereby an optical carrier is modulated with unicast or multicast baseband data while subcarriers operating far beyond the frequency range of the baseband data carry multicast or unicast data. In [114], the 1.25-Gb/s unicast data was modulated at the baseband while the 155-Mb/s broadcast digital video signal was modulated at 2.5-GHz RF carrier. The selective broadcasting was fulfilled by controlling the DFB laser bias.

When the laser is set below the threshold current, the video signal is badly distorted and cannot be recovered by the ONU. In [115], a dual-drive Mach-Zehnder modulator (MZM) is used to generate a sub-carrier double-sideband (DSB) DPSK signal in the OLT for each WDM channel. All central carriers are separated and subsequently modulated to deliver the multicast data, while the remaining sub-carrier DPSK signals carry the downstream unicast traffic. The presence of multicast services was controlled by switching the modulation format of unicast signal between DSB-DPSK and optical carrier suppressed (OCS) DPSK. In such schemes, high-speed optoelectronic components are needed in both OLT and ONUs.

Another method exploited to enable broadcast/multicast service would be orthogonal modulation [116-120]. The frequently-used combination of two modulation formats are phase shift keying (PSK) and amplitude shift keying (ASK). The DPSK-formatted multicast signal could be overlaid on the NRZ on-off keying (OOK) or IRZ-OOK unicast signal. The availability of the multicast service was controlled by adjusting the extinction ratio of the NRZ-OOK unicast data [116] or by switching the modulation format of the unicast signal between IRZ and NRZ [117]. Inversely, the unicast data could be in DPSK format while the multicast data was NRZ-OOK-modulated [118]. Optical orthogonal frequency division multiplexing (OFDM) was adopted for multicast overlay services with different rate requirement. A total 40-Gb/s frequency shift keying (FSK) point-to-point signal and 6.3-Gb/s OFDM overlay with three kinds of variable-rate multicast services were experimentally demonstrated [119]. In [120], the 2.5-Gb/s broadcast data was encoded on the 10-Gb/s 16 quadrature amplitude modulation (QAM)-OFDM unicast signal by polarization shift keying. In general, a trade-off between the

downlink unicast data and multicast data exists in these overlay schemes. The downlink unicast data would suffer from system penalty in order to enable the multicast service.

Time-interleaving the unicast and broadcast data was proposed in [121]. The broadcast and unicast DPSK signals with the same bit rate were temporally offset by *T/2*, with *T* being the bit period. Error-free transmission of 5-Gb/s bidirectional unicast data and 5-Gb/s broadcast data was experimentally demonstrated at the same carrier wavelength over a 20-km SMF. Besides all the methods discussed above, the nonlinear effect-cross gain modulation (XGM)-in a SOA was utilized to generate multiple wavelength signals for broadcast delivery [122].

We have proposed and demonstrated two new schemes to enable broadcast capability over WDM-PONs based on polarization multiplexing and offset polarization multiplexing, respectively. The proposed WDM-PON architectures and the experiment results will be discussed in detail in Chapters 5 and 6.

2.3 Other research aspects in WDM-PON technologies

Besides colorless ONUs and broadcast/multicast delivery for WDM-PON systems, other technical issues, including integration of wired and wireless signal in WDM-PONs, extension of WDM-PON reach, and protection and fault management, have been intensively studied. This section gives a brief summary of existing research work in these fields.

2.3.1 Convergence of wired and wireless: WDM-RoF-PONs

There is an increasing demand from broadband telecommunication end-users to have instant access to high-capacity information services, whether from a fixed or a mobile

terminal. Recently, radio-over-fiber technology has attracted more and more attention to provide wireless connectivity due to its advantages of low transmission loss and high bandwidth of optical fibers. Therefore, the consolidation of RoF and high-speed baseband signals been delivered over a common optical infrastructure is foreseen to pave the way for a seamless broadband experience for the end-users [123].

RoF refers to a technology where light is modulated by a radio signal and transmitted over an optical fiber link to facilitate wireless access. RoF system operating at 60-GHz has gained much attention for the huge bandwidth availability over 7-GHz unlicensed millimeter-wave (MMW) band set aside by the Federal Communications Commission in 2001. The radio signals in MMW band, especially in 60-GHz region, are extremely prone to atmospheric attenuation, making them of very little use over longer wireless distances. Thus, numerous antenna base stations (BS) are needed to cover a larger service area. In this respect, integrating MMW RoF system with WDM-PON (i.e., WDM-RoF-PON) is a very attractive solution to significantly increase the overall capacity and coverage area of the RoF access networks [124]. Nonetheless, the successful implementation of such WDM-RoF-PON systems considerably depends on the spectrally-efficient multiplexing and demultiplexing of the optical channels carrying MMW radio signals. The generation and detection of the MMW is the key issue in RoF systems.

The MMW can be generated through an external intensity or phase modulator driven by the required radio frequency (RF) [125, 126]. By controlling the bias voltage and modulation index, several modulation formats can be realized such as double sideband modulation with/without suppressed carrier, single sideband (SSB) modulation

with/without suppressed carrier. Nonlinear effects, e.g. cross gain modulation, four-wave mixing, and nonlinear polarization rotation, are introduced to perform all-optical up-conversion of radio signal. These techniques, based on nonlinear effects in SOAs or highly nonlinear fibers, exhibit low conversion efficiency and need very high optical input power [127-130]. Other techniques to generate MMW signals include two-mode locked FP slave lasers [131], dual parallel injection-locked FP laser [132] and an optical heterodyne technique using two single mode lasers [133].

The MMW signal can be recovered by direct detection with a high-speed photodiode. The detected radio frequency is sent into the air by an antenna located at BS. Another horn antenna placed at several meters away receives the signal which is down-converted to baseband data by self-mixing and low-pass filtering in the RF receiver. Fig. 2.11 shows the schematic of a converged wired and wireless access network. The MMW was generated by driving a phase modulator with 30-GHz RF in the central office. At the base station, the wired data was detected by a low-bandwidth receiver while the wireless data was received by a 60-GHz PIN photodetector. The 10-Gb/s wireless data carried by a 60-GHz RF was transmitted into the air by a horn antenna and received by the subscribers several meters away. The signal was down-converted by mixing with a 60-GHz clock.

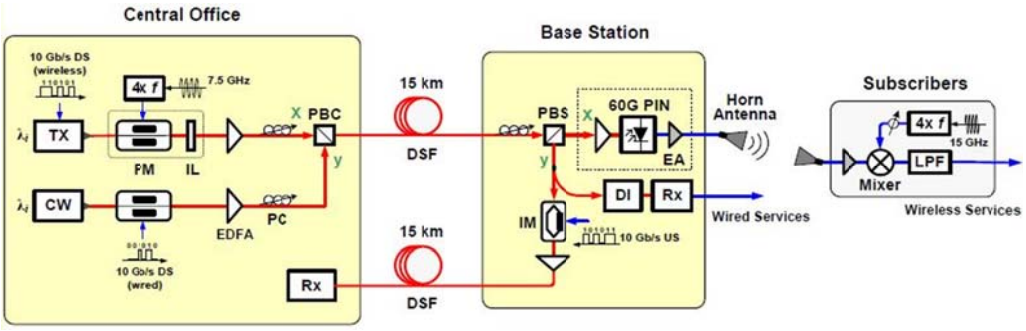

Fig. 2.11. Schematic of a converged wired and wireless access network [126].

2.3.2 Long-reach WDM-PONs

Network operators are currently looking for valid solutions to deploy long-reach PONs. The access and metro networks can be merged into one by extending the back-haul fiber possibly to 100 km in length to incorporate protection path and mechanisms [134]. The overall network would be simplified due to the reducing of the amount of equipment, network elements, and central offices. However, for the prevalent colorless WDM-PONs based on external-seeded RSOAs or external-injected FP-LDs, extending the link would pose power budget issue, especially for upstream transmission since the seeding power may not be sufficient to injection-lock FP-LDs or drive RSOAs into saturation region.

The link loss could be compensated by adding a bidirectional EDFA in the RN. While the traditional way of electrically powering the EDFA violates the rule of being fully passive in the RN, a remote pumping scheme is proposed [135]. Distributed Raman amplification is also employed to boost the power in long-reach WDM-PONs [136]. The fiber link could be extended by adopting coherent detection. For example, error-free transmission of the 5-Gbps QPSK signal over 100-km long fiber link without using any optical amplifiers and electronic equalizers was demonstrated in [137]. A novel line coding combination (IRZ for downlink and RZ for uplink) was proved to extend the reach of WDM-PON to 80 km [138]. Self-seeding of FP-LDs or RSOAs removes the need of remote seeding light and therefore partially alleviates the insufficient power budget induced by extending the transmission link. Directly modulation of self-injected FP-LDs at 2.5 Gb/s and transmission of 85-km SMF was demonstrated in [34].

2.3.3 Fiber fault protection in WDM-PONs

Fault management is a crucial aspect in network management to enhance the network reliability. In conventional PONs, tree topology is commonly employed. Whenever there is a fiber link break from the RN to one of the ONUs, the affected ONU will become unreachable from the OLT which leads to enormous data and business loss [139]. Common practice to achieve network protection is to implement duplicated network resources such as fiber links or ONUs to provide network resource redundancy. Automatic protection switching shall be used to reroute the affected data traffic into those alternate protection paths [140-143]. Fig. 2.12 shows several protection schemes applicable to WDM-PON systems. With the structures in Fig. 2.12 (a) and (b), the fault in the feeder fiber can be protected and restored; with the structures in Fig. 2.12 (c) and (d), the failure in both feeder fiber and distribution fibers can be recovered.

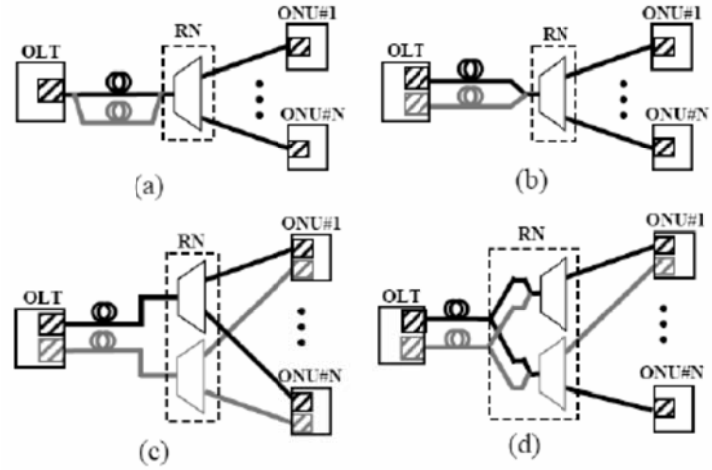

Fig. 2.12. Protection architectures for WDM-PONs using the similar approaches suggested by ITU-T G.983 [144].

In [140], the affected ONU could communicate with the OLT by rerouting the wavelength channels via the adjacent ONU in case of a fiber cut in the distribution fiber.

By utilizing the routing characteristics of an N×N AWG, automatic protection against any fiber cut between central office and ONUs was guaranteed in [145]. Beside tree topology, a dual-ring architecture was proposed to protect and restore any fiber fault in a ring-based WDM-PON [146].

2.3.4 Energy-saving in WDM-PONs

Environmental sustainability has become an important social and business movement in the past years. Energy consumption of the information and communication technologies (ICT) is increasing at a high rate since more computers, networks, and communication equipment are being deployed every year. It is estimated that ICT consumes around 8% of total electricity all over the world [147]. Telecom networks constitute a significant part of ICT. It is estimated that access network consumes around 70% of overall telecom network energy consumption due to the presence of huge number of active devices [148]. In addition, estimation shows that access networking equipment are less than 15% utilized and a large portion of energy is therefore consumed by the idle devices, as the networks are engineered for satisfying the peak traffic load requirement. Hence, reducing energy consumption in access networks can lead to major saving in Internet energy consumption.

A monitoring technique with the modulation of the ASE generated by free-running RSOA by the pilot-tone monitoring signal at the ONU was demonstrated to achieve power saving in RSOA-based WDM-PONs [149]. In [150], a polling scheme of a supervisor transceiver in a WDM-PON was proposed to build a power saving structure. It is suitable for the PON system in which traffic is relatively concentrated during certain times. An efficient energy-saving scheme incorporating dozing and sleep modes for

WDM-PONs with centralized light sources was proposed in [151]. The scheme was based on simple power detection and local transmission request. Two logic control units were designed to switch the operation modes of the respective ONUs and their associated transceivers in the OLT.

2.4 Summary

In this chapter, the existing technologies enabling colorless operation of ONUs in WDM-PONs have been thoroughly summarized. Their characteristics, advantages, and corresponding technical issues are briefly introduced. These schemes will be evaluated and compared in terms of cost-effectiveness, transmission capacity, and operation complexity in Section 3.3. Various existing broadcast/multicast-enabling schemes are also discussed in this chapter. Together with our two proposed broadcast-enabling schemes, they will be evaluated in terms of cost-effectiveness, spectral efficiency, operation complexity, and system transparency in Section 6.5. Other related research aspects are briefly mentioned in order to give a comprehensive understanding of the current development of WDM-PON technologies. Our investigation on self-seeded RSOAs, multimode-injected FP-LDs, and the two proposed broadcast-enabling techniques will be presented and discussed individually in the following chapters.

CHAPTER 3

Self-Seeded RSOAs—Low-Cost Colorless Light Sources for WDM-PONs

The self-seeding technique provides a cost-efficient solution for colorless operation of ONUs in WDM-PONs. Colorless WDM-PONs based on self-seeding scheme could avoid the backreflection-induced performance degradation, which is the primary drawback for the prevalent carrier-distributed or wavelength-remodulated WDM-PONs. As discussed in Section 2.1.5, several studies have been contributed to investigate the technical issues in self-seeded RSOAs such as polarization dependence [105], operating wavelength range [107], and multi-channel operation [152]. However, the influences of several crucial system parameters on the transmission performance of WDM-PONs based on self-seeded RSOAs remain unexplored. Furthermore, except for [47], no effort is made to increase the bit rate of self-seeded RSOAs which is primarily limited by the RSOA modulation bandwidth.

This chapter first investigates the effects of several system parameters on the transmission performance of a WDM-PON based on self-seeded RSOAs. Then, some feasible techniques to increase the bit rate of self-seeded RSOAs are proposed and studied. Finally, various schemes for colorless operation of ONUs in WDM-PONs are compared.

3.1 Characterization of self-seeded RSOAs in WDM-PONs

In this section, the influences of several system parameters including the signal extinction ratio, the stable seeding power to the self-seeded RSOA, the pattern length dependency, the bandwidth and shape factor of the wavelength multiplexer within the self-seeding cavity, and the length of the self-seeding cavity, on the transmission performance of a colorless WDM-PON based on directly modulated self-seeded RSOAs are investigated through experiments. Besides, the polarization evolution of the light circulated in the self-seeding cavity with a low- or high-PDG RSOA is analyzed intuitively. The power evolution in the establishment of the self-seeding operation is also discussed through simulation.

3.1.1 System architecture and experimental setup

The WDM-PON architecture with directly modulated self-seeded RSOAs as the colorless upstream transmitters is shown in Fig. 3.1. The downstream and upstream wavelength channels for each ONU are separated by one or multiple FSRs of the cyclic AWG. They could be separated by CWDMs in each ONU and the OLT. The output of a RSOA is spectrum-sliced by the AWG channel which the RSOA is connected to and the resultant spectrum slice is reflected back and forth between the RM in the RN and the RSOA in the corresponding ONU.

The RM is composed of an FRM providing 90° rotation of polarization at 1550 nm to the reflected signal with respect to the coming signal. The RM based on an FRM instead of a circulator has been proved to successfully stabilize the system performance of the directly modulated self-seeded RSOA by addressing the system polarization dependence [105]. A bandpass filter with a pass band comparable to the FSR of the AWG

within the self-seeding cavity is added in the RM to ensure that only one spectrum slice from each AWG channel could circulate in the self-seeding cavity. Stable self-seeding is established when the gain of the RSOA equals the loss of the self-seeding cavity after the light circulates in the self-seeding cavity for several roundtrips.

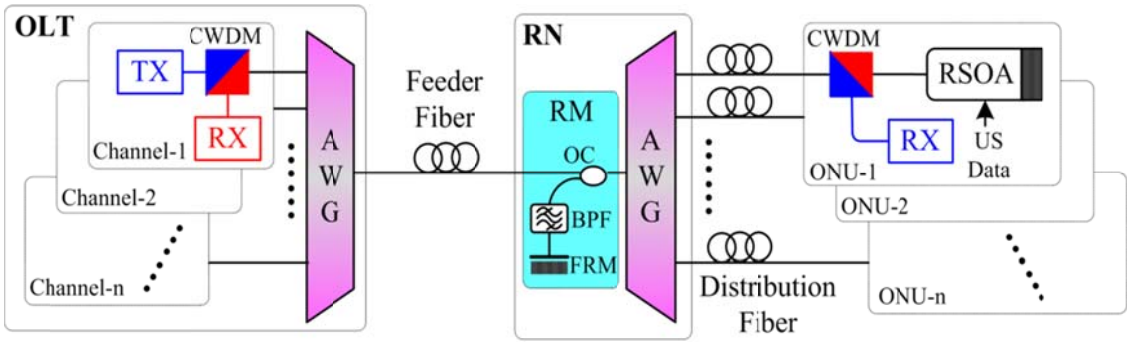

Fig. 3.1. Schematic of a colorless WDM-PON system based on the directly modulated self-seeded RSOAs.

In a RSOA structure, a usual SOA chip has a rear facet with a high-reflectivity (HR) coating and a front facet with an anti-reflectivity coating. Light incident onto the front facet is amplified while progressing in an active waveguide, is then reflected from the HR rear facet on the backside, and is then output through the front facet [153].

The RSOA used in the experiments is housed in a pigtailed coaxial package based on a TO56 can with a FC/APC fiber connector. It utilizes InP-based buried heterostructure design with a ~1.2 μm wide InGaAsP tensile bulk active region. The active region of the RSOA may have a length of 200-600 μm. In order to facilitate the application as a WDM-PON transmitter, it is designed with a low front facet reflectivity of $<10^{-5}$ and a high reflectivity coating for the rear facet [154]. It has a small signal gain of 23 dB, a low PDG of 1 dB, and a saturated output power of 5 dBm when it is biased at 80 mA. The electrical bandwidth of the RSOA is around 1.1 GHz. The free-running optical spectrum and gain characteristic of the RSOA when it is biased at 80 mA are

shown in Fig. 3.2 and 3.3, respectively. The ripples exhibited in the free-running spectrum are induced by Fresnel reflection occurred during the measurement. The 3-dB bandwidth of ASE generated by the free-running RSOA is about 55 nm. The output power of the RSOA would still slightly increase with the seeding power in the saturation regime.

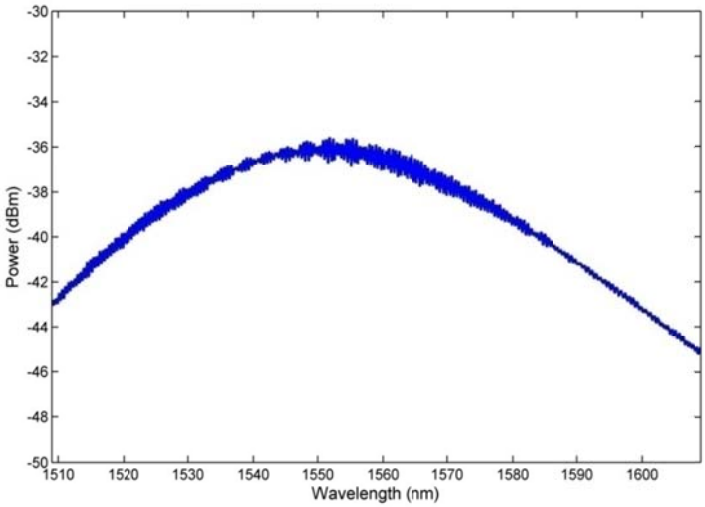

Fig. 3.2. The free-running optical spectrum of the RSOA biased at 80 mA.

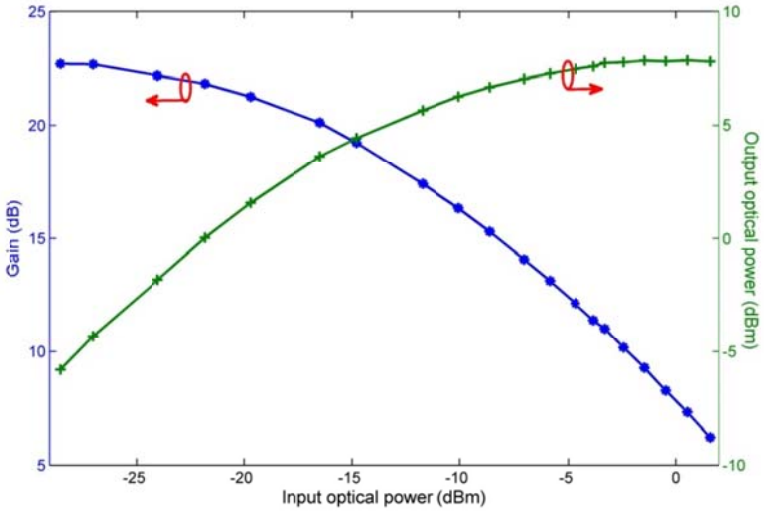

Fig. 3.3. The gain characteristic of the RSOA biased at 80 mA.

Since we focus on the performance characterization of the directly modulated self-seeded RSOAs, only the upstream transmission performance of the WDM-PON system is investigated and the experimental setup is shown in Fig. 3.4. The RSOA is directly modulated with a 1.25-Gb/s NRZ pseudo-random binary sequence (PRBS). The output signal of the self-seeded RSOA is fed to an optical coupler after passing through the distribution fiber and the wavelength multiplexer. As shown in Fig. 3.4, the incident power of the optical coupler is split into two portions. One portion, P_r, is reflected by the FRM to continuously feed the directly modulated RSOA while the other portion, P_t, is transmitted over a 20-km SSMF and detected by a 1.25-Gb/s APD receiver in the OLT. The coupling ratio of the optical coupler is defined as P_r/P_t.

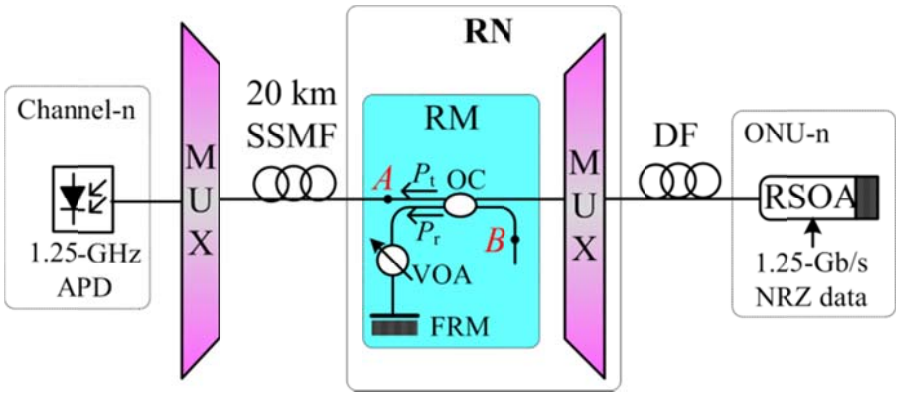

Fig. 3.4. Experimental setup for investigating the transmission performance of the directly modulated self-seeded RSOA. DF: Distribution Fiber; MUX: Multiplexer.

Two 1×4 flat-top wavelength multiplexers (3-dB bandwidth is 0.6 nm and insertion loss is 4 dB) are employed in the experiments. Since the wavelength multiplexer used in our experiments are not cyclic, a variable optical attenuator (VOA) is inserted inside the cavity to emulate the loss of the BPF in Fig. 3.1. The loss of the self-seeding cavity and the seeding power to the RSOA can be adjusted by tuning the VOA. The seeding power is defined as the optical power fed into the RSOA. Therefore, we can estimate the stable

seeding power, which is the seeding power to the RSOA when the stable lasing is established, by measuring the optical power at point 'B', the coupling ratio of the optical coupler, and the insertion losses of the multiplexer and distribution fiber. The power of the transmitted signal from the RN to the OLT, P_t, could be measured at point 'A'.

3.1.2 Analysis of polarization evolution in self-seeding scheme

The nonzero PDG of RSOAs results in instability of the self-seeding operation. In [105], the authors demonstrated that the system performance of a self-seeded RSOA with a low PDG could be stabilized by employing a 90° FRM as the RM in the RN. In this subsection, the polarization evolution in the self-seeding cavity is analyzed and illustrated graphically. It explains how a 90° FRM could help to stabilize the system performance of a self-seeded RSOA with a low (1~2 dB) or much higher (20 dB) PDG.

Fig 3.5 shows the experimental setup to investigate the polarization evolution in the self-seeding scheme. An inline polarimeter is inserted in the self-seeding cavity to measure the state of polarization (SOP) and degree of polarization (DOP) of the self-seeded RSOA output. A 90° FRM is employed as the reflection module. A bandpass filter is used to simulate the AWG in the RN. Besides, a 1-km SMF and a polarization controller (PC) are inserted in the self-seeding cavity.

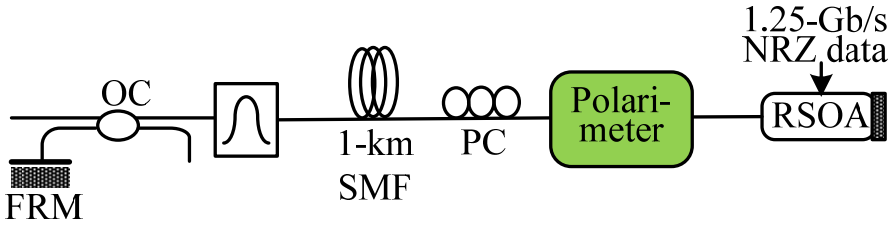

Fig. 3.5. Experimental setup to measure the SOP and DOP of the self-seeded RSOA output.

Fig. 3.6 illustrates the polarization evolution in the self-seeding cavity with a self-seeded low-PDG RSOA. For the RSOA with a low PDG, the output of the self-seeded RSOA always consists of two orthogonal polarization beams with comparable powers. Due to the small nonzero PDG of the RSOA, one polarization mode (e.g. TE mode) is a bit stronger than the other (TM mode). The FRM simply provides 90° rotation of polarization to the reflected light (②) with respect to the incoming light (①). As a result, the incoming TE becomes TM and the incoming TM becomes TE after reflection. Therefore, the resultant TM is now a bit stronger than the resultant TE. When the light travel from 'P' to 'Q', the two polarizations experience same cavity loss (including the insertion losses of various components in the self-seeding cavity) but the RSOA provides slightly larger gain for the TE mode, therefore TE and TM become comparable in power (③).

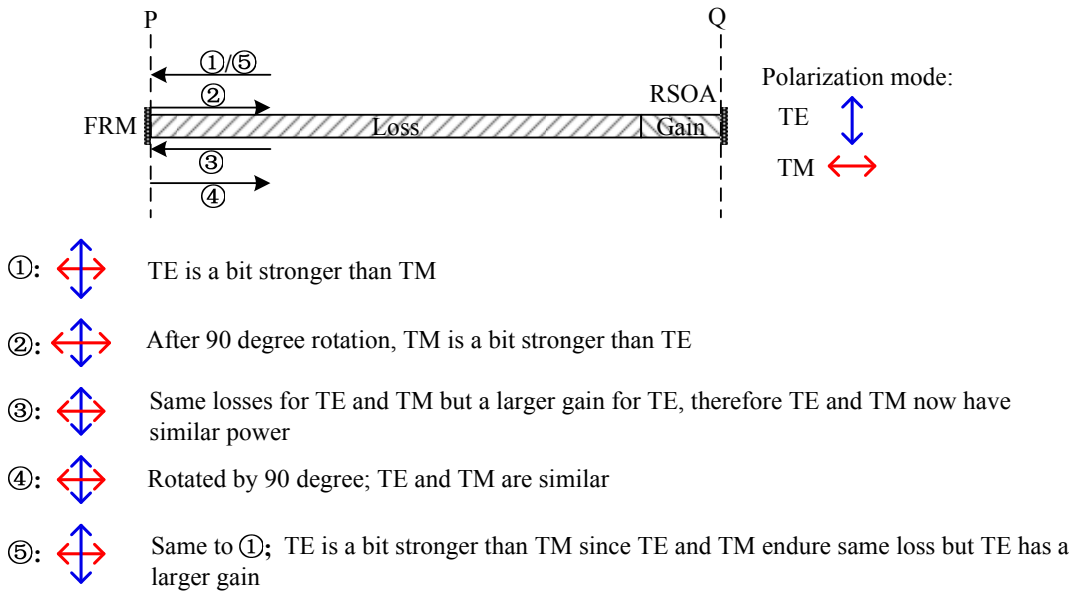

Fig. 3.6. Analysis of polarization evolution in the self-seeding cavity with a low-PDG RSOA.

Because of the coexistence of the two orthogonal polarizations, the DOP measured by the inline polarimeter is small (~10%). Self-seeding could be established in both polarizations. In fact, no matter whether a FRM or a simple fiber mirror is used, self-seeding operation could always be built due to the considerable gain in both TE and TM.

Fig. 3.7 illustrates the polarization evolution in the self-seeding cavity with a self-seeded high-PDG RSOA. For a RSOA with high PDG, the output is dominated by one polarization, e.g. TE (①). The DOP measured by the inline polarimeter is near 100%. After being reflected by the FRM, the polarization direction is changed to TM (②). When the light travels to 'Q', it is simply reflected back by the RSOA without being amplified since it is perpendicular to the polarization direction which the RSOA favors. Therefore, the power is reduced significantly when it arrives at 'P' (③) due to the cavity loss. The light is again reflected by the FRM with 90° polarization rotation and turns to TE-polarized (④). When it travels to 'Q', it obtains a large gain provided by the RSOA. In short, the light could only be amplified by the RSOA once after it is circulated in the cavity twice. That is to say, the self-seeding operation could be established when the gain provided by the RSOA is larger than twice of the cavity loss.

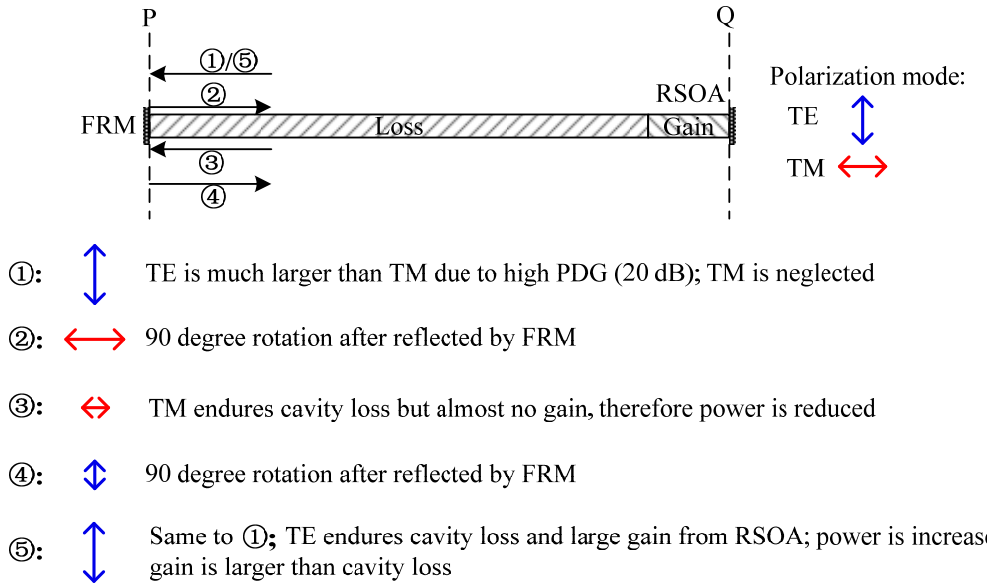

Fig. 3.7. Analysis of polarization evolution in the self-seeding cavity with a high-PDG RSOA.

One method enabling stable self-seeding operation with a high-PDG RSOA is to insert a 45° Faraday rotator before the RSOA, as proposed in [155]. The light would be rotated by a 90° in total through propagating the FR in the forward and reserve direction in one loop. By inserting an additional FR in the self-seeding cavity, the light would acquire gain in each loop. Self-seeding operation could be established as long as the RSOA gain is larger than the cavity loss.

For RSOAs with a low PDG, a Faraday rotator mirror and a simple fiber mirror bring little difference in establishing the self-seeding operation. However, when a fiber mirror is adopted, the BER would change dramatically by rotating the PC, which emulating the possible polarization perturbation in the cavity. Instead, a FRM would bring a more stable BER performance.

For RSOAs with a high PDG, as long as the RSOA gain is larger than twice of the cavity loss, self-seeding operation could be established. An open eye could be observed

when a FRM is adopted no matter how to rotate the PC in the cavity. However, the open eye would become completely close by rotating the PC to some positions when a FM is adopted. This demonstrates that employing a FRM as the reflection module can make a self-seeding scheme insensitive to the polarization perturbation for both low- and high-PDG RSOAs.

3.1.3 Simulation of the self-seeding establishment

The gain characteristic of the RSOA used in the experiment could be extracted by fitting the discrete measured values at different seeding powers, as shown in Fig. 3.8. The insertion losses of all the components in the self-seeding cavity including the wavelength multiplexer, the optical coupler (90/10), and the FRM are measured individually. Therefore, the cavity loss could be estimated.

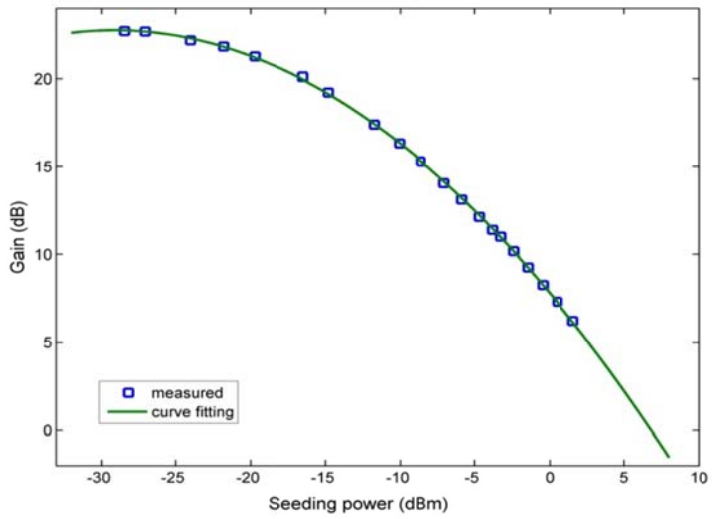

Fig. 3.8. Curve fitting of the gain characteristic of the RSOA.

The establishing of the self-seeding operation could be simulated with the known RSOA gain characteristic and the cavity loss. The initial seeding power could be measured in an open self-seeding cavity as illustrated in Fig. 3.9. An optical circulator is

inserted before the RSOA and disrupts the closed cavity. The initial seeding power could be measured at point 'C' shown in Fig. 3.9. When the RSOA is biased at 80 mA, the initial seeding power is measured to be -22.1 dBm.

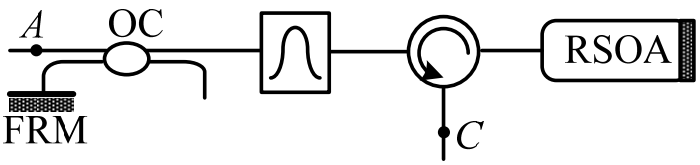

Fig. 3.9. Measurement of the initial seeding power.

Fig. 3.10 gives the simulated power evolution in the establishment of self-seeding operation. It shows that self-seeding operation becomes stable only after the light circulates in the cavity for five loops. At the beginning, the initial seeding power is low and the gain provided by the RSOA is high. Consequently, the gain is larger than the cavity loss and therefore the seeding power is increased in the next loop. As a result, the RSOA gain is dropped due to the increased seeding power. After around five loops, the RSOA output power and the seeding power become stable when the gain provided by the RSOA equals to the cavity loss. As shown in Fig. 3.10, the stable seeding power is about -3.5 dBm which could drive the RSOA into the deep gain saturation region. Since stable self-seeding operation could be established after the light is circulated in the cavity for a few loops, the establishment of stable self-seeding operation would take up to one microsecond considering that the cavity length is usually several kilometers long.

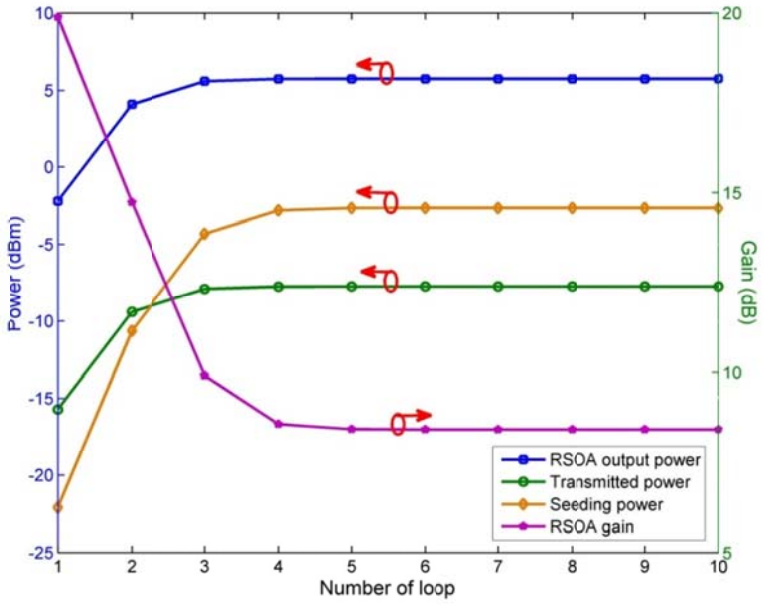

Fig. 3.10. Power evolution in the self-seeding establishment.

3.1.4 Analyses of transmission performances

The influences of several system parameters on the transmission performance of the directly modulated self-seeded RSOAs are investigated and analyzed. In each of the following subsections, the impact of one parameter is studied while other parameters are kept unchanged to exclude their influences. To make the description succinct, the values of related system parameters in each subsection are summarized in Table 3.1.

Table 3.1. Related experimental parameters in each subsection.

Subsection	Stable seeding power	Coupling ratio	Mux type & bandwidth	Cavity length	Attenuation of VOA	Transmission distance
3.1.4.1	-10.0 dBm	90/10	Flat-top & 0.6 nm	1 km	3 dB	20 km
	varied	90/10	Flat-top & 0.6 nm	1 km	varied	20 km
3.1.4.2	varied	varied	Flat-top & 0.6 nm	1 km	3 dB	20 km
3.1.4.3	-10.7 dBm	90/10	varied	1 km	3 dB	varied
3.1.4.4	-10.0 dBm	90/10	Flat-top & 0.6 nm	varied	varied	20 km

3.1.4.1 Impact of ER, seeding power, and pattern length

Since the RSOA is directly modulated with the upstream data, the reflected seeding light that continuously feeds the RSOA is also modulated. However, thanks to the high-pass characteristic of the RSOA operating in the saturation region [35], the modulation on the seeding light, especially the low-frequency components, could be suppressed to some degree and therefore error-free transmission (defined as bit error rate (BER) < 10^{-9}) of the directly modulated self-seeded RSOAs could be achieved. Nevertheless, the transmission performance of the directly modulated self-seeded RSOAs is sensitive to the ER of the RSOA output signal. This is because a low ER will degrade the upstream receiver sensitivity and may fail the error-free transmission, whereas a high ER will increase the remodulation crosstalk and jeopardize the self-seeding operation due to the inadequate seeding power during the spaces (binary "0"s) of the modulated seeding light. Therefore, there exists an optimal ER which results in the best transmission performance.

The attenuation of the VOA is tuned to be 3.0 dB to simulate the insertion loss of the BPF in the RM in Fig. 3.1. Fig. 3.11 (a) shows the upstream receiver sensitivities at a BER of 10^{-9} under different ERs of the upstream signal. The best upstream receiver sensitivity is measured to be -31.5 dBm when the ER is 5.8 dB. Based on the power measured at point 'B' in Fig. 3.4, the stable seeding power is calculated to be -10.0 dBm, which could drive the RSOA into the saturation region. The inset in Fig. 3.11 (a) shows the eye diagram with the optimal ER. When the ER is larger than 7.5 dB, a BER of 10^{-9} could not be achieved due to the unacceptable remodulation crosstalk.

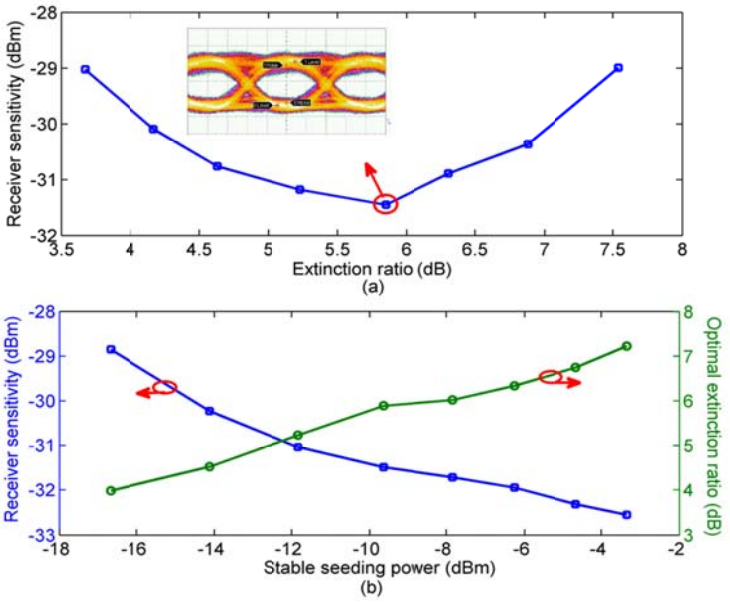

Fig. 3.11. (a) The upstream receiver sensitivity at a BER of 10^{-9} as a function of the signal extinction ratio; (b) the optimal extinction ratio and the corresponding receiver sensitivity as a function of the stable seeding power.

The seeding power determines to what extent the modulation on the seeding light can be suppressed by the RSOA. This is because as the seeding power increases, the RSOA will be driven into deeper saturation region. The impact of the stable seeding power on the optimal ER is investigated. The loss of the self-seeding cavity could be varied by tuning the VOA. Since the gain of the RSOA should equal to the cavity loss when the stable self-seeding is established, a higher cavity loss corresponds to a higher RSOA gain which implies a lower stable seeding power.

In the experiments, the attenuation of the VOA is varied from 0 to 6 dB. The corresponding stable seeding power is reduced from -3.3 to -16.6 dBm. Fig. 3.11 (b) illustrates how the optimal ER and the corresponding receiver sensitivity are affected by the stable seeding power. The optimal ER increases with the stable seeding power and meanwhile the corresponding receiver sensitivity is improved from -28.8 to -32.5 dBm. It

could be explained that the increase in the stable seeding power would drive the RSOA into deeper saturation which in turn suppresses stronger modulation on the seeding light. Further increase in the attenuation of the VOA would fail the error-free transmission resulting from the increased remodulation crosstalk and would eventually lead to the failure of initiating the self-seeding operation.

For the transmission system employing the remodulation technique in which the upstream OOK data are overlaid onto the downstream OOK data, the upstream transmission performance will be affected by the downstream ER as well as the downstream pattern length [87, 116]. The transmission system based on the directly modulated self-seeded RSOAs may also suffer the same problems since the output of the directly modulated RSOA self-seeds itself and the modulated seeding light is remodulated with the subsequent upstream data.

Next, the pattern dependence of the directly modulated self-seeded RSOAs is studied by increasing the PRBS pattern length from 2^7-1 to 2^{31}-1 and the ER is readjusted to optimize the transmission performance. As shown in Fig. 3.12, the receiver sensitivity at a BER of 10^{-9} is degraded by 1.2 dB when the pattern length is increased from 2^7-1 to 2^{31}-1. The corresponding optimal ER is reduced from 6.0 to 4.9 dB. To demonstrate that the pattern dependence observed in the directly modulated self-seeded RSOA is not induced by device imperfection, the transmission performances of the CW-seeded RSOA are also plotted in Fig. 3.12. Negligible power penalties are observed when the pattern length is increased. Hence, the pattern dependence is an intrinsic characteristic of the directly modulated self-seeded RSOA-based systems and the signal ER should be decreased to accommodate a long PRBS.

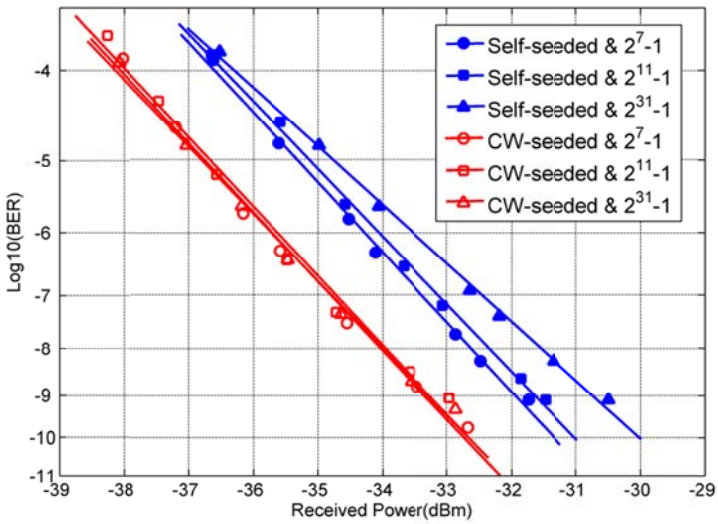

Fig. 3.12. Pattern dependences of the directly modulated self-seeded RSOAs and continuous-wave-seeded RSOAs.

Pattern dependence originates from remodulation crosstalk as it is also observed in wavelength-remodulated WDM-PONs in which the downstream signal adopts intensity modulation. A longer PRBS pattern contains longer continuous marks (bit "1") or spaces (bit "0"), which corresponds to more frequency components existing within the same frequency range. The high-pass characteristic of a saturated RSOA will remove the low frequency components in the seeding light to some degree but for a longer pattern the remaining low frequency components would be definitely stronger than that of a shorter pattern. Therefore, more residual remodulation crosstalk is induced by a longer PRBS pattern and the BER performance of the self-seeded RSOA is degraded. The signal ER is a critical parameter considering the trade-off between the remodulation crosstalk and signal detection. The ER is adjusted to optimize the BER of the self-seeded RSOA when the pattern length is increased. In order to compensate for the increased remodulation crosstalk, the ER can be decreased but a smaller ER is negative for signal detection. And it is found that the optimal ER drops for a longer PRBS pattern. This means that the

overall effect of a reduced ER can alleviate the BER degradation induced by a longer PRBS pattern.

3.1.4.2 Impact of the coupling ratio

The coupling ratio of the optical coupler in the RM determines the loss of the self-seeding cavity and the link loss for upstream transmission. In this subsection, the 90/10 optical coupler is replaced by a variable-ratio optical coupler. The attenuation of the VOA is fixed at 3.0 dB. The losses of the self-seeding cavity and upstream transmission link are varied by tuning the coupling ratio. The dependences of the upstream receiver sensitivity and the transmitted power from the RN, P_t, on the coupling ratio P_r/P_t are depicted in Fig. 3.13. The power budget shown in Fig. 3.13 is the power difference between the transmitted power from the RN, P_t, and the upstream receiver sensitivity.

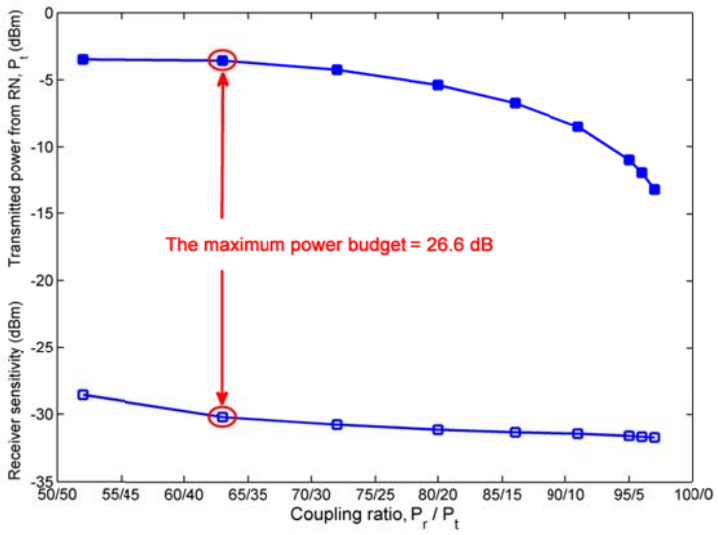

Fig. 3.13. The upstream receiver sensitivity and the transmitted power from the RN as a function of the coupling ratio of the optical coupler.

Since the cavity loss decreases with the increase in the coupling ratio and hence the stable seeding power increases with the coupling ratio, the upstream receiver sensitivity

is improved as the coupling ratio increases considering the enhanced suppression of the modulation on the seeding light by the saturated RSOA. However, as shown in Fig. 3.13, the improvement of the receiver sensitivity slows down when the coupling ratio reaches 80/20. Further increase in the coupling ratio does not bring a significant improvement of the upstream receiver sensitivity since the RSOA has been already in deep saturation, but it reduces the transmitted power P_t remarkably as the loss of the upstream transmission link is increased significantly. Meanwhile, error-free transmission cannot be achieved when the coupling ratio is smaller than 50/50 due to the high cavity loss.

The experimental results show that the power budget for upstream transmission reaches its maximum value, i.e., 26.6 dB, when the coupling ratio is around 63/37. Considering the link loss after the RN, including the insertion losses of the 20-km SSMF feeder fiber, the CWDM, and the AWG in the OLT, a considerable power margin is guaranteed. The optimal coupling ratio shall be determined by both the gain properties of the RSOA and the insertion losses of other passive components within the self-seeding cavity.

3.1.4.3 Impact of the wavelength multiplexer

The wavelength multiplexer located in the RN acts as a filter for each upstream wavelength channel. It spectrum-slices the output of the RSOAs and determines the shape and bandwidth of the seeding light. The influences of the filter characteristics, including the 3-dB bandwidth and the shape factor, on the upstream receiver sensitivity are studied in this subsection. A programmable optical processor (Finisar WaveShaper) whose bandwidth and shape factor could be varied flexibly was utilized to simulate one channel of the wavelength multiplexer [156]. The insertion loss at the central wavelength

of the programmable filter remains unchanged when its bandwidth or shape factor is varied. Hence, the cavity loss or the stable seeding power stays almost the same and its impact on the receiver sensitivity could be excluded. The stable seeding power is calculated to be about -10.7 dBm.

Two most common passbands, flat-top and Gaussian-shaped, are studied and their 3-dB bandwidths are varied. The various spectra of the filter passbands and the corresponding output spectra of the directly modulated self-seeded RSOAs measured at point 'A' are depicted in Fig. 3.14. As shown, the 3-dB spectral width of the directly modulated self-seeded RSOA is much narrower than the 3-dB bandwidth of the corresponding filter. The most notable feature of the spectra is that the peak of the RSOA output is shifted to a longer wavelength with respect to the center wavelength of the corresponding filter. This is because of the self-phase modulation caused by the carrier-induced index change in the RSOA [107, 157]. The self-phase modulation results in frequency chirp which is imposed on the seeding light. Since the frequency chirp is negative, the center frequency of the seeding light is downshifted (the red shift).

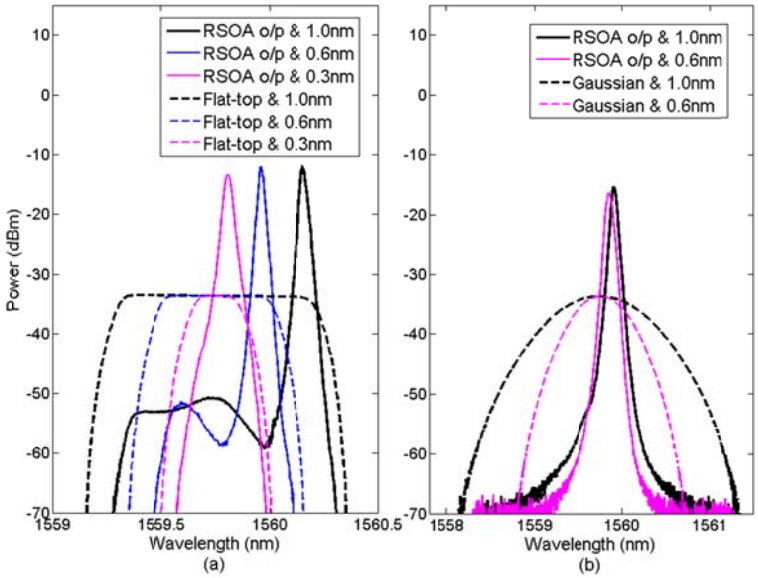

Fig. 3.14. Optical spectra of the directly modulated self-seeded RSOAs and the corresponding filters with (a) a flat-top passband and (b) a Gaussian-shaped passband.

For the case of the flat-top passband, the peak of the output spectrum is drifted closely to the upper cut-off wavelength of the filter passband due to the even attenuation within the passband; for the case of the Gaussian-shaped passband, the peak of the output spectrum stays closely to the central wavelength of the filter since the incremental attenuation from the central wavelength to the cut-off wavelength within the passband prohibits farther drifting. The peak of the RSOA output is locked to the longer wavelength at which the attenuation of the corresponding filter is increased by 0.1~0.3 dB compared to the filter center.

The back-to-back receiver sensitivities at a BER of 10^{-9} of the directly modulated self-seeded RSOA are plotted in Fig. 3.15 when the 3-dB bandwidth of the flat-top or Gaussian-shaped filter is varied from 0.2 to 1.5 nm. Since the WaveShaper is utilized as the wavelength multiplexer in the RN, there is no matched wavelength demultiplexer in the OLT. Hence, the back-to-back receiver sensitivity is measured at the point "*A*" in Fig.

3.4 without considering the potential power penalty induced by the filtering effect of the wavelength demultiplexer in the OLT. This power penalty would be similar to the value obtained in Subsection 3.1.2.1 where it is measured to be 0.5 dB when two 1×4 wavelength multiplexers are employed.

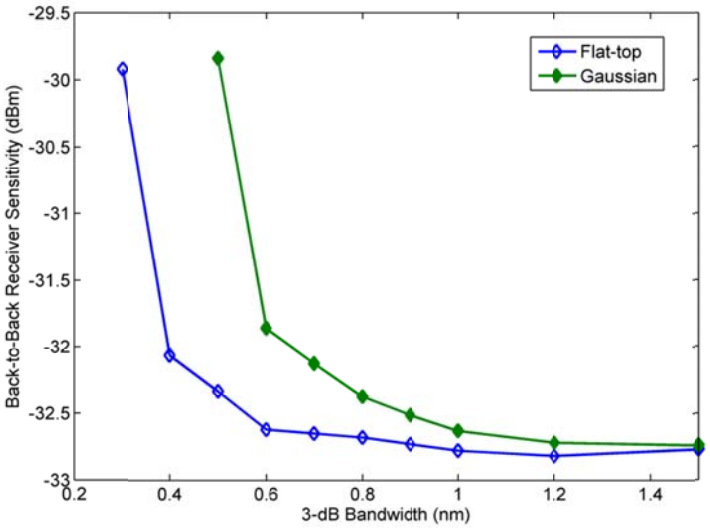

Fig. 3.15. The back-to-back receiver sensitivity as a function of the 3-dB bandwidth of the flat-top and Gaussian-shaped filters.

As shown in Fig. 3.15, the 3-dB bandwidth of the flat-top and Gaussian-shaped filters has a significant effect on the upstream receiver sensitivity. The BER performances are degraded as the filter bandwidths decrease. The two filter shapes bring comparable performance when the 3-dB bandwidth is larger than 1.0 nm. As the filter bandwidth decrease, the flat-top filter outperforms the Gaussian-shaped filter. The self-seeding operation could not be initiated when the 3-dB bandwidths of the filters are smaller than certain values due to the low initial seeding powers, e.g. for the flat-top filter, a BER of 10^{-9} could not be achieved when the bandwidth is smaller than 0.3 nm whereas it is measured to be 0.5 nm for the Gaussian-shaped filter. As demonstrated by the optical spectra in Fig. 3.14, a reduced filter bandwidth causes an increase in the 3-dB bandwidth

of the self-seeded RSOA output and hence an increased dispersion effect of the upstream signal after transmission. Therefore, the BER performance is degraded when the filter bandwidth is reduced.

Fig. 3.16 shows how the transmission performance of the directly modulated self-seeded RSOA is degraded as the transmission distance is extended. When the flat-top filter with a 3-dB bandwidth of 0.6 nm is adopted, the receiver sensitivities are -32.1 dBm and -31.0 dBm after 20 and 50-km transmission, respectively. Compared to the back-to-back performance, the respective dispersion-induced power penalties are around 0.5 dB and 1.6 dB. When the Gaussian-shaped filter with a 3-dB bandwidth of 0.6 nm is adopted, an error floor at 10^{-9} is observed after transmission over 50 km.

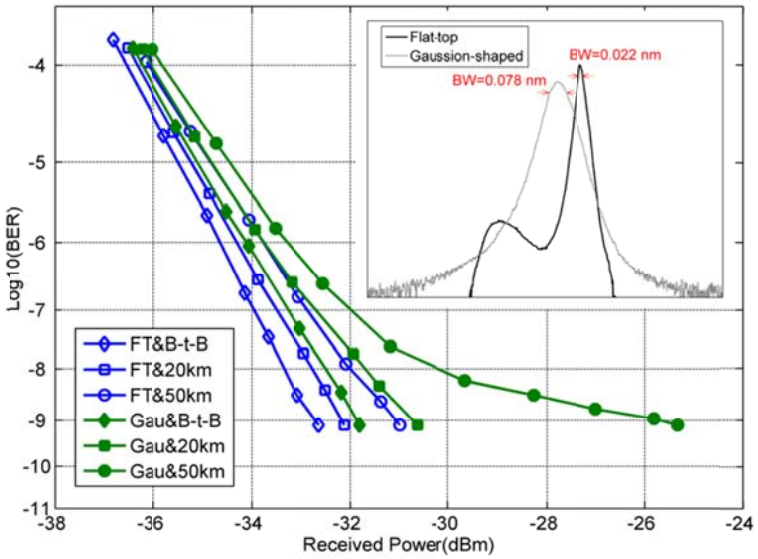

Fig. 3.16. The transmission performances with different transmission distances. The inset shows the measured optical spectra of the self-seeded RSOA when either the flat-top or Gaussian-shaped filter with a 3-dB bandwidth of 0.6 nm is employed.

The inset in Fig. 3.16 depicts the optical spectra of the RSOA output when the flat-top and Gaussian-shaped filters with a 3-dB bandwidth of 0.6 nm are employed. The narrower 3-dB bandwidth of the RSOA output when the flat-top filter is adopted might

explain the better transmission performance compared to the one with the Gaussian-shaped filter. Based on these observations, we can conclude that a flat-top passband is a desirable feature for the AWG used in the self-seeding scheme. The inferior performance of the Gaussian-shaped filter might be attributed to the contradiction between the red-shifted peak of the self-seeding RSOA output and the incremental attenuation from the filter center to longer wavelength.

3.1.4.4 Impact of the length of self-seeding cavity

Since the reflection module is located in the RN, the length of the self-seeding cavity, defined as the distance between the reflection module in the RN and the rear facet of the RSOA, could be several kilometers long considering the length of the distribution fiber connecting the RN and ONUs in typical WDM-PONs. In the following analysis, the cavity length is varied from meters to kilometers by adopting different lengths of the distribution fibers and its impact on the transmission performance of the directly modulated self-seeded RSOAs is studied.

The VOA is tuned to keep the cavity loss unchanged when the length of the distribution fiber is varied. The stable seeding power is kept at around -10.0 dBm. The ER is readjusted to optimize the transmission performance after the length of the distribution fiber is changed. Fig. 3.17 shows the upstream transmission performances with various lengths of the distribution fiber. The experiment results indicate that the transmission performance of the directly modulated self-seeded RSOA is deteriorated by extending the length of the self-seeding cavity. The receiver sensitivity is -31.5 dBm at a BER of 10^{-9} when the length of the distribution fiber is 1 km. It is degraded by 1.8 dB

when the distribution fiber is increased to 2 km. An error floor at a BER of 10^{-9} is observed when the distribution fiber is extended to more than 4 km.

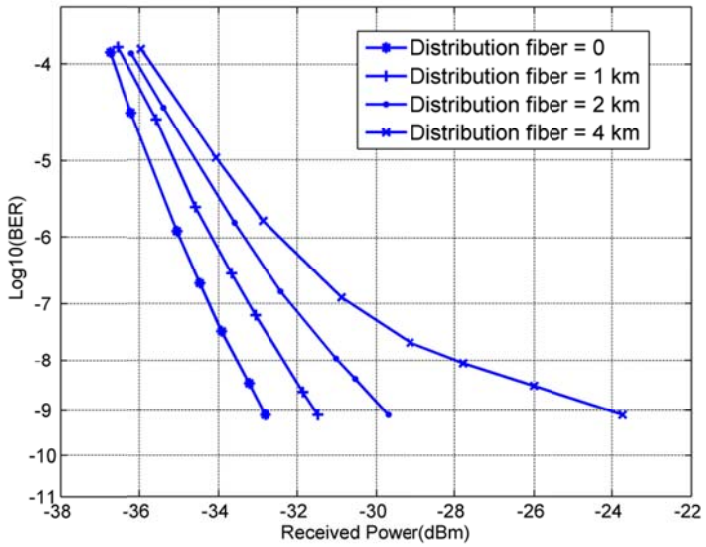

Fig. 3.17. The transmission performances with different distribution fiber lengths.

The reason of the performance degradation induced by extending the cavity length is investigated by measuring the electrical spectrum of the self-seeded RSOA output. Fig. 3.18 shows the electrical spectra of the self-seeded RSOA output over a frequency span of 10 MHz. The high peak at 9.84 MHz is the first spectral line resulting from the direct modulation with a 2^7-1 PRBS (spectral line spacing = (bit rate) / (pattern length) = 9.84 MHz) [158]. Besides the spectral lines resulted from direct modulation, the beat frequency between the longitudinal modes associated with the length of the self-seeding cavity is also observed. The longitudinal mode spacing can be calculated as $\Delta\upsilon = \frac{c}{2nL}$, where n is the fiber refractive index and L is the distance between the two mirrors (i.e., the FRM and the rear facet of RSOA).

When there is no additional distribution fiber in the self-seeding cavity, the mode spacing is measured to be around 6.202 MHz. The cavity length is therefore 16.6 m approximately, which is composed of fiber pigtails of various components in the cavity. When a 50-m distribution fiber is added, the mode spacing is reduced to 1.552 MHz. And it is further decrease to 0.096 MHz when the distribution fiber is about 1-km long.

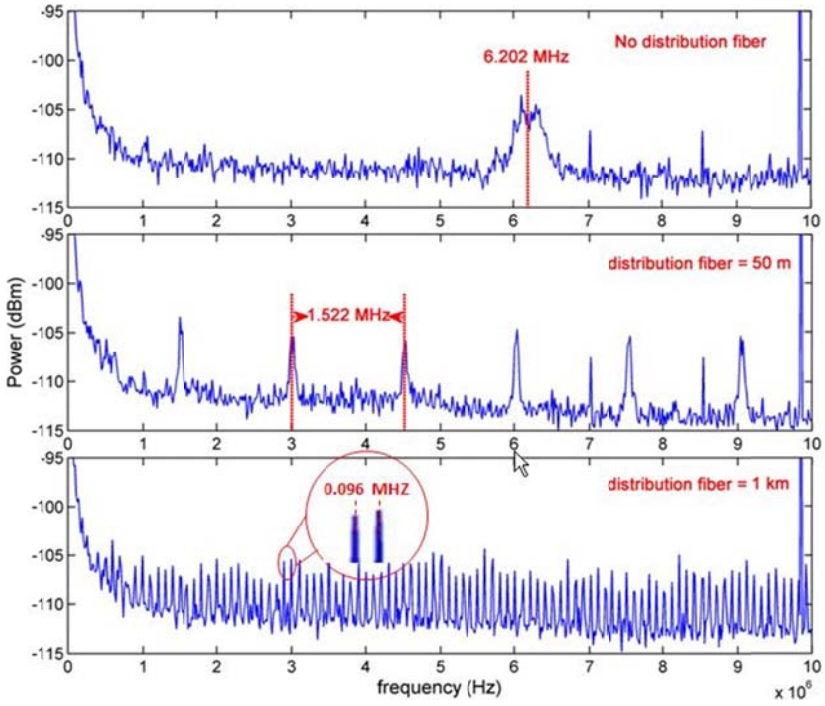

Fig. 3.18. Electrical spectra of the self-seeded RSOA with different lengths of distribution fibers.

The longer the cavity length, the smaller the frequency spacing between two adjacent longitudinal modes. As a result, more beating noise falls in the baseband after the detection. As mentioned in [107], the degradation of the transmission performance could be attributed to the increased beating noise generated by the multiple longitudinal modes associated with the length of the self-seeding cavity.

Another interesting fact observed from measuring the electrical spectrum is that the beating noise generated by the longitudinal modes could be suppressed by imposing

direct modulation on the self-seeded RSOA. For example, Fig. 3.19 shows the measured electrical spectra of the self-seeded RSOA output with and without direct modulation when the distribution fiber is 1-km long. The magnitudes of the beating frequencies are obviously suppressed with direct modulation.

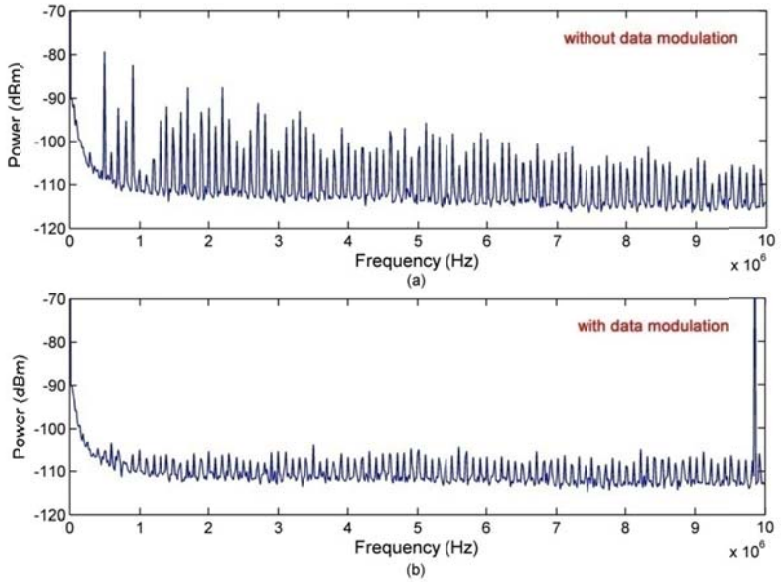

Fig. 3.19. Electrical spectra of the self-seeded RSOA (a) without and (b) with direct modulation.

The external pressure or temperature fluctuations will slightly change the cavity length and therefore induce phase perturbation to the light propagating in the self-seeding cavity. To investigate whether the system performance is sensitive to the phase perturbation induced by the imperceptible change in the cavity length, a tunable optical delay line (ODL) is inserted between the RSOA and the distribution fiber. The VOA is varied to keep the cavity loss unchanged. The ODL is tuned manually by a rotary knob with a resolution of 318 micrometers per turn. In the experiment, the received power is fixed at -31.0 dBm and the BER is recorded for each 10° rotation of the ODL knob, which approximately corresponds to a change of 8.83 micrometers in the cavity length.

As shown in Fig. 3.20, the BER fluctuates slightly around the BER of 10^{-10}, which indicates that the transmission performance of the directly modulated self-seeded RSOAs is robust against the phase perturbation to the light circulated in the self-seeding cavity.

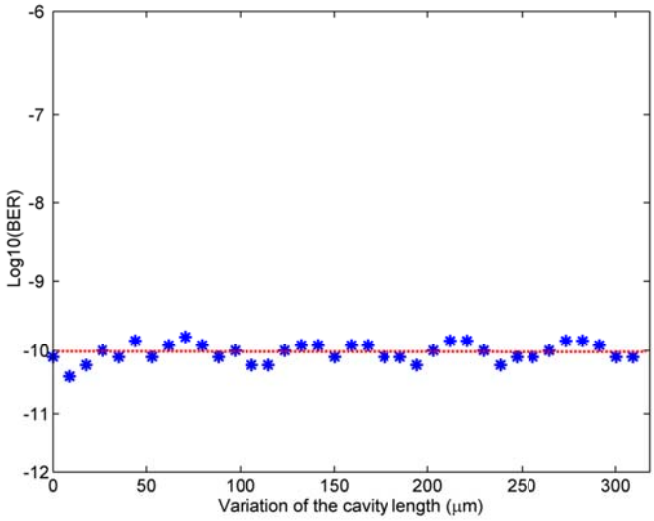

Fig. 3.20. The measured BER at a fixed received power of -31 dBm as a function of the minute variation in the cavity length.

3.2 A low-cost WDM-PON based on self- and remote-seeded RSOAs with enhanced bit rate

Similar to other RSOA-based transmission systems, the data rate that can be supported by the directly modulated self-seeded RSOAs is restricted by the limited electrical bandwidth of the RSOAs. As summarized in Section 2.1.2.2, several techniques including electronics equalization, detuned optical filtering, and high-order modulation formats have been demonstrated to enhance the data rate of directly modulated CW-seeded RSOA-based systems. Some of these techniques are only applicable to coherent signals and therefore ineffective to increase the bit rate of self-seeded RSOA whose output has a low degree of coherence. In this section, the bit rate of a directly modulated self-seeded

RSOA is increased by boosting the seeding power as well as employing off-line electronic equalization. A low-cost WDM-PON system whose downlink is based on self-seeded RSOAs with enhanced bit rate and uplink is based on remote-seeded RSOAs is investigated and experimentally demonstrated.

3.2.1 Bit rate enhancement by increasing the seeding power

The modulation bandwidth of a RSOA could be enhanced by external seeding and it increases with the external seeding power. As shown in Fig. 3.21, the 3-dB bandwidth of a free-running RSOA is 0.57 GHz. When it is fed by an external seeding light with a power of -15 dBm, the 3-dB bandwidth is increased to 0.63 GHz. The 3-dB bandwidth is further enhanced to 0.95 GHz when the seeding power is -10 dBm.

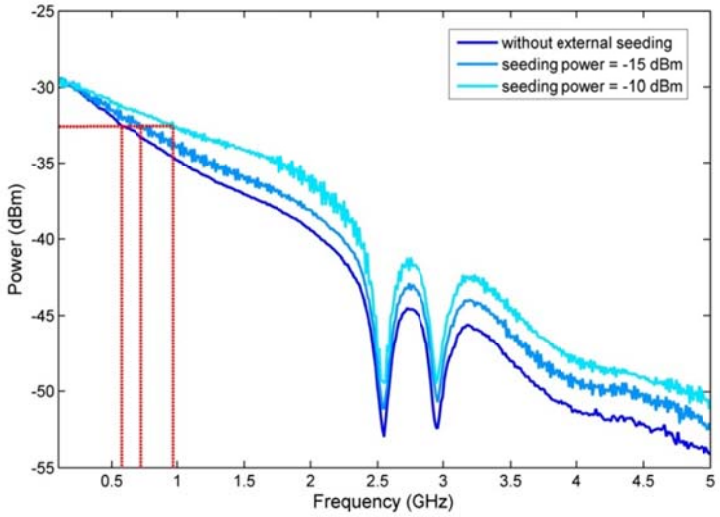

Fig. 3.21. Frequency response of the RSOA with and without external seeding.

This feature is not exploited to increase the bit rate of the remote-seeded RSOAs since increasing the remote seeding light power would inevitably enhance the RBS-induced crosstalk. As a result, the transmission performance would be degraded.

However, this feature can be utilized in the self-seeding scheme in which RBS is avoided by removing the remote seeding light.

The self-seeding schemes with two different refection modules are shown in Fig. 3.22. The RSOA is biased at 80 mA and directly modulated with 2.5-Gb/s NRZ PRBS. The filter inside the cavity for selecting the circulated wavelength spectrum is a 1×4 wavelength multiplexer with 0.6-nm 3-dB-bandwidth flat-top passbands. The coupling ratio of the optical coupler is 90/10 where 90% of the light entered into the coupler is reflected by reflection modules. In order to boost the stable seeding power to the RSOA, the FRM is replaced by a reflection module composed of an optical circulator and an EDFA, as shown in Fig. 3.22 (b).

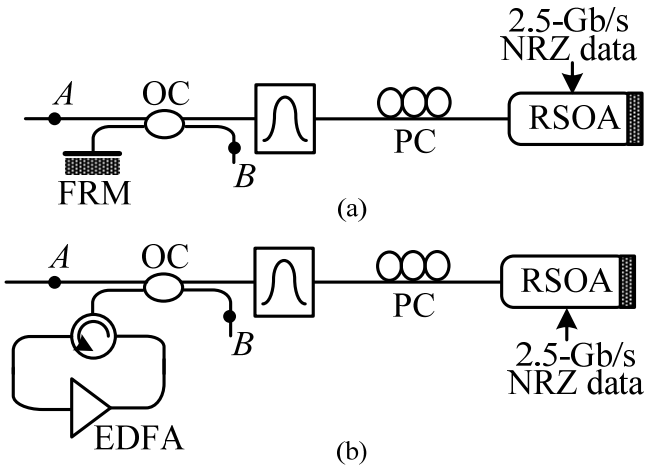

Fig. 3.22. Self-seeding with two different reflection modules; (a) Structure I based on a FRM and (b) Structure II based on a circulator.

When stable self-seeding is established, the gain and loss in the cavity become equal. For Structure I, it has $loss_1 = gain_1^{RSOA}$; while for Structure II, the equation becomes $loss_2 = gain_2^{RSOA} + gain_2^{EDFA}$. Since the cavity losses of the two structures are similar, the fact that the gain is partially contributed by the EDFA in Structure II would result in

$gain_2^{RSOA} < gain_1^{RSOA}$. That is to say, the stable seeding power in Structure II is larger than that in Structure I. This can be also demonstrated by measuring the power at point 'B' in Fig. 3.22. After self-seeding is established, the power at point 'B' is measured to be -7.5 dBm in Structure I while it is -3.0 dBm in Structure II when the pumping current of the EDFA is 120 mA. Therefore, the seeding power is approximately 4 dB higher with the presence of an additional EDFA in the cavity.

The BER measurement is carried out when the data rate is 2.5 Gb/s. For Structure II, the receiver sensitivity at a BER of 10^{-9} without transmission is -29.2 dBm as shown in Fig. 3.23. After 20-km transmission, the BER performance is degraded by the chromatic dispersion and the receiver sensitivity at a BER of 10^{-9} is reduced to -24.9 dBm. However, with Structure I a BER < 10^{-9} cannot be achieved even at the back-to-back condition. An error floor at around 10^{-6} is observed.

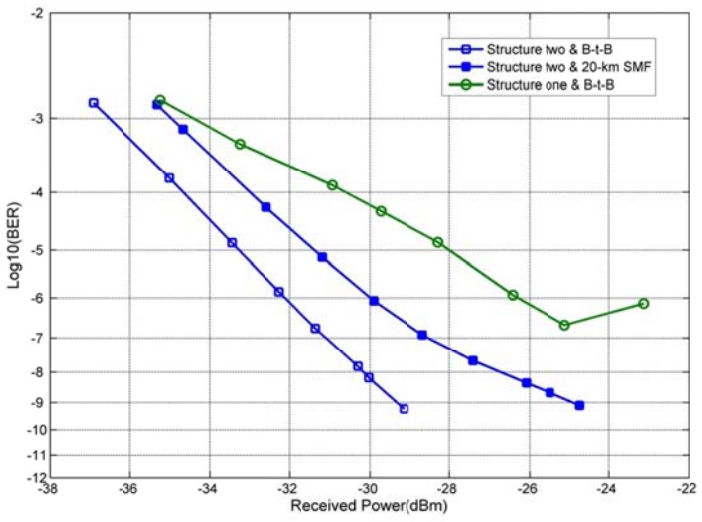

Fig. 3.23. The BER performances of the self-seeded RSOA in Structure I and II.

Based on the above results, we can conclude that increase of the seeding power by employing an additional optical amplifier in the self-seeding cavity can improve the

modulation bandwidth of the corresponding RSOA and therefore enable direct modulation of the self-seeded RSOA with a higher bit rate. This scheme may not be suitable for uplink which is based on self-seeded RSOAs in ONUs since the remote node is no longer passive due to the presence of an active optical amplifier in the reflection module. However, this scheme could be applied in the OLT for downstream transmission.

3.2.2 Bit rate enhancement by electronic equalization

It has been widely demonstrated that electronic equalization could compensate the limited bandwidth of RSOAs so that the bit rate of RSOAs seeded by coherent CW light can achieve 10 Gb/s or even higher [48, 50, 51]. The frequency response of a RSOA exhibits a smooth roll-off without a relaxation oscillation peak while its modulation has a good linearity. These properties are ideal for the electronic equalization using the decision feedback equalizer consisting of feed-forward and feedback filters.

The idea behind equalization is to use the voltage levels of the other bits to correct the voltage level of a given bit [159]. A feed-forward equalizer is the simplest structure and the most cost-effective solution, which is shown in Fig. 3.24. It is given by the sum of the voltage levels of the bits received prior to the bit of interest multiplied by correction factors. It is linear and only uses information from previously received bits. The limitation of a FFE can be improved by introducing a delay so that both previous and current bits can be used in the correction.

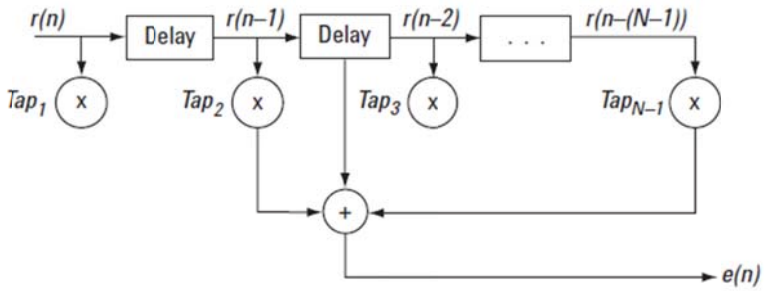

Fig. 3.24. The structure of a (N-1)-tap feed-forward equalizer [159].

.

A DFE uses a feedback loop of the digital signal after it has been decoded from the output of a FFE. The DFE introduces M additional taps that are applied to the decoded digital signal and usually includes a delay between the FFE and the feedback loop. A diagram of a FFE-DFE is given in Fig. 3.25. The received signal enters the FFE. The output of the FFE is added to the feedback loop resulting in the equalized signal. The equalized signal is fed back through a symbol detector and delayed. The M-tap feedback filter is applied to the decoded symbols. The output of the feedback filter is added to the output of the FFE to yield the equalized signal. With a FFE-DFE the total number of filter coefficients is much less compared to the linear FFE for the same amount of ISI mitigation [160].

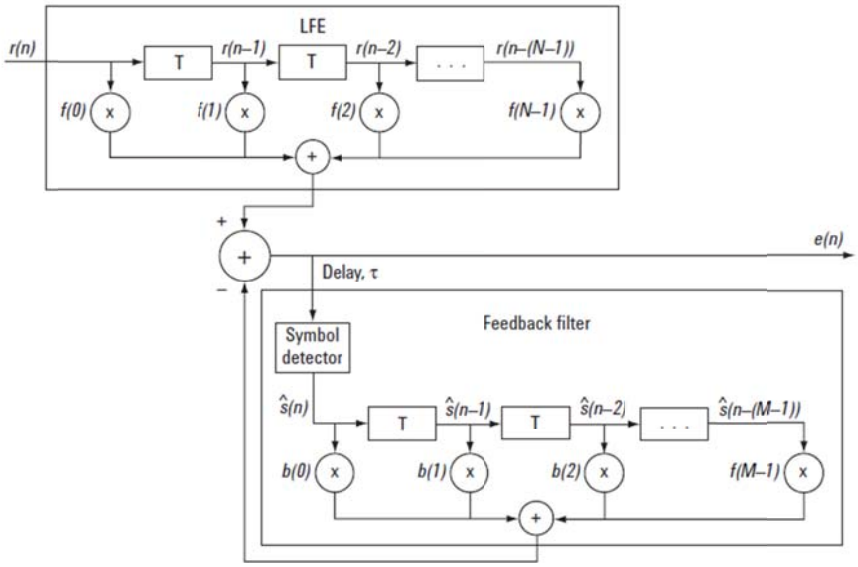

Fig. 3.25. The structure of a (N, M)-tap FFE-DFE [159].

The tap values are derived by using optimization techniques for either a FFE or a DFE. The standard methods are called least mean square error and minimum mean square error. The ability to set taps can also be dynamic. Adaptive equalization means a system can optimize its own taps as conditions evolve.

Based on the setup shown in Fig. 3.22 (b), the bit rate of a self-seeded RSOA is further increased to 5 Gb/s with offline electronic equalization. The received electrical signal is sampled by a real-time oscilloscope and the samples are post-processed by a Matlab program functioning as a feed-forward-decision feedback equalizer (FFE-DFE). Measurements have been repeated with different received power at the PIN photodetector. The resultant BER performance of the self-seeded RSOA directly modulated by a 5-Gb/s PRBS with electronic equalization is shown in next section.

3.2.3 A low-cost bidirectional WDM-PON system based on RSOAs

Fig. 3.26 shows a cost-effective bidirectional 5/1.25-Gb/s WDM-PON based on self-seeded RSOAs for downlink and remote-seeded RSOAs for uplink. The self-seeding scheme with an optical amplifier in the reflection module is adopted for downstream transmission and located in the OLT. The optical amplifier can be shared among all the downstream channels. The downstream signal distributed to the corresponding ONU is divided into two portions. One is for downstream detection and the other is fed into the RSOA at the ONU for upstream remodulation.

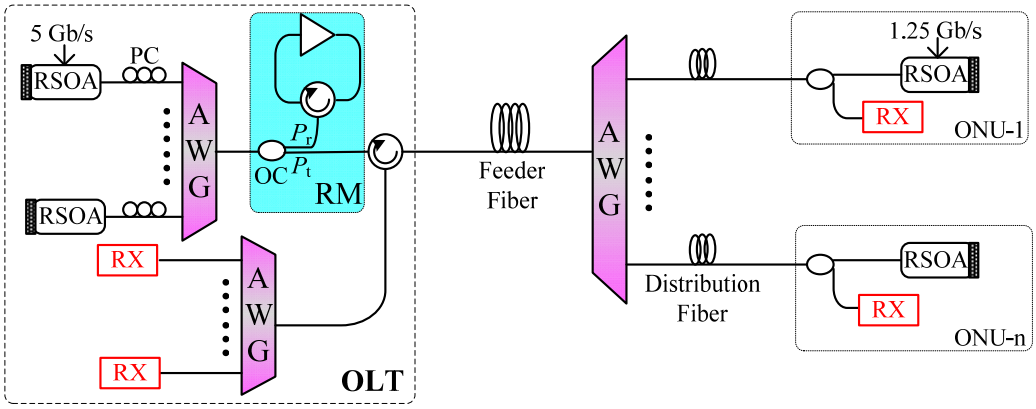

Fig. 3.26. A cost-effective bidirectional WDM-PON based on self- and remote-seeded RSOAs.

Unlike conventional WDM-PONs in which an arrays of DFB lasers are employed for high-speed downstream transmission (e.g. 10 Gb/s), the proposed WDM-PON architecture simply based on RSOAs has a limited downstream data rate (e.g. 5 Gb/s with electronic equalization). However, its high cost-effectiveness makes it a potential solution for access networks with end users having moderate bandwidth requirement. Fig. 3.27 shows the experimental setup to investigate the system transmission performance.

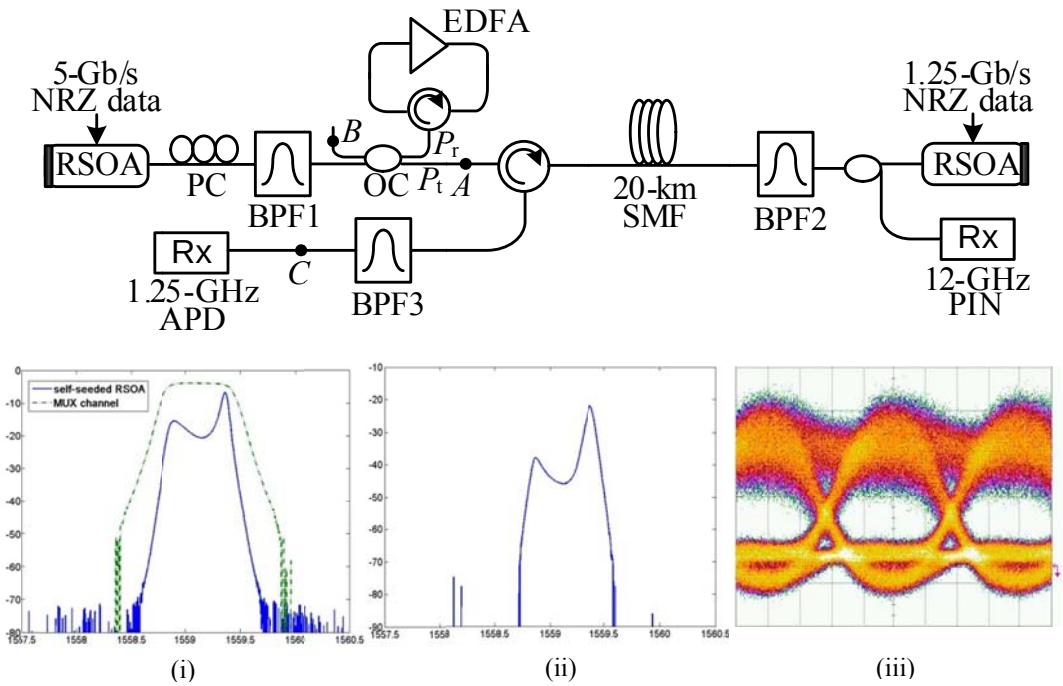

Fig. 3.27. Experimental setup. Insets: (i) optical spectrum measured at point 'A' and the shape of BPF1; (ii) optical spectrum measured at point 'C'; (iii) eye diagram measured at point 'C'.

3.2.3.1 Downstream transmission

The downstream transmission in this WDM-PON system is based on self-seeded RSOAs which are directly modulated by 5-Gb/s PRBS with a pattern length of 2^{15}-1.The RSOA used in the experiments has a small signal gain of 23 dB, a low PDG of 1 dB, and a saturated output power of 5 dBm when it is biased at 80 mA. A 1×4 flat-top wavelength multiplexers (BPF1 with 3-dB bandwidth = 0.6 nm and insertion loss = 4 dB) is employed in the self-seeding cavity. Since the RSOA has a small non-zero PDG, a polarization controller is added before the RSOA to adjust the polarization state and optimize the BER performance. The coupling ratio (P_r/P_t) of the optical coupler in the reflection module is chosen to be 50/50 instead of 90/10 to ensure that the transmitted power P_t meets the power budget for both downstream detection and upstream

remodulation. Although the cavity loss is increased due to the reduced coupling ratio, the stable seeding power could be maintained by increasing the pump current of the EDFA.

When the pump current of the EDFA is 120 mA, the transmitted power P_t is measured to be -0.8 dBm. The downstream signal is transmitted over 20-km SMF feeder fiber. BPF2 is another 1×4 wavelength multiplexer having the same parameters as BPF1. The downstream signal distributed to the corresponding ONU is divided by a 50/50 optical coupler. One portion is detected by a 12.5-GHz PIN photodetector. Then the received electrical signal is sampled by a 6-GHz real-time oscilloscope at 10 GSamples/s giving 2 samples/bit. 2×10^6 samples stored by the oscilloscope are post-processed by a Matlab program functioning as a decision feedback equalizer consisting of half-symbol-spaced 11-tap FFE and 3-tap DFE. After changing the number of taps for FFE and DFE, a (11, 3) FFE-DFE is found to be the optimal choice. The adaptive tap coefficients are determined according to the least mean square algorithm. Fig. 3.28 shows the BER curves of 5-Gb/s self-seeded RSOA with electronic equalization before and after transmission over a 20-km SMF. Assuming a proper FEC code (e.g. the second generation FEC—concatenated RS(239,223)+RS(255,239)) is adopted, a coded BER of 1×10^{-12} could be achieved [161].

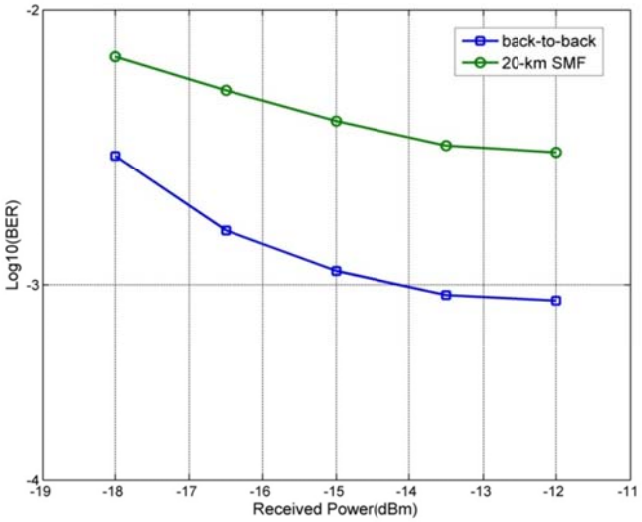

Fig. 3.28. BER performance of the self-seeded RSOA at 5-Gb/s with electronic equalization.

The 3-dB bandwidth of the wavelength multiplexer within the self-seeding cavity is a critical parameter. As discussed in [162], a larger bandwidth would improve the back-to-back BER performance due to the reduced relative intensity noise. However, the accumulated chromatic dispersion becomes the limiting factor when downstream signal at 5 Gb/s or even higher data rate is transmitted over a 20-km SMF. Therefore, the 3-dB bandwidth of the wavelength multiplexer should be carefully chosen considering the trade-off between the RIN-reduced and chromatic dispersion-induced penalties.

3.2.3.2 Upstream transmission

The upstream transmission reuses the downstream carrier by utilizing directly modulated remote-seeded RSOAs. The RSOA used for upstream transmission in the experiment has a small signal gain of 15 dB, a low PDG of 1 dB, and a saturated output power of 0 dBm when it is biased at 40 mA. Since the transmitted power P_t of the downstream signal is measured to be 0.8 dBm, the attainable seeding power to the upstream RSOA is around -12 dBm considering the insertion losses of the feeder fiber (4.2 dB), the wavelength

multiplexer in remote node (4.0 dB), the 50/50 coupler in ONU (3.3 dB) and others losses including the circulator and distribution fiber. The seeding power of -12 dBm could drive the upstream RSOA into saturation region and the downstream modulation on the seeding light could be suppressed to some degree.

Although the upstream RSOA has a small non-zero PDG (1 dB), polarization control of the external seeding light is not required since the seeding light, i.e., the output of the self-seeded RSOA, is incoherent to a great extent. The upstream RSOA is directly driven by a 1.25-Gb/s PRBS with a pattern length of 2^{31}-1. The driving voltage of the NRZ signal is set to be 2.0 V_{pp}. The upstream signal is detected by a 1.25-Gb/s APD receiver in the OLT. The upstream transmission performances of three different setups depicted in Fig. 3.29 (a) are shown in Fig. 3.29 (b). The seeding power to the upstream RSOA is kept the same in the three setups.

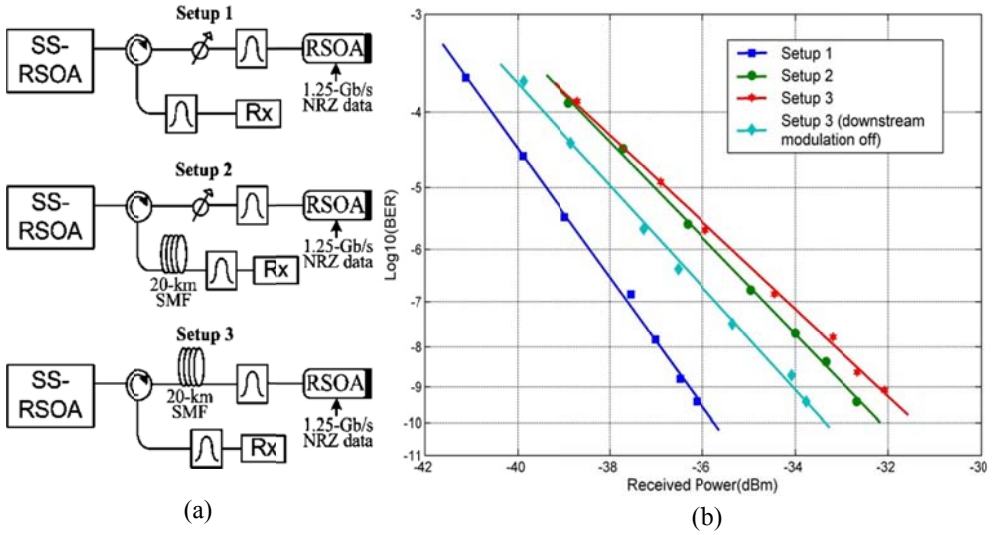

(a) (b)

Fig. 3.29. (a) Experiment setups to investigate the RB-induced and remodulation crosstalk; (b)the corresponding BER performances.

The back-to-back BER performance of the upstream external-seeded RSOA can be measured with Setup 1. The receiver sensitivity at a BER of 10^{-9} is -36.3 dBm for the back-to-back case. In Setup 2, the upstream signal is transmitted over a 20-km SMF and the receiver sensitivity at a BER of 10^{-9} is measured to be -32.9 dBm. Therefore, the power penalty induced by the chromatic dispersion is 3.4 dB. Setup 3 corresponds to the practical implementation in which the seeding light is delivered from the central office and the remodulated upstream signal is transmitted back to the OLT through the same feeder fiber. Due to the bidirectional loopback configuration, the upstream signal would be degraded by RBS-induced crosstalk. The receiver sensitivity at a BER of 10^{-9} is -32.2 dBm. Compared to the BER measurement of Setup 2, the power penalty induced by RBS is 0.7 dB.

The power penalty induced by the remodulation crosstalk is also investigated by turning off the downstream modulation. The CW light generated by the self-seeded RSOA is externally fed into the upstream RSOA. As Fig. 3.29 (b) shows, the receiver sensitivity at a BER of 10^{-9} is -34.0 dBm when the downstream modulation is turned off. Compared to the BER measured when the downstream modulation is turned on, the remodulation crosstalk induces a power penalty of 1.8 dB. When the remodulation scheme is involved, the downstream ER is a critical value which should be determined by considering the trade-off between downstream and upstream transmission performances. Usually the downstream ER is set to be within a range of 3-6 dB [87, 163]. A lower or higher ER would result in unacceptable power penalty in downstream or upstream transmission, respectively. In the WDM-PON architecture discussed here, the downstream signal comes from the directly modulated self-seeded RSOA and therefore it

naturally has an appropriate ER for upstream remodulation. For downstream transmission based on self-seeded RSOA, a higher ER will not improve but degrade the downstream performance, as discussed in Section 3.1.4.1. Reference [162] has studied the effect of downstream ER on both self-seeded RSOA-based downstream and remote-seeded RSOA-based upstream transmission performances.

3.3 Comparison of schemes for colorless ONUs in WDM-PONs

Various proposed schemes for colorless operation of ONUs, including broadband light sources, incoherent remote-seeded RSOAs or injection-locked FP-LDs, coherent remote-seeded RSOAs or injection-locked FP-LDs, and self-seeded RSOAs or FP-LDs, are compared in terms of their cost-effectiveness, bit-rate capacity, and operation complexity. The technical issues in implementing each of the schemes are also listed in the table. A reasonable choice could be made only by considering the requirements and constraints in real deployment in conjunction with the pros and cons of each scheme.

Table 3.2. Comparison of schemes for colorless operation of ONUs

	Cost-effectiveness	Bit-rate capacity	Operation complexity and technical issues	References
① Broadband light sources (BLS)	★★★★ A BLS (LED, SLD, or EDFA) in each ONU.	★ Suffer from spontaneous-spontaneous beat noise, bit rate limited to 1.25 Gb/s.	★ Simple operation; transmission distance limited by the BLS output power.	[28], [31], [41]
②Incoherent remote-seeded RSOAs	★★★ A RSOA at each ONU and a BLS in OLT.	★★ Suffer from spontaneous-spontaneous beat noise, typical bit rate 1.25 Gb/s.	★★★ Suffer from backreflection-induced crosstalk.	[164]
③Incoherent injection-locked FP-LDs	★★★ A FP-LD at each ONU and a BLS in OLT.	★★★ Suffer from spontaneous-spontaneous beat noise, typical bit rate 1.25/2.5 Gb/s.	★★★★ Suffer from backreflection-induced crosstalk; wavelength alignment between FP-LD and AWG needed.	[75-77]

④ Coherent remote-seeded RSOAs	★★ A RSOA at each ONU and an array of DFB lasers in OLT.	★★★★ Bit rate limited by RSOA modulation bandwidth (typically 1-2 GHz); 10 Gb/s or ever higher data rate achieved by utilizing other techniques.	★★★ More sensitive to backreflection-induced crosstalk than ②;	[44], [46]
⑤Coherent injection-locked FP-LDs	★★ A FP-LD at each ONU and an array of DFB lasers in OLT.	★★★★★ Up to 10 Gb/s demonstrated with a butterfly-packaged FP-LD having high modulation bandwidth.	★★★★★ More sensitive to backreflection-induced crosstalk than ③; accurate wavelength alignment needed for high-speed operation.	[80], [87]
⑥ Self-seeded RSOAs	★★★★★ A RSOA at each ONU	★★ 1.25 Gb/s typically; bit rate limited by RSOA modulation bandwidth as well as self-seeding characteristics.	★★ Suffer from remodulation crosstalk;	[35], [105] [107]
⑦ Self-injected FP-LDs	★★★★★ A FP-LD at each ONU	★★★ Up to 2.5 Gb/s; bit rate limited by self-seeding characteristics.	★★★ Suffer from remodulation crosstalk; wavelength alignment between FP-LD and AWG needed.	[34], [103]
★★★★★indicates the highest grade of cost-effectiveness, bit rate, and operation complexity.				

3.4 Summary

Performance characterization of self-seeded RSOAs utilized as the colorless light sources for WDM-PONs was carried out. An optimal ER existed for each fixed cavity loss since remodulation is involved in the self-seeding operation. Either by tuning the attenuation of the VOA or by varying the coupling ratio of the optical coupler in the reflection module, the cavity loss and the resultant stable seeding power could be modified. The results showed that low cavity loss or the resultant high stable seeding power brought better transmission performances. Considering the trade-off between the upstream link loss and the self-seeding cavity loss, the power budget for upstream transmission could be optimized with a certain coupling ratio of the optical coupler.

The RSOA with a high signal gain, high saturated output power, and a low PDG was preferred for the self-seeding application. For other passive components in the self-seeding cavity, e.g. the AWG, low insertion loss was a desirable feature. The experiment results also showed that the AWG with flat-top passband outperformed the one with Gaussian-shaped passband in terms of transmission performance and the minimum 3-dB bandwidth. Therefore, a low-loss flat-top AWG met all the requirements on the wavelength multiplexer for the WDM-PON system based on the directly modulated self-seeded RSOAs. The system transmission performance was robust against the phase perturbation but degraded by extending the length of the self-seeding cavity. Nonetheless, error-free transmission was guaranteed for the typical WDM-PON system with the length of the distribution fiber up to 4 km.

The performances of the systems based on the directly modulated self-seeded RSOAs are strongly dependent on the intrinsic characteristics of the RSOA, e.g. gain dynamics and saturation property. The quantitative results presented in Section 3.1 may only be applied to the RSOA used in our experiments but the qualitative analyses extracted from the experiment data are applicable to all RSOAs with variant characteristics.

Bidirectional transmission of the upstream signal based on a self-seeded RSOA and the downstream signal based on an externally modulated laser source has been investigated and the crosstalk-induced power penalty is negligible [106]. The wavelength operating range of a self-seeded RSOA is decided by the gain profile of the RSOA. RSOAs with flat and high gain spectra are desirable for self-seeding application to cover a wide wavelength range. For example in [107], experiment results show the wavelength

of the self-seeded RSOA output could be tuned from 1530 to 1595 nm. The fluctuation of the receiver sensitivity at a BER of 10^{-9} is around 1 dB. Simultaneous upstream transmission of 16 or 32 channels of self-seeded RSOAs has been demonstrated in [152]. After 20 km transmission, the power penalty is only 0.5 dB and 0.3 dB at a BER of 10^{-10} for the 32- and 16-channel systems, respectively.

Self-seeded RSOA is a promising solution for low-cost colorless WDM-PONs. When it is applied to upstream transmission, remote seeding sources are not required and therefore the RBS-induced crosstalk is avoided. When it is applied to downstream transmission, it is more cost-efficient than an array of DFB lasers in conventional WDM-PONs. The data rate of self-seeded RSOAs is not only limited by the modulation bandwidth of RSOAs but also by the remodulation crosstalk and incoherent characteristic involved in the self-seeding scheme. In Section 3.2, we demonstrated a cost-effective bidirectional 5/1.25-Gb/s WDM-PON based on self-seeded RSOAs for downlink and remote-seeded RSOAs for uplink. The bit rate of a directly modulated self-seeded RSOA with a modulation bandwidth < 1GHz could be enhanced to 5 Gb/s by increasing the seeding power and employing offline electronic equalization. So far, 10.7-Gb/s self-seeded RSOA was demonstrated with a RSOA having 4-GHz E/O bandwidth and the help of electronic equalization [47]. All the above have shown that self-seeded and external-seeded RSOAs are very promising for the future deployment of low-cost colorless WDM-PONs.

CHAPTER 4

A Multimode-Injected FP-LD—a Common Noise Suppressor for Multiple Injected ASE Spectrum Slices

In addition to RSOAs, FP-LDs are considered as low-cost light sources for wavelength-independent ONUs in WDM-PONs. FP-LDs located at ONUs are injection-locked by remote seeding light sent from the central office. The seeding light can be a coherent CW laser, whereby a free-running multi-wavelength FP-LD is converted to a quasi-single-wavelength light source. However, this may not be cost-effective as an array of CW lasers is required for uplink. Spectrum-sliced ASE source has been proposed as a low-cost seeding light but its noise characteristic severely limits the modulation bandwidth of injection-locked FP-LDs. To improve the transmission performance of incoherent light injection-locked FP-LDs, we propose a new remote seeding light scheme and verify it by simulations. Instead of a spectrum-sliced ASE source, we use a spectrum-sliced multimode-injected FP-LD as the remote seeding light.

In this chapter, a theoretical model of injection-locked FP-LDs is first introduced. Based on this model, the transient response and the steady-state longitudinal-mode spectrum of a FP-LD before and after external injection are examined by simulation. Then the characteristics of free-running and injection-locked FP-LDs are explored through experiments. A multimode-injected (MI) FP-LD is proposed as a broadband light source. After being spectrum-sliced (SS), the resultant SS-MI FP-LD is employed as an

optical carrier and its performance is compared with a spectrum-sliced ASE source. At last, the SS-MI FP-LD is proposed as a seeding light to injection-lock another FP-LD located at the ONU. The corresponding transmission performance is investigated through simulations.

4.1 Theoretical analysis of injection-locked FP-LDs

The theoretical models to describe the dynamic behaviors of injection-locked lasers have been developed in [165, 166]. In-depth investigations have been carried out to analyze the significant benefits of injection-locking technique, including relative intensity noise reduction [167], suppression of nonlinear effects [168], and modulation bandwidth enhancement [169]. In the free-running state, a FP-LD will generate multiple longitudinal modes. The theoretical model of injection-locked lasers is further developed to describe an injection-locked FP-LD.

4.1.1 Rate equations of injection-locked FP-LDs

The differential rate equation governing a free-running laser, neglecting spontaneous emission, is [170]:

$$\frac{dE(t)}{dt} = \frac{1}{2} g \Delta N (1 + j\alpha) E(t) \tag{4.1}$$

where *E(t)* is the complex electric field, *g* is the linear gain coefficient, *ΔN* is the carrier number above threshold, and α is the linewidth enhancement factor. $\Delta N = N(t) - N_{th}$, where *N* is the carrier number and N_{th} is the threshold carrier number.

A theoretical model of the injection-locked FP-LD based on the rate equations for semiconductor laser diodes was proposed in [171]. The dynamics of a FP-LD with the

external injection can be described with the following rate equations for carrier density inside the active region N and the electric field of the active region E which is normalized, such that $|E(t)|^2$ corresponds to the photon density:

$$\frac{dE_0}{dt} = \frac{1}{2}(1+j\alpha)(G_0 - \gamma)E_0(t) + F_E^0(t) + k_c E_{inj}\exp(j2\pi\Delta f) \tag{4.2}$$

$$\frac{dE_i}{dt} = \frac{1}{2}(1+j\alpha)(G_i - \gamma)E_i(t) + F_E^i(t) \tag{4.3}$$

$$\frac{dN}{dt} = \frac{I}{qV} - \gamma_e N - \sum_i G_i |E_i|^2 \tag{4.4}$$

with

$$G_i = \frac{\Gamma \upsilon_g a(N - N_0)}{\left[1 + \left(\frac{2i\Delta f_{mode}}{\Delta f_g}\right)^2\right] \cdot \left(1 + \varepsilon \sum |E_i|^2\right)} \tag{4.5}$$

$$\gamma = \upsilon_g(\alpha_{int} + \alpha_m) \tag{4.6}$$

$$\alpha_m = \frac{1}{2L} \cdot \ln\left(\frac{1}{R_f R_b}\right) \tag{4.7}$$

$$\gamma_e = A_{nr} + BN + CN^2 \tag{4.8}$$

$$\Delta f = f_{inj} - f_0^{th} \tag{4.9}$$

$$k_c = \frac{\upsilon_g(1 - R_f)}{2L\sqrt{R_f}} \cdot \sqrt{\frac{\eta\left(\sqrt{R_f} + \sqrt{R_b}\right)\left(1 - \sqrt{R_f R_b}\right)}{\sqrt{R_b}(1 - R_f)\ln\left(\frac{1}{\sqrt{R_f R_b}}\right)}} \tag{4.10}$$

where E_i is the complex amplitude of the i^{th} mode, f_0^{th} the frequency of the zeroth mode at the threshold, f_{inj} the frequency of the external injection light, G_i the gain of the i^{th} mode, γ the loss of the cavity, α the linewidth enhancement factor, k_c the coupling

efficiency, Δf the frequency offset between the free-running longitudinal mode and the injection light, α_m the facet loss, and γ_e is the carrier recombination rate. The gain of the i^{th} mode G_i is approximated by the Lorentzian function with the gain compression effect. $F_E^i(t)$ is the spontaneous emission noise coupled into the i^{th} mode. The values of various physical parameters adopted in the simulation are summarized in Table 4.1.

Table 4.1. Physical parameters used in simulation of injection-locked FP-LDs [171, 172]

λ	Peak wavelength (main mode)	1550 nm
L	Cavity length	250 μm
w	Width of the active region	2.0 μm
d	Depth of the active region	0.2 μm
τ_e	Carrier lifetime	2.2 ns
τ_p	Photon lifetime	1.6e-3 ns
Γ	Confinement factor	0.3
n_g	Group index	4.0
k	Coupling efficiency	100ns^{-1}
α	Linewidth enhancement factor	5
β_{sp}	Spontaneous emission factor	1e-4
α_{int}	Internal loss	30 cm^{-1}
α_{m}	Facet loss	45 cm^{-1}
a	Gain constant	2.5e-16 cm^2
N_0	Transparent carrier density	1e18 cm^{-3}
A_{nr}	Non-radiative recombination rate	1e8 s^{-1}
B	Radiative recombination coefficient	1e-10cm^3/s
C	Auger recombination coefficient	4e-29 cm^6/s
ε	Gain compression factor	6e-19 cm^3
h	Planck constant	6.626e-25J·ns
c	Speed of light	30 cm/ns
$\Delta\omega_{\text{mod}}$	Mode spacing of FP-LD	0.8 nm

4.1.2 Simulation results

An approximate physical description of the FP-LD threshold and the resultant light-current (L-I) curve can be obtained based on the single-mode rate equations. Fig 4.1 shows the calculated L-I curve of a FP-LD with the physical parameters listed in Table 4.1. As the L-I curve indicates, the threshold current is around 15 mA.

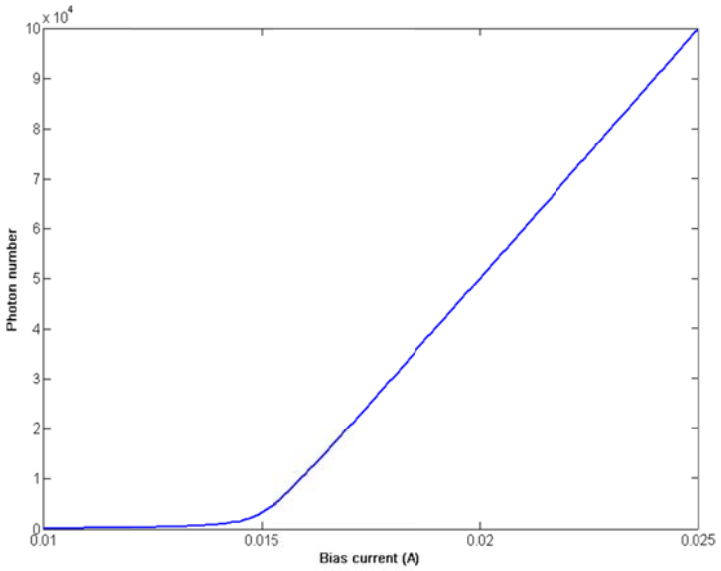

Fig. 4.1. The calculated L-I curve.

Then the dynamic characteristics of a free-running and injection-locked FP-LD biased at 20 mA are investigated by calculating the rate equations (4.2)-(4.4). Fig. 4.2 shows the free-running spectrum of a FP-LD in the steady state with 19 longitudinal modes are calculated. The mode spacing is set to be 0.8 nm. The SMSR, which is defined as the power ratio between the mode with the highest power (the main mode "0") and the mode with the second highest power (the side mode "+1"), is around 2.5 dB.

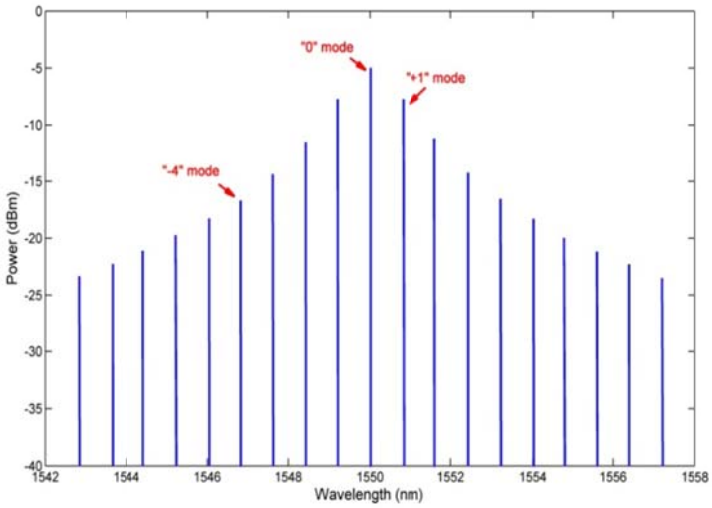

Fig. 4.2. The simulated optical spectrum of a free-running FP-LD.

When a semiconductor laser is turned on by changing the bias current, a relative long time (~10 ns) elapses before the steady state is reached [172]. In the transient regime, the power distribution among various longitudinal modes varies periodically as the laser goes through relaxation oscillations. Fig. 4.3 shows the transient responses of the carrier number and photon numbers in different modes when the FP-LD is turned on. After about 10 ns, the oscillations of the carrier and photon numbers vanish and the laser is in steady state. The main mode (the "0" mode) contains the most photons which contribute to the highest power as shown in Fig. 4.2.

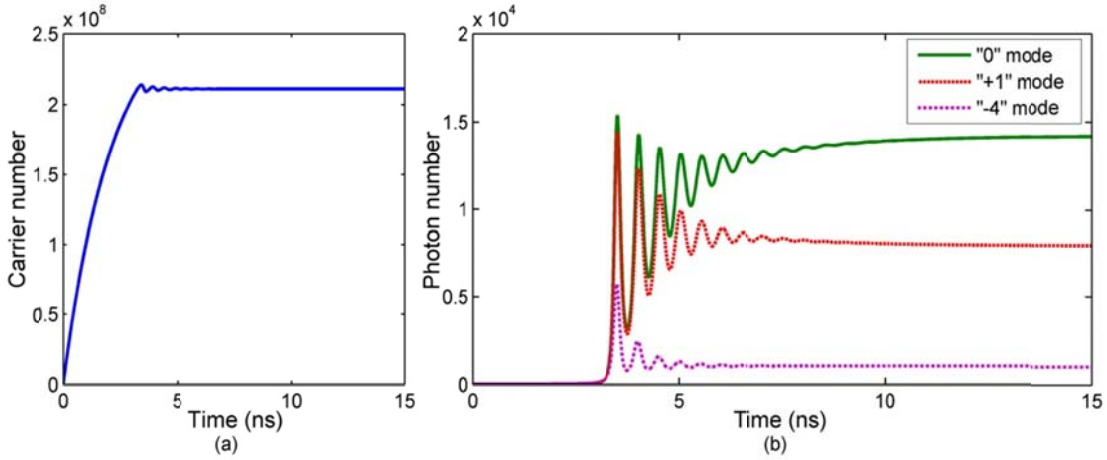

Fig. 4.3. Time evolution of (a) the carrier and (b) photon numbers when the laser is turned on.

Fig. 4.4 and 4.5 show the optical spectrum and transient responses of a FP-LD injection-locked by a coherent CW light at the main mode. The injection power is around -6.7 dBm. The side modes are significantly suppressed and the resultant SMSR is 22.9 dB. Fig. 4.4 shows how the carrier and photon populations in different modes are changed when a CW external light is injected into the FP-LD. The external injection is introduced after the FP-LD has been turned on for 20 ns when it has already been operated in the steady state. Before the external injection, the behavior of carrier and photon numbers are exactly same with those shown in Fig. 4.3. The external injection results in a strong instantaneous surge of the photon number in the main mode. After the FP-LD returns to steady state with external injection, the photon number in the injection-locked mode (the "0" mode) is increased whereas the photon numbers in other modes are reduced. Consequently, the injection-locked mode is amplified and the other modes are suppressed. The SMSR is therefore increased.

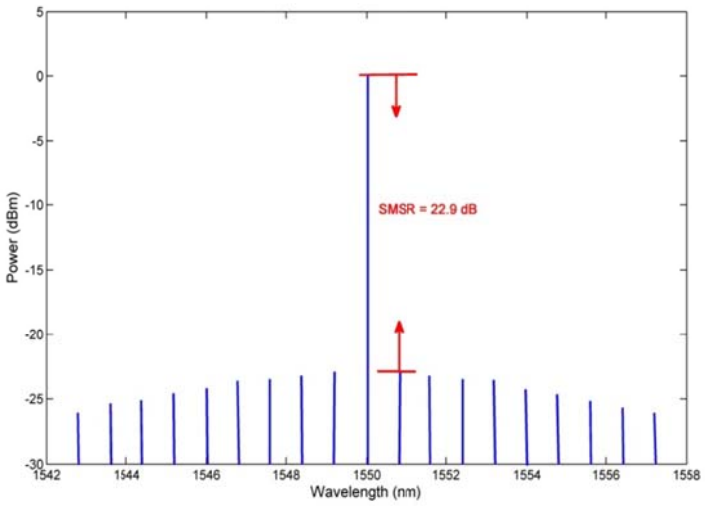

Fig. 4.4. The simulated optical spectrum of a FP-LD injection-locked at the main mode.

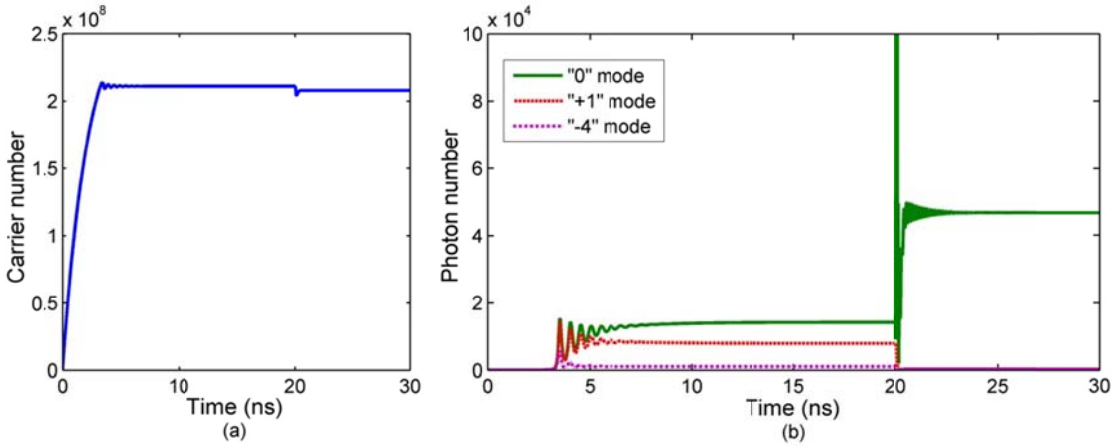

Fig. 4.5. Time evolution of (a) the carrier and (b) photon numbers in the FP-LD switched from free-running to injection-locking (the main mode is injection-locked).

The same investigation is carried out for the case when a side mode (the "-4" mode) is injection-locked by the external coherent CW light. Fig. 4.6 shows the corresponding optical spectrum. The injection power is -5.2 dBm. The SMSR after injection-locking is 30.8 dB. Fig. 4.7 shows similar behavior as Fig. 4.5. The difference lies in that the injection-locked mode now is the "-4" mode. After injection-locking, the "-4" mode is amplified while the other modes are suppressed. The carrier number drops a bit after external injection.

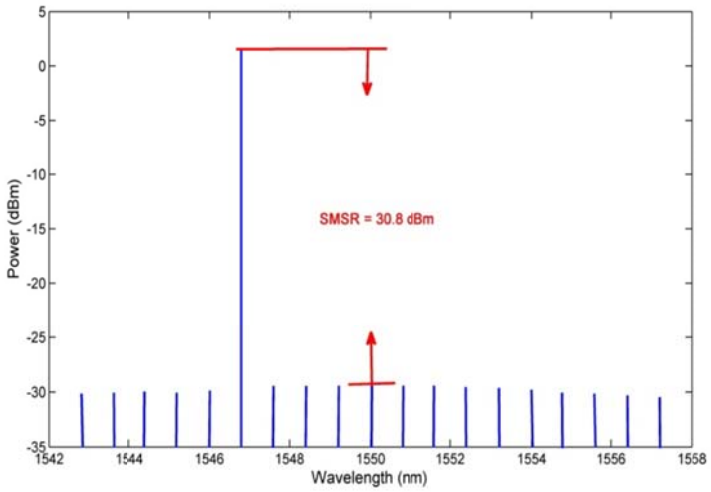

Fig. 4.6. The simulated optical spectrum of a FP-LD injection-locked at the "-4" mode.

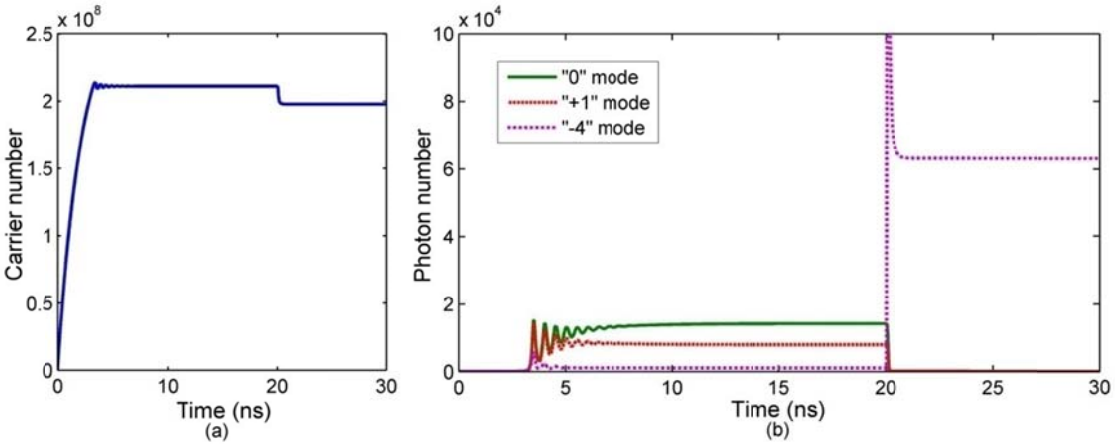

Fig. 4.7. Time evolution of (a) the carrier and (b) photon numbers in the FP-LD switched from free-running to injection-locking (the side mode "-4" is injection-locked).

4.2 Experimental characterization of FP-LDs

A Fabry-Perot laser diode is an oscillator in which two mirrors separated by an amplifying medium with an inverted population make a FP cavity. FP-LDs are the most common type of diode laser and are the most economical, but they are generally slower and noisier than DFB lasers. The two FP-LDs used in our experiments are a conventional FP-LD housed in a butterfly package and a weak-resonant-cavity (WRC) FP-LD housed in a transistor outlook (TO)-can package. In general, butterfly-packaged FP-LDs exhibit high modulation bandwidth compared to TO-can-packaged FP-LDs; WRC FP-LDs have a larger locking range than conventional FP-LDs. In the following experimental demonstration, the two FP-LDs are selected according to their characteristics.

4.2.1 Free-running FP-LDs

The free-running FP-LD exhibits many longitudinal modes. The spacing $\Delta\nu_L$ between the longitudinal modes is constant if the frequency dependence of refractive index n is ignored. The mode spacing is calculated by $\Delta\nu_L = c/2nL$, where L is the cavity length.

The free-running spectra of a FP-LD (butterfly-packaged conventional FP-LD) with mode spacing of 0.8 nm under different bias currents are depicted in Fig. 4.8. As the bias current increases, the main mode which has the highest power among all the longitudinal modes shifts towards the longer wavelength side.

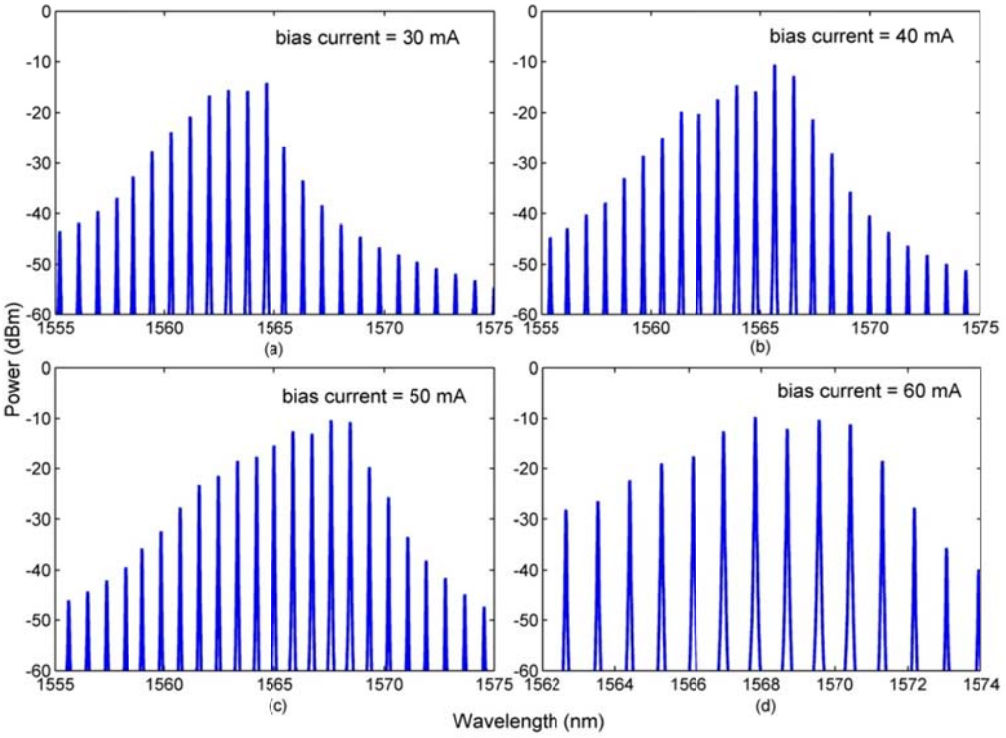

Fig. 4.8. Free-running spectra of a FP-LD under different bias currents.

Although the free-running spectrum observed from an optical spectrum analyzer (OSA) looks stable and the total optical power measured by power meter (PM) is almost invariable, the power of each longitudinal mode fluctuates dramatically due to mode partition noise. Mode partitioning in semiconductor lasers describes how the intensities of all longitudinal modes fluctuate as they compete with each other for a common injected-carrier population [173]. The mode partition noise (MPN) cannot be captured by an OSA or a PM since the intensity fluctuation is much faster than the responding speed of these

instruments. Therefore, if one longitudinal mode is filtered out, the optical spectrum still looks stable by an OSA and its power seldom changes when observed by a PM. However, due to the existence of MPN, a single longitudinal mode selected from a free-running FP-LD could hardly be used as an optical carrier.

The modulation bandwidth of a FP-LD increases with the bias current. Fig. 4.9 shows the frequency response of the free-running butterfly-packaged FP-LD under different bias currents measured by a vector network analyzer. The 3-dB bandwidths are 6.0 GHz, 8.0 GHz, 9.6 GHz, and 10.7 GHz when the bias currents are 30 mA, 40 mA, 50 mA, and 60 mA, respectively.

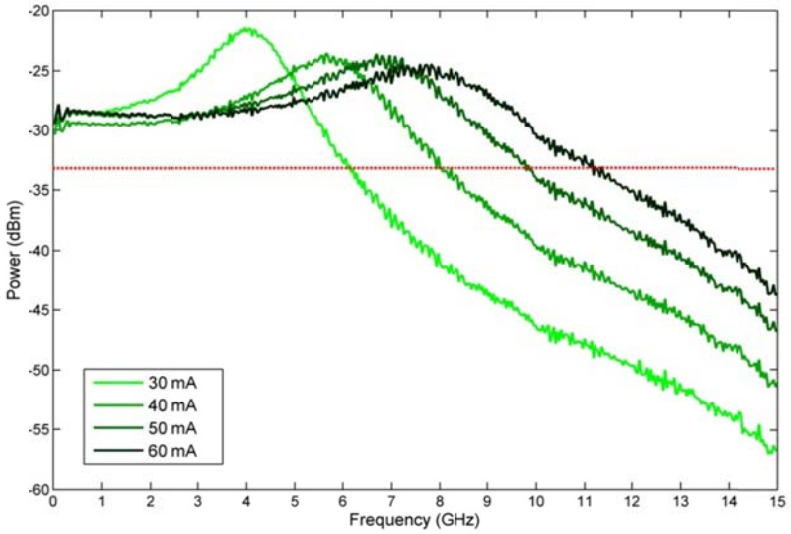

Fig. 4.9. Frequency response of a free-running FP-LD under different bias currents.

The free-running spectrum drifts with the changing temperature. It moves to the longer wavelength side when the temperature increases. The output spectra of the FP-LDs used in our experiments shifts 0.1 nm/°C approximately. The main mode also shifts to a longer-wavelength longitudinal mode. Due to the temperature sensitivity, a

thermoelectric cooling (TEC) module may be required to control the operating temperature of the FP-LD in some applications.

4.2.2 Injection-locked FP-LDs

When a semiconductor laser is strongly injection-locked in a stable locking state, the benefits of a significantly enhanced modulation bandwidth, a broadband noise reduction, and a large modulation dynamic range can be attained [174]. Although a free-running FP-LD is not a suitable light source for high-speed data transmission, injection-locked FP-LDs play an important role in colorless WDM-PON systems.

The mode frequencies will shift to the longer wavelength side after injection-locking due to the carrier-induced refractive index change [175]. Therefore, stable injection-locking can be achieved by tuning the wavelength of seeding light slightly longer than that of the target longitudinal mode of free-running FP-LD. A FP-LD will not be injection-locked beyond certain detuning range (locking range) between the seeding light and the target longitudinal mode exists. A larger locking range is observed for a lower bias current [176]. The injection-locking threshold is also affected by bias current. A higher seeding power is needed when the bias current of the FP-LD is increased. The reason for the increase of the required seeding power with an increase of the bias current is related to the ratio of number of photons in the free-running regime and the number of injected photons. The injected photons can prevail and sustain stimulated emission at a certain mode much easier if the number of existing free-running photons is smaller, which means the bias current is lower [177].

Fig. 4.10 illustrates a free-running FP-LD (TO-can-packaged WRC FP-LD) injection-locked by coherent seeding light. The threshold current of the FP-LD is 20 mA and it is biased at 30 mA. It is directly modulated with 2.5-Gb/s 1.5 V_{pp} 2^{23}-1 PRBS data. The wavelength of the seeding light is 1554.23 nm and the target free-running longitudinal mode locates at 1554.11 nm.

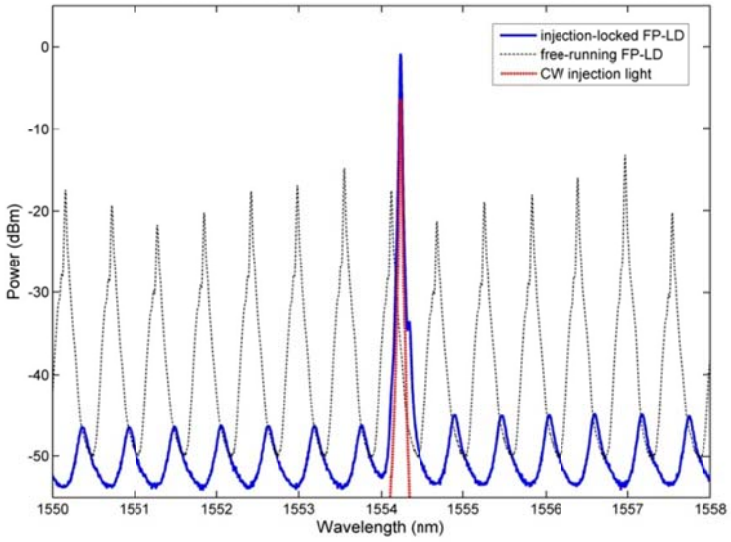

Fig. 4.10. Optical spectra of the free-running FP-LD, coherent injection light, and coherent light injection-locked FP-LD.

Fig. 4.11 shows the same FP-LD injection-locked by incoherent seeding light. The incoherent seeding light is obtained by spectrum-slicing a broadband ASE source with a 0.6-nm 3-dB bandwidth bandpass filter. The seeding power is around -9 dBm. The red-shift of the longitudinal modes could be observed in both the coherent and incoherent injection-locking.

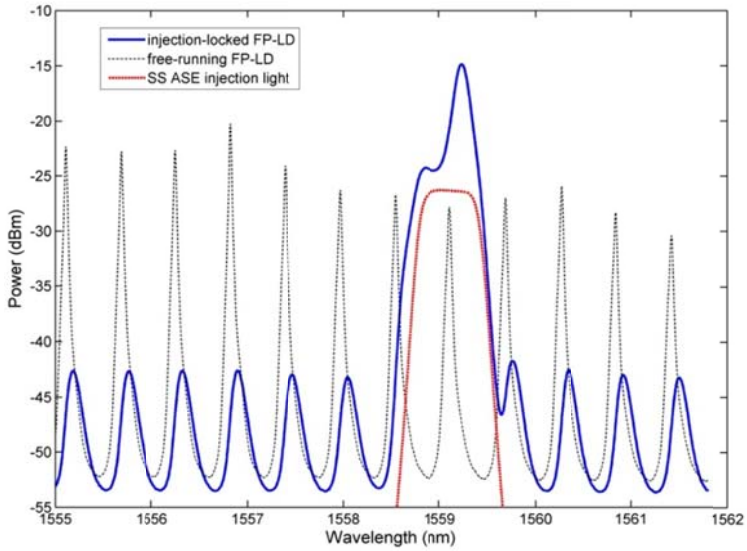

Fig. 4.11. Optical spectra of the free-running FP-LD, incoherent injection light (a spectrum-sliced ASE), and incoherent light injection-locked FP-LD.

The polarization dependence of injection-locking a polarization-sensitive FP-LD (butterfly-packaged conventional FP-LD) is demonstrated next. The polarization direction of the linearly polarized coherent injection light is altered by passing through a half-wave plate before it is injected into the FP-LD. By rotating the half-wave plate, the polarization direction of the seeding light could be changed from parallel to the TE mode of the FP-LD to parallel to the TM mode of the FP-LD. When the seeding light is aligned to the TE mode of the FP-LD, the FP-LD will be injection-locked; when the seeding light is aligned to the TM mode of the FP-LD, it is absorbed by the FP-LD and fails injection

locking. Fig. 4.12 depicts the FP-LD injection-locked by linear-polarized seeding light with different polarization directions, from TE-polarized to TM-polarized.

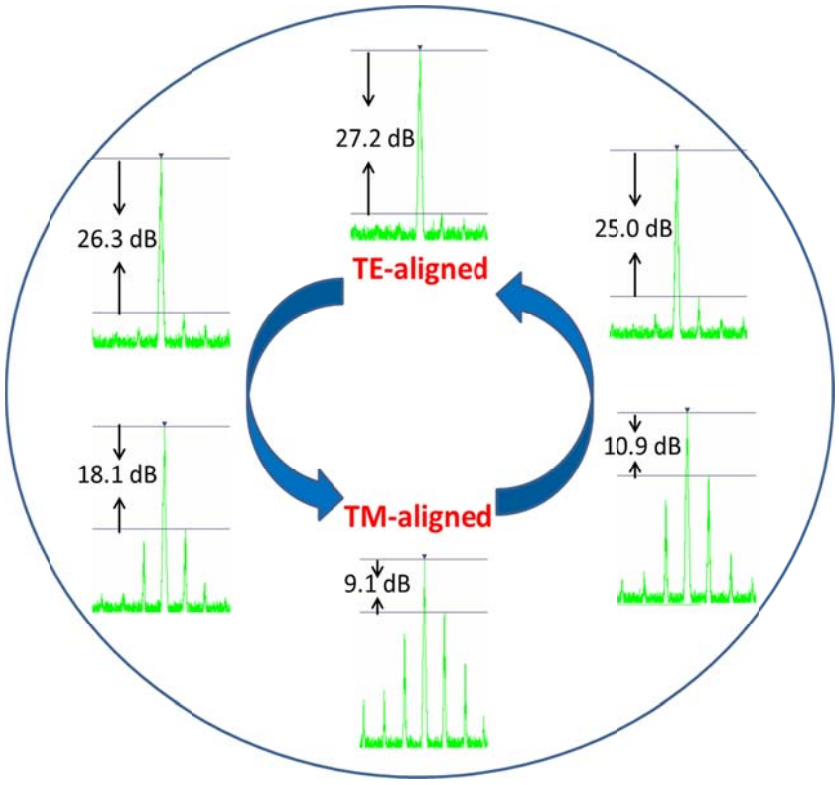

Fig. 4.12. Optical spectral of a FP-LD injection-locked by linearly polarized seeding light with different polarization directions. The SMSR is given in each case.

We have proposed a multimode-injected FP-LD (MI FP-LD) which could be used as the seeding light source for multiple FP-LDs or RSOAs. The scheme of a WDM-PON employing a multimode-injected FP-LD as the remote seeding light will be introduced in Section 4.4 in detail. Some optical spectra of the MI FP-LD are given here. Fig. 4.13 shows the optical spectra of a FP-LD (butterfly-packaged conventional FP-LD) injected by two and three coherent CW seeding lights aligned to its longitudinal modes. Coherent multimode injection-locking is difficult to implement since the wavelength of each

seeding light has to be controlled precisely within the locking range. It is difficult to obtain high SMSR.

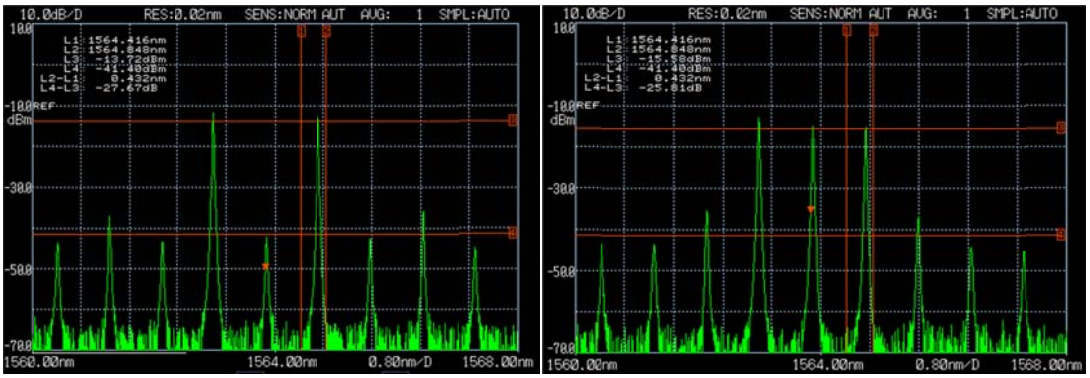

(a) (b)

Fig. 4.13. Optical spectra of coherent (a) two-mode IL FP-LD and (b) three-mode IL FP-LD.

Fig. 4.14 shows the optical spectra of a FP-LD (TO-can-packaged WRC FP-LD) injected by multiple incoherent spectrum slices aligned to its longitudinal modes. The injected spectrum slices depicted in Fig. 4.14 (b) have a spacing of 0.57 nm which equals to the longitudinal mode spacing of the FP-LD. The 3-dB bandwidth of each spectrum slice is 80 GHz (~0.64 nm) which is larger than the longitudinal mode spacing. Hence, the four spectrum slices are overlapped. The total seeding power is -7 dBm. The spacing between the injected spectrum slices depicted in Fig. 4.14 (d) is twice of the mode spacing and the 3-dB bandwidth is 50 GHz which is smaller than the longitudinal mode spacing. The total seeding power is -13 dBm. Fig. 4.14 (c) and (e) show the corresponding optical spectra of multimode-injected FP-LDs. As shown in the figures, the shape of the injection-locked spectrum is primarily decided by the external seeding light. The SMSRs achieved in these two cases are both around 30 dB.

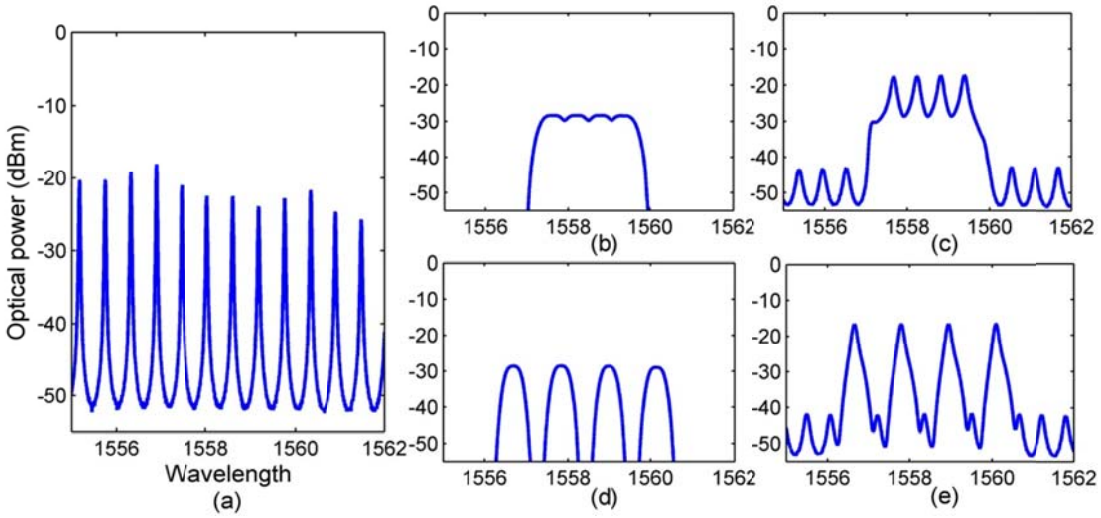

Fig. 4.14. Optical spectra of (a) the free-running FP-LD, (b) injected light containing four overlapped spectrum slices, (c) FP-LD injection-locked by the injected light shown in (b), (d) injected light containing four separate spectrum slices, and (e) FP-LD injection-locked by the injected light shown in (d).

4.3 A multimode-injected FP-LD used as optical carriers

The characteristics of an injection-locked FP-LD strongly depend on the characteristics of the injected light. The spectrum of the injection-locked mode is primarily determined by the spectrum of the injected light. However, the RIN of the incoherent seeding light, e.g. a spectrum-sliced ASE, could be suppressed by feeding it to a free-running FP-LD [175, 178]. Enlightened by this fact, we propose a MI FP-LD as a common noise suppressor for multiple ASE spectrum slices.

The configuration to obtain a MI FP-LD is introduced in this section firstly. To demonstrate the proposed MI FP-LD has better noise characteristic than an ASE source, it is spectrum-sliced and externally modulated with 622-Mb/s data for transmission. The transmission performance is compared with that based on the externally modulated spectrum-sliced ASE source.

4.3.1 Configuration of a multimode-injected FP-LD

As shown in Fig. 4.15, an ASE source is firstly spectrum-sliced by a wavelength demultiplexer (DEMUX_1) and then the spectrum slices coming out from different channels are combined by a wavelength multiplexer (MUX_1). The combined spectrum slices are injected into a FP-LD which is used as the common noise suppressor for all injected spectrum slices. The channel spacing of DEMUX_1 and MUX_1 should be same as the longitudinal mode spacing of the FP-LD. More importantly, the longitudinal modes of the free-running FP-LD should be aligned to the center frequencies of the spectrum slices.

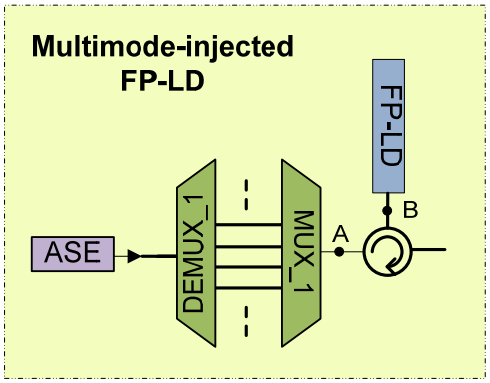

Fig. 4.15. Configuration of a multimode-injected FP-LD.

The simulations are carried out with VPItransmissionMaker 7.6 and the simulated spectra of the multimode-injected FP-LD are shown in Fig. 4.16. For comparison, the spectra of a free-running and single-mode injection-locked FP-LD are given in Fig. 4.16 (a). Cavity resonance shift can be observed in Fig. 4.16 (a) by comparing the optical spectra of the free-running and injection-locked FP-LD. The cavity modes are shifted to the longer wavelength side after injection-locking. The injection-locked mode becomes broader than when it is in the free-running state simply because the seeding light which is a spectrum-sliced ASE source is much wider than the longitudinal mode of the free-running FP-LD. The 3-dB bandwidth of MUX_1 and DEMUX_1 is 0.48 nm. The seeding power of one channel (i.e., the power of each spectrum slice) is around -8 dBm. Thus, the total seeding power in Fig. 4.16 (b) is around 1 dBm which is made up of eight ASE spectrum slices. The spectrum of the multimode-injected FP-LD is shown in Fig. 4.16 (c).

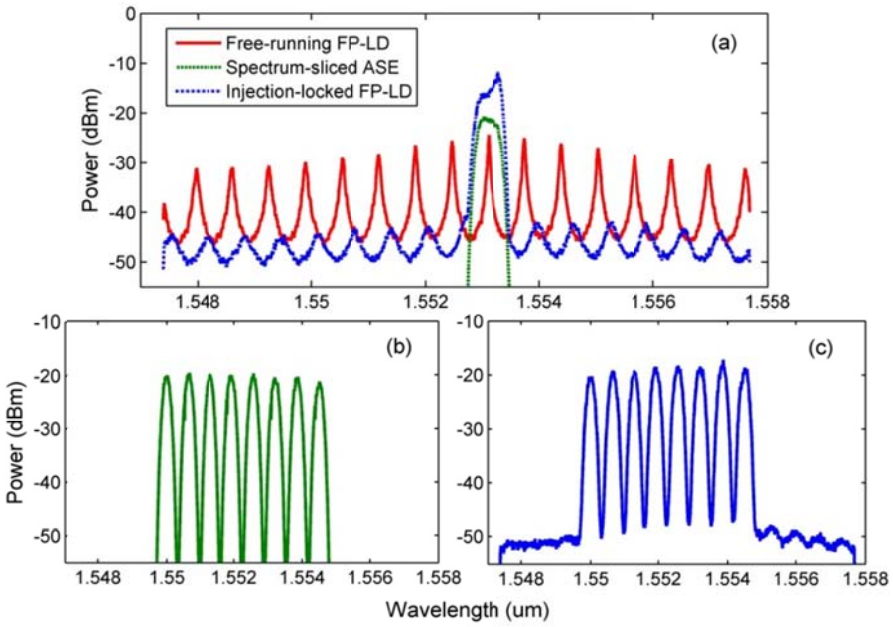

Fig. 4.16. The simulated optical spectra of (a) the free-running FP-LD, one ASE slice used as the seeding light, and single-mode injection-locked FP-LD; (b) the seeding light consisting of eight ASE spectrum slices; (c) the corresponding multimode-injected FP-LD.

4.3.2 Transmission performance of the multimode-injected FP-LD

To demonstrate that the RIN of the ASE spectrum slices is suppressed after being fed into a FP-LD (i.e. the RIN of a spectrum-sliced multimode-injected FP-LD is smaller than that of a spectrum-sliced ASE), we investigate the transmission performance of the system shown in Fig. 4.17. The broadband ASE source is a two-stage EDFA, whereas the multimode-injected FP-LD is obtained by the configuration shown in Fig. 4.15. The 3-dB bandwidth of the filter is 0.48 nm. The optical power after the filter is kept the same for the two types of sources. After spectrum-slicing, the optical carrier is externally modulated by a polarization-insensitive MZM with 622-Mb/s data. The signal is detected by a PIN receiver after being transmitted over a 20-km SMF followed by a 4-km dispersion compensation fiber (DCF). The dispersion-induced intensity noise might diminish the benefit of the noise suppression offered by the multimode-injected FP-LD when the output of the multimode-injected FP-LD was transmitted over a 20-km SMF [179]. Thus, a 4-km DCF is added in the feeder fiber to reduce the dispersion-induced intensity noise of the signal and improve the BER performance.

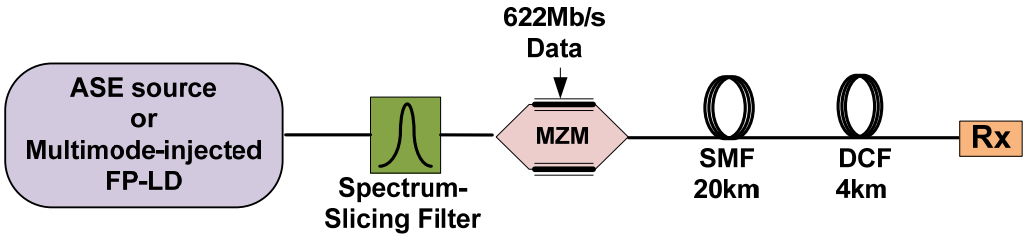

Fig. 4.17. Setup to investigate the transmission performance of a spectrum-sliced ASE and a spectrum-sliced multimode-injected FP-LD used as the optical carrier.

Fig. 4.18 shows the BER performances with the two different light sources. Compared to an ASE source, the receiver sensitivity is improved by 3.6 dB at BER of 10^{-9} with the multimode-injected FP-LD. Since the only difference between these two cases is the light source, we can conclude that the sensitivity improvement is brought by the multimode-injected FP-LD and the RIN of a spectrum-sliced ASE is suppressed after being fed into a FP-LD.

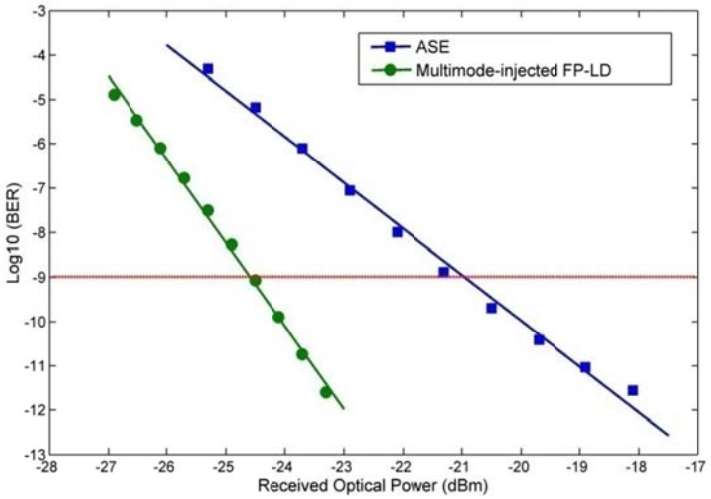

Fig. 4.18. BER performances of a spectrum-sliced ASE and a spectrum-sliced multimode-injected FP-LD used as the optical carrier.

4.4 A multimode-injected FP-LD utilized as the remote seeding source in a colorless carrier-distributed WDM-PON

It has been demonstrated that a spectrum-sliced multimode-injected FP-LD exhibits better noise performance than a spectrum-sliced ASE source. Based on this observation, the spectrum-sliced multimode-injected FP-LD is utilized as the remote seeding source to injection-lock the FP-LDs at ONUs in a colorless carrier-distributed WDM-PON system. Its transmission performance is compared with that of a colorless carrier-distributed WDM-PON with a spectrum-sliced ASE as the remote seeding source.

4.4.1 Proposed WDM-PON structure

The schematic of the proposed WDM-PON architecture is shown in Fig. 4.19. Since the proposed scheme is intended to improve the upstream transmission performance, the downlink is not included in Fig. 4.19. The downstream transmission scheme should be same with any conventional WDM-PONs.

A multimode-injected FP-LD is employed in the OLT as the remote seeding light for colorless upstream operation. The output of the multimode-injected FP-LD is delivered to the RN where the injected-locked modes from the FP-LD are separated by an AWG. The spectrum of the multimode-injected FP-LD and the AWG channels should be aligned with each other. This ensures that each of the injection-locked modes of the MI FP-LD could pass the AWG with minimum insertion loss. After being separated by the AWG, each spectrum slice is distributed to the attached ONU to injection-lock the FP-LD (FP-LD_B) resided there.

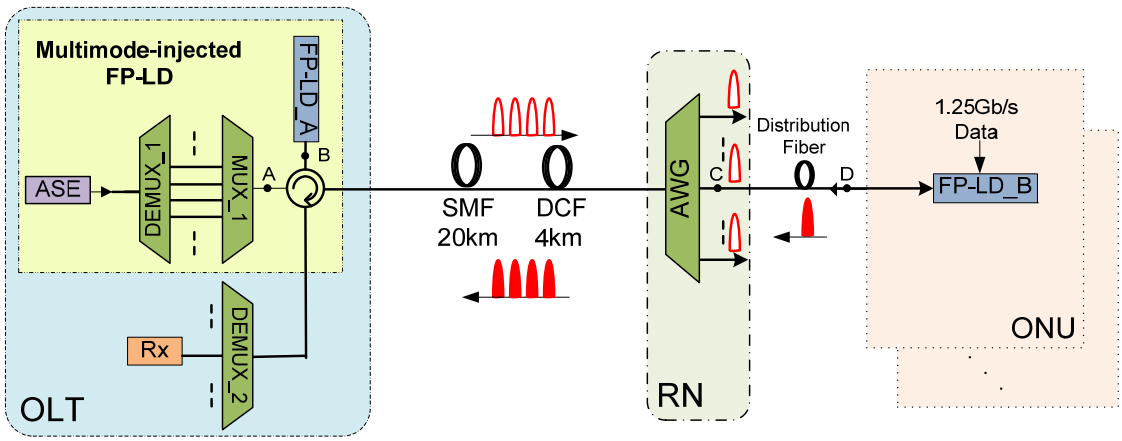

Fig. 4.19. Proposed WDM-PON architecture with the multimode-injected FP-LD as the remote seeding light (upstream transmission only).

4.4.2 Transmission performance analysis

In order to demonstrate the feasibility of using the spectrum-sliced multimode-injected FP-LD as the seeding light, the transmission performances of upstream signals generated by the directly-modulated injection-locked FP-LD with different seeding light sources are analyzed and compared. The simulation is based on the architecture shown in Fig. 4.19. Eight consecutive longitudinal modes of FP-LD_A are injection-locked by eight spectrum slices of an ASE source, which is given in Fig. 4.16 (b). The output of multimode-injected FP-LD is shown in Fig. 4.16 (c). For comparison, the transmission performance of the spectrum-sliced ASE injection-locked FP-LD is also examined by simply replacing the multimode-injected FP-LD with an ASE source. The FP-LD_B is injection-locked by a spectrum-sliced ASE or a spectrum-sliced multimode-injected FP-LD and directly modulated with 1.25 Gb/s 2^{31}-1 PRBS. The upstream signal is transmitted back to the OLT and detected by a PIN receiver after being demultiplexed by a wavelength multiplexer (DEMUX_2).

Fig. 4.20 shows the BER performance of the upstream signal. At the BER of 10^{-9}, the receiver sensitivity is -17.3 dBm when an ASE source is used as the remote seeding light, but this is improved to -21.2 dBm when the remote seeding light is a multimode-injected FP-LD. Thus, a 3.9-dB sensitivity improvement is achieved by using the proposed seeding light. Error floor at BER < 10^{-9} is observed for both cases, which is mainly attributed to the unsuppressed relative intensity noise originated from the ASE source and the back-reflection noise.

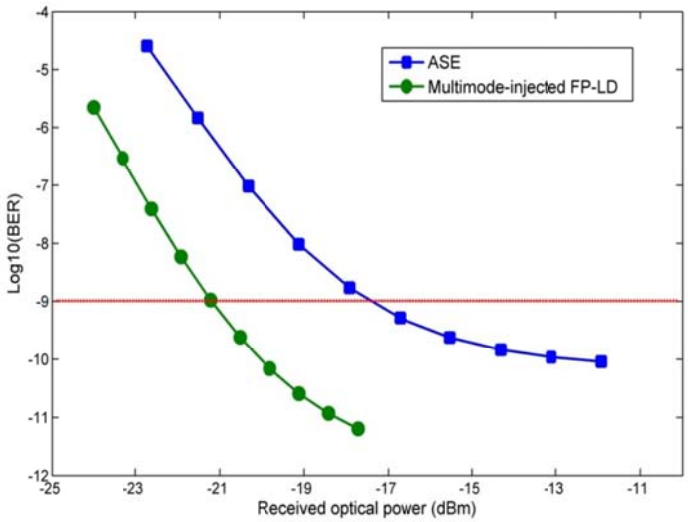

Fig. 4.20. BER performances of the injection-locked FP-LD with different remote seeding light sources.

4.5 Summary

The injection-locking of a FP-LD was theoretically analyzed and simulated. Some basic properties of FP-LDs including frequency response and polarization sensitivity were experimentally characterized. A multimode-injected FP-LD was proposed as a low-cost remote seeding source for carrier-distributed WDM-PONs. The improvement of the transmission performance of the carrier-distributed WDM-PON utilizing a spectrum-sliced multimode-injected FP-LD as the seeding source was mainly due to the fact that the RIN of a spectrum-sliced ASE could be suppressed by injected into an additional FP-LD which acts as a common noise suppressor shared by all the injected spectrum slices.

The feeder fiber was composed of 20-km SMF followed by 4-km DCF which were employed to reduce the dispersion-induced intensity noise of the seeding light. Furthermore, the filtering effect would also increase the RIN of the seeding light when it is demultiplexed by the AWG at the remote node. The intensity noise induced by filtering is inversely proportional to the bandwidth of the filter [180]. Therefore, the bandwidth of

AWG located at the RN should be a bit larger than that of the wavelength multiplexer/demultiplexer used to generate the multimode-injected FP-LD.

CHAPTER 5

Broadcast Service Delivery over a WDM-PON Based on Polarization Multiplexing

Chapters 3 and 4 focus on developing low-cost colorless light sources for WDM-PON systems. Another important research aspect is to improve the viability of WDM-PON systems by addressing issues like delivery of broadcast/multicast service. Chapters 5 and 6 are devoted to introduce two feasible techniques that enable broadcast delivery over WDM-PON architectures.

The capability of delivering broadcast/multicast services over a WDM-PON system is a desirable feature for next-generation optical access network. In this chapter, a colorless WDM-PON with broadcast capability based on polarization multiplexing (PolMUX) technique is proposed and experimentally demonstrated. The downstream unicast and broadcast data are respectively carried by two orthogonally polarized optical beams from a single light source. At each ONU, the downstream signals are injected into a FP-LD for the uplink remodulation. Unlike the scheme in [80] where the CW seeding light had to be depolarized before being injected into a polarization-sensitive FP-LD, the seeding light in our scheme consists of two uncorrelated orthogonally polarized beams which acts as a depolarized light source and hence it can constantly injection-lock the FP-LD without any polarization control. Simultaneous transmissions of 10-Gb/s downstream unicast and broadcast signals as well as the 2.5-Gb/s upstream signal are demonstrated

through experiment. Detailed analyses of injection polarization dependence, injection-locking range, and power budget are provided.

5.1 Polarization multiplexing and demultiplexing

PolMUX technique has been employed to double the capacity of long-haul transmission systems [181]. Two independent data streams could be polarization-multiplexed into the same wavelength channel by two orthogonally polarized optical beams. Due to the doubled spectral efficiency and the convenience to separate different data services, PolMUX is a potential and attractive candidate for dual-service fiber-based access networks [182]. Although polarization-mode dispersion and polarization-dependent loss (PDL) during propagation may induce the loss of orthogonality of the polarization-multiplexed signals, the signal crosstalk for a short-haul distance (e.g. 20 km) would be insignificant if optical components are carefully chosen to have low PDL.

In practical implementations, automatic polarization demultiplexing is required to separate the two polarization-multiplexed data streams at the receiver side. Automatic polarization demultiplexing is generally realized by a feedback control system, which analyzes the SOP of the incoming optical signal and generates a control signal accordingly for an electronically driven polarization controller to track the SOP of the incoming optical signal and achieve desired polarization transformation.

Recently, several potentially cost-effective automatic polarization demultiplexing schemes have been proposed and demonstrated, including (i) utilizing the radio frequency power of the detected incoming signal from a low frequency RF power detector as the control signal [183], and (ii) employing the power imbalance between the two polarization-multiplexed channels as the feedback signal [184]. These schemes simplify

the structure of the feedback systems and reduce the implementation cost by avoiding using high-speed photodetectors and electronics. A relatively low-cost electronically driven PC with response time of tens of microseconds would be enough to track the fastest polarization perturbation which is on the order of milliseconds in installed buried or aerial fibers [185-188].

Furthermore, polarization-multiplexing is a modulation format and line-rate transparent technique compared to other broadcast/multicast-enabling techniques introduced in Section 2.2. Therefore, it is a potential and attractive solution to provide broadcast services in access networks considering the doubled spectral efficiency and the flexible upgradability in both the line-rate and the modulation format of the unicast or broadcast signals.

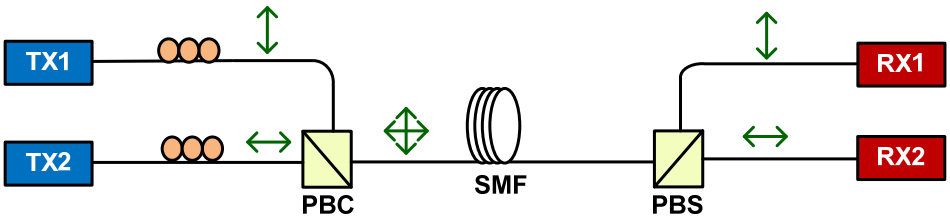

Fig. 5.1. Polarization multiplexing and demultiplexing

Fig. 5.1 illustrates the optical polarization multiplexing and demultiplexing concept. The electrical field emitted by TX1 and TX2 can be expressed as [189]:

$$\overrightarrow{E_1} = A_1 e^{i\varphi_1(t)} \hat{x} \tag{5.1}$$

$$\overrightarrow{E_2} = A_2 e^{i\varphi_2(t)} \hat{y} \tag{5.2}$$

where the parameters A_1 and A_2 are the time varying amplitudes and are different from each other, i.e., they represent different data sequences. The parameters φ_1 and φ_2 are the

time-varying phases of the two signals, respectively. Since the two signals are orthogonally polarized to each other, the output signal after transmission over a short distance can be expressed as (the attenuation is neglected):

$$\vec{E} = A_1 e^{i\varphi_1(t)}\hat{x} + A_2 e^{i\varphi_2(t)}\hat{y} \tag{5.3}$$

The transmission functions of the two output ports of the polarization beam splitter (PBS) are:

$$\vec{T_1} = \cos\theta\hat{x} + \sin\theta\hat{y} \tag{5.4}$$

$$\vec{T_2} = \sin\theta\hat{x} - \cos\theta\hat{y} \tag{5.5}$$

where the angle θ is the relative angle between the polarization of the incoming light and the polarization direction of the PBS. The output powers at the two output arms of the PBS can be expressed as:

$$\begin{aligned} P_1 &= \left|\vec{E}\cdot\vec{T_1}\right|^2 = \left|\left(A_1 e^{i\varphi_1(t)}\hat{x} + A_2 e^{i\varphi_2(t)}\hat{y}\right)\cdot\left(\cos\theta\hat{x} + \sin\theta\hat{y}\right)\right|^2 \\ &= A_1{}^2\cos^2\theta + A_2{}^2\sin^2\theta + A_1A_2\sin 2\theta\cos\left(\varphi_1(t) - \varphi_2(t)\right) \end{aligned} \tag{5.6}$$

$$\begin{aligned} P_2 &= \left|\vec{E}\cdot\vec{T_2}\right|^2 = \left|\left(A_1 e^{i\varphi_1(t)}\hat{x} + A_2 e^{i\varphi_2(t)}\hat{y}\right)\cdot\left(\sin\theta\hat{x} - \cos\theta\hat{y}\right)\right|^2 \\ &= A_1{}^2\sin^2\theta + A_2{}^2\cos^2\theta - A_1A_2\sin 2\theta\cos\left(\varphi_1(t) - \varphi_2(t)\right) \end{aligned} \tag{5.7}$$

When $\theta = 0^\circ$, $P_1 = A_1{}^2$ and $P_2 = A_2{}^2$; when $\theta = 90^\circ$, $P_1 = A_2{}^2$ and $P_2 = A_1{}^2$. The two cases correspond to the scenario when the polarizations of the orthogonally polarized signals are exactly aligned to the polarization directions of the PBS. The only difference is the two signals are switched between the two output ports.

However, θ is not always perfectly controlled to be 0° or 90° in real implementation. A slightly deviation from the perfect alignment would induce crosstalk to the demultiplexed signals from one another. Furthermore, when $\sin 2\theta \neq 0$, the output powers P_1 and P_2 will fluctuate significantly if the phases of the two electrical fields, φ_1 and φ_2, are correlated. The crosstalk induced by imperfect polarization demultiplexing could be tolerated since it is usually small when compared to the signal power. However, the severe power fluctuation resulted from the correlation between the two signals is devastating for signal detection. Therefore, it is necessary to decorrelate the two electrical fields in polarization multiplexing applications. In another word, the optical phases of the two beams should be independent from each other without a fixed phase relationship.

Decorrelation is naturally satisfied when two different light sources are adopted. If the two beams are extracted from the same laser source, the phase of one beam should be scrambled relative to the other beam. Alternatively, one of the beams should be delayed with respect to the other with a relative delay larger than the coherence length of the laser. When the two beams are uncorrelated, φ_1 and φ_2 have no phase relationship. The term $\cos\left(\varphi_1(t)-\varphi_2(t)\right)$ varies rapidly and averages to zero in a slow photodetector. Consequently, the powers in the two arms are:

$$P_1 = A_1^2 \cos^2\theta + A_2^2 \sin^2\theta \tag{5.8}$$

$$P_2 = A_1^2 \sin^2\theta + A_2^2 \cos^2\theta \tag{5.9}$$

5.2 Proposed WDM-PON architecture

This subsection describes how the polarization multiplexing technique can be applied to WDM-PON systems to enable the broadcast capability. Fig 5.2 shows the schematic of

the proposed WDM-PON architecture. At the OLT, the output of each DFB laser is first split into two equal portions by a 50/50 optical coupler. One portion is modulated by the downstream unicast data through a Mach-Zehnder modulator (MZM) and then combined with other downstream unicast signals by a wavelength multiplexer. The other portion is first combined with other channel carriers by another wavelength multiplexer and then modulated with broadcast data through another MZM. A piece of SSMF is added into one of the two branches to decorrelate the phase of the two optical beams from a single light source. The downstream unicast signals are then polarization-multiplexed with the broadcast signals by a polarization beam combiner (PBC).

The polarization-multiplexed signals are transmitted through a feeder fiber to the remote node where they are demultiplexed by a wavelength demultiplexer. At each ONU, a small portion of the downstream unicast and broadcast signals are polarization-demultiplexed by a PBS and detected separately. The remaining is fed into a FP-LD which is directly modulated with the upstream data. After being multiplexed, the respective upstream signals are transmitted back to the OLT through the same feeder fiber and detected by upstream receivers.

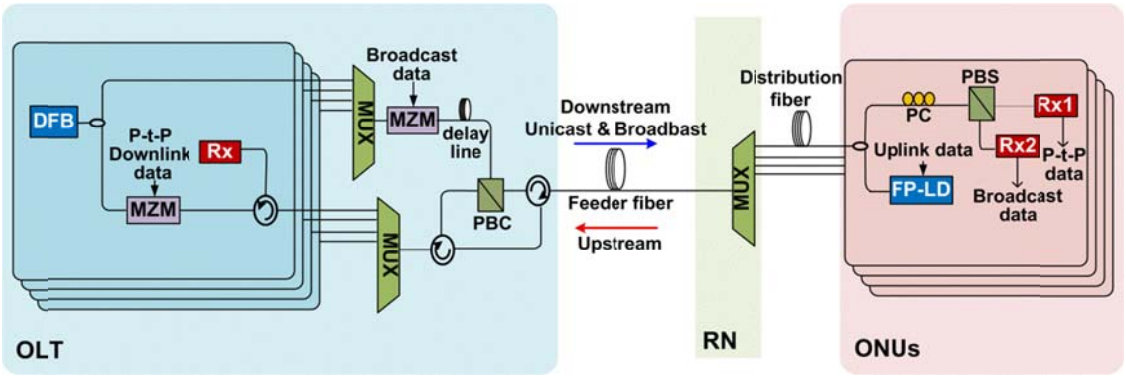

Fig. 5.2. Proposed WDM-PON architecture providing broadcast service based on polarization multiplexing technique.

It is noted that in this architecture the FP-LD is injection-locked by the polarization-multiplexed depolarized light rather than by the polarization-demultiplexed polarized light from one of the PBS outputs. A question may be raised that why not utilize the polarized light from one of the two PBS outputs as the external injection light. Although the FP-LD is polarization-sensitive, the polarization of the light coming out from the PBS could be controlled with the existence of the automatic polarization demultiplexing device in the ONU.

The reason of adopting the polarization-multiplexed depolarized light as the injection light is to decouple the upstream operation from the downstream operation and also to avoid the power loss induced by automatic polarization demultiplexing. As will be discussed later, the power budget of the proposed scheme is limited by the minimum required seeding power of the FP-LD and thus the proposed scheme is designed to maximize the injection power into the FP-LD. Another reason lies in that the proposed scheme allows us to utilize FP-LDs pigtailed with conventional SSMF instead of polarization-maintaining fiber (PMF). Since the use of PMF always involves complicated alignment procedure during device packaging, the proposed scheme will help to lower the implementation costs of FP-LDs.

5.3 Experimental setup and results

The feasibility of the proposed scheme is demonstrated by the experimental setup shown in Fig. 5.3. A CW light from a DFB laser at 1545.1 nm is split into two equal portions by a 50/50 optical coupler. The two beams are modulated with 10-Gb/s PRBS data streams with a pattern length of 2^{31}-1, representing the respective unicast and broadcast data, through two separate MZMs. A polarization controller (denoted as PC1 or PC2 in Fig.

5.3) is inserted in each branch to align the SOP of the optical beam to one of the principal axes of the PBC independently.

A 1-km optical fiber is added into one of the branches. The length is long enough to effectively decorrelate the phase of the two optical beams coming from the 5-MHz linewidth DFB laser. A variable attenuator is employed in one branch to equalize the powers of the two optical beams before the PBC. This would minimize the degree of polarization of the combined downstream signals. The polarization-multiplexed signals are transmitted through a 20-km SSMF feeder fiber.

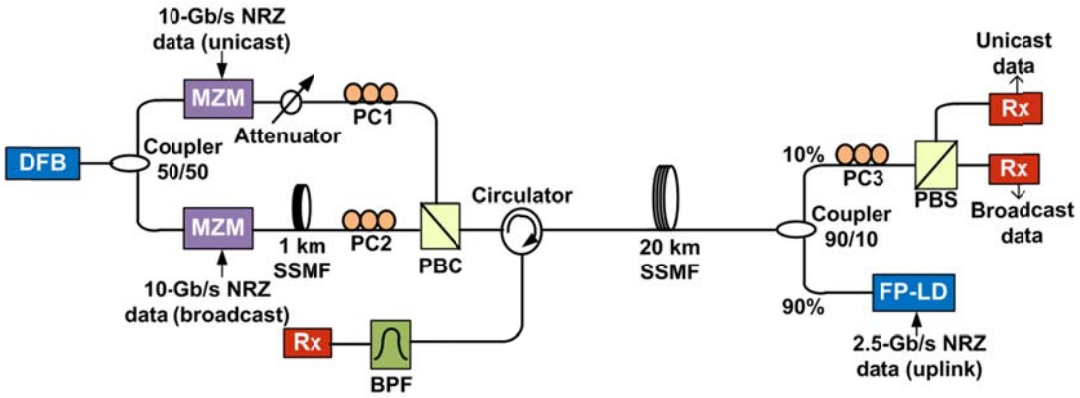

Fig. 5.3. Experimental setup

At the ONU, the downstream signals are divided into two portions by a 90/10 optical coupler. The small portion is polarization-demultiplexed by a PBS. The PC (i.e., PC3) before the PBS is adjusted to ensure at least 30 dB polarization extinction ratio for each polarization component. The downstream unicast and broadcast signals are detected and recovered by 10-Gb/s APD receivers separately. The large portion is fed into a FP-LD which is directly-modulated with a 2.5-Gb/s NRZ PRBS with a pattern length of 2^{31}-1. The FP-LD with a threshold current of 17 mA is biased at 30 mA. The seeding power

is -13 dBm from each polarization component and therefore the total injection power is -10 dBm.

After injection, the upstream signal is transmitted back to the OLT through the same feeder fiber and detected by a 2.5-Gb/s APD receiver. The depolarized seeding light helps to reduce the Rayleigh backscattering-induced crosstalk in the single-fiber loopback configured network since the beating between the signal and the Rayleigh backscattering is polarization-sensitive. An optical filter with a flat-top passband whose 3-dB bandwidth is 0.4 nm is used before the receiver to emulate an AWG in the OLT. The insertion loss of the BPF is around 1.5 dB.

5.3.1 Analysis of polarization dependence

When an external light is injected into a polarization-sensitive FP-LD, the output of the FP-LD is dependent on the SOP of the seeding light [88]. Thus, the seeding light should be depolarized before entering the FP-LD to achieve stable injection-locking. A polarimeter is employed to measure the DOP of various light sources. The DOP of the DFB laser is around 100%; whereas the DOP of an ASE source generated by an EDFA fluctuates between 2-5%.

The setup shown in Fig. 5.4 is used to measure the DOP of the seeding light in our proposed scheme. When the 1-km optical fiber delay line is removed, the two input light of the PBC are still correlated and therefore the DOP of the combined light is nearly 100% and the SOP changes dramatically. When the 1-km optical fiber delay line is present, since it decorrelates the two polarization-multiplexed optical beams, the DOP of the combined light is reduced to ~4%.

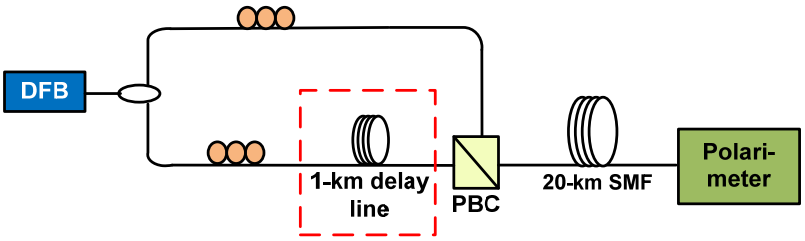

Fig. 5.4. Setup for DOP measurement.

A spectral comparison of the FP-LD injection-locked by different seeding sources is carried out. The corresponding optical spectra are shown in Fig. 5.5. Fig. 5.5 (a) is the optical spectrum of the free-running FP-LD and Fig. 5.5 (b) shows the optical spectra of the polarized (solid line) and depolarized (dash line) seeding light, respectively. Fig. 5.5 (c) and (d) show the measured optical spectra of the FP-LD output when the SOP of the seeding light is changed from TE-aligned to TM-aligned, confirming high polarization dependence when a polarized light is used as the seeding source. When the linearly polarized seeding light is aligned to the TE mode of the FP-LD, it would injection-lock the FP-LD. The injection-locked mode is amplified and the others are suppressed as shown in Fig. 5.5 (c); when the linearly polarized seeding light is aligned to the TM mode of the FP-LD, it is absorbed by the FP-LD, as shown in Fig. 5.5 (d).

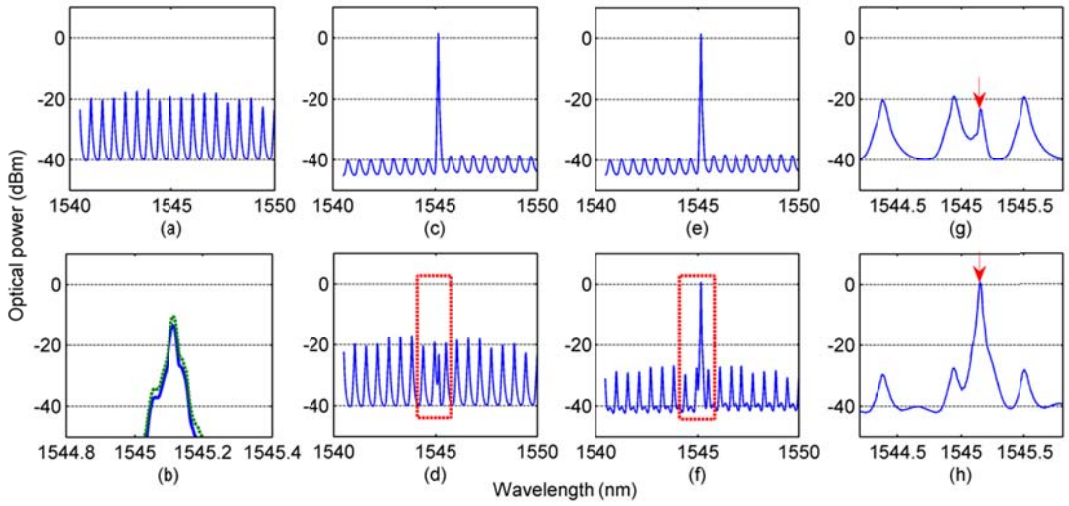

Fig. 5.5. Measured optical spectra of (a) free-running FP-LD, (b) the polarized (solid line) and depolarized (dash line) seeding light sources, (c) FP-LD injected by TE-mode-aligned polarized seeding light, (d) FP-LD injected by TM-mode-aligned polarized seeding light, (e) FP-LD injected by depolarized seeding light with the best polarization alignment, (f) FP-LD injected by depolarized seeding light with the worst polarization alignment, (g) and (h) are close look of the spectra in the dotted rectangles of (d) and (f), respectively (the arrows indicate where the seeding light sources are located).

A quantitative investigation of the polarization dependence of injection-locking the FP-LD is carried out and the results are given in Fig. 5.6. In this experiment, the polarization direction of the linearly polarized seeding light is rotated from the TE to the TM mode of the FP-LD while the seeding power is maintained at -13 dBm. θ denotes the angle between the polarization direction of the seeding light and the TE mode of the FP-LD. Thus, $\theta = 0°$ means the seeding light is TE-mode-aligned whereas the seeding light is TM-mode aligned when $\theta = 90°$. The gain of the seeding light provided by the FP-LD and the corresponding SMSR are measured at the output of the FP-LD with different angles θ.

Here, the SMSR is defined as the power ratio between the main mode, i.e., the injection-locked mode, and the highest longitudinal side mode at the output of the FP-LD with external injection. The results clearly exhibit high polarization dependence of the

FP-LD. For example, the polarization dependence gain of the device, a gain difference between $\theta = 0°$ and $\theta = 90°$, is measured to be 19.2 dB. The SMSR is also degraded as the polarization of the seeding light is changed from the TE-aligned to TM-aligned. As shown in Fig. 5.6, the angle θ should be smaller than 50° to keep the SMSR greater than 30 dB.

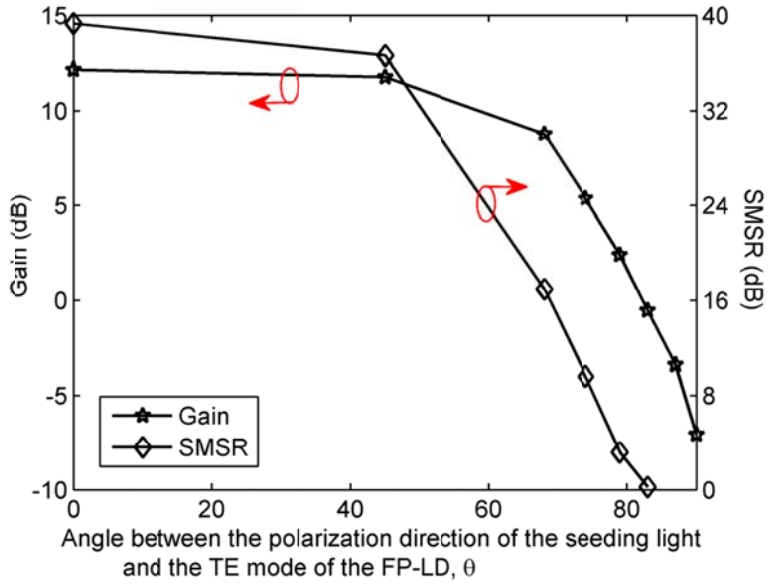

Fig. 5.6. Charaterization of the polarization dependence of the FP-LD when linearly polarized light is used as the seeding source.

In contrast, the seeding light in our proposed scheme, consisting of two uncorrelated orthogonally linearly polarized optical beams, could injection-lock the FP-LD constantly. Fig. 5.5 (e) and (f) depict the spectra of the FP-LD externally injected by the proposed seeding light with the best and the worst polarization alignment in terms of SMSR, respectively. Note that a small polarization dependence could still be observed due to the non-zero DOP of the seeding source. For example, the SMSRs are 39.7 dB with the best polarization alignment (also referred to as the best case) and 27.4 dB with the worst polarization alignment (also referred to as the worst case). This SMSR

degradation induced by polarization dependence could deteriorate the signal's performance since the relative intensity noise is inversely proportional to the SMSR [190].

To investigate how much the SMSR degradation affects the bit-error rate performance of the upstream signal, we have measured the BERs under these two cases and plotted them in Fig. 5.7. After transmission over 20-km SMF, the receiver sensitivity at the BER of 10^{-9} is -30.4 dBm in the best case. An error floor at ~10^{-8} is observed in the worst case but error-free transmission could still be achieved by using forward error correction. The receiver sensitivities (at BER of 10^{-4}) are -36.1 dBm for the best case and -34.0 dBm for the worst case, which implies that only 2.1 dB power penalty is induced by the polarization dependence.

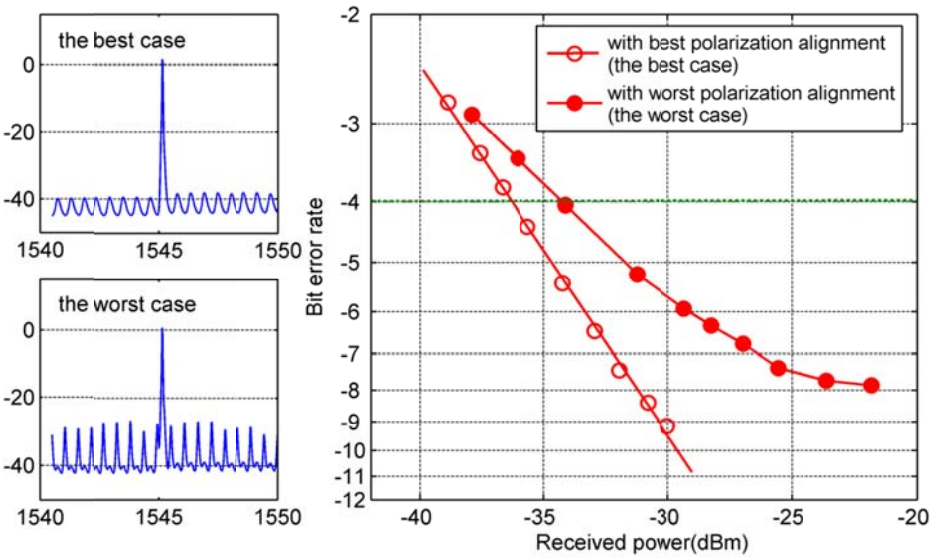

Fig. 5.7. The best and worst BER performance of the upstream signal when the wavelength offset is 0.21 nm (The dash-dot line shows the FEC threshold).

5.3.2 Analysis of wavelength offset

The FP-LD used in the experiment has a weak-resonant cavity. The front-facet and rear-facet reflectivity are 1% and 99%, respectively. The highly asymmetric coating design

increases the seeding efficiency and reduces the power leakage at the rear-facet [191]. The weak-resonant-cavity FP-LD exhibits wider injection-locking range compared to conventional FP-LDs.

The longitudinal mode spacing of the free-running FP-LD is 0.56 nm. The wavelength offset$\left(\lambda_{SE}-\lambda_{FP}\right)$, where λ_{SE} is the wavelength of the seeding light and λ_{FP} is the wavelength of the reference longitudinal mode of free-running FP-LD, is tuned from 0 to 0.56 nm in our experiment. Fig. 5.8 includes a series of the optical spectra of the injection-locked FP-LD at the best polarization alignment with different wavelength offsets.

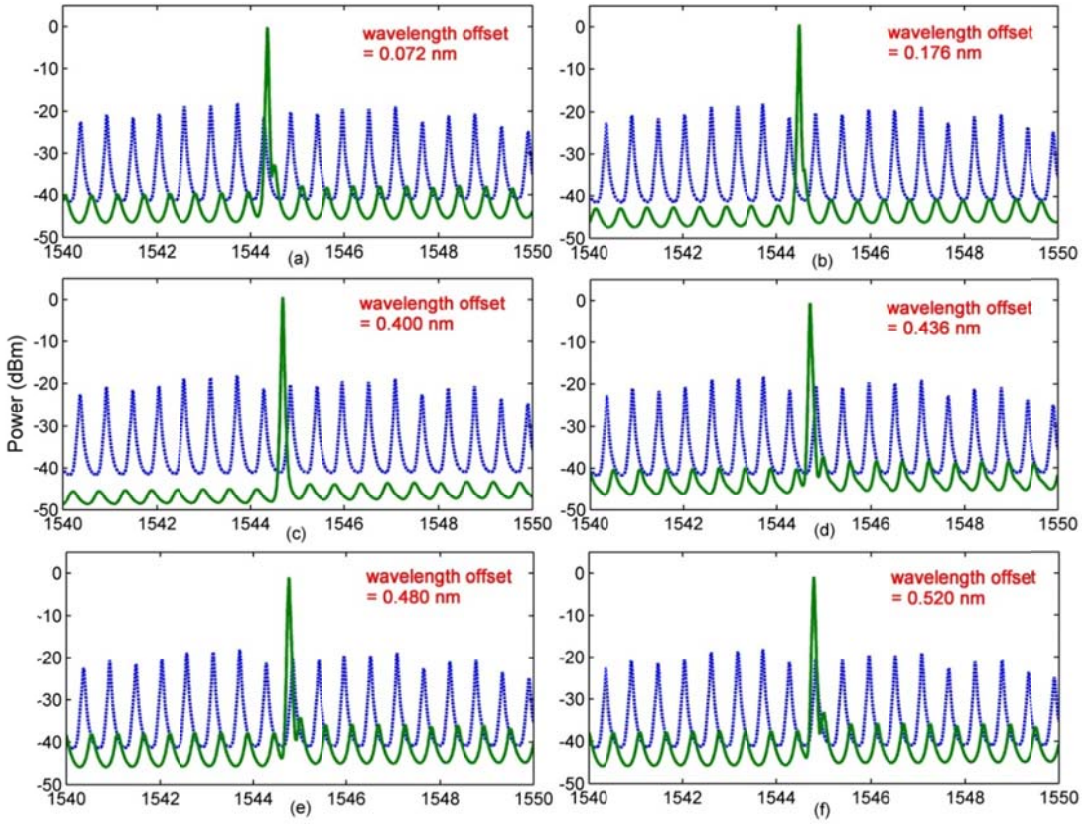

Fig. 5.8. Optical spectra of the injection-locked FP-LD with different wavelength offsets (dotted line: free-running FP-LDs; solid line: injection-locked FP-LDs).

As each subplot demonstrated, the wavelength spectrum would shift to the longer wavelength side after injection-locking. A relative larger SMSR is obtained when the wavelength offset is between 0.2-0.4 nm approximately and thus results in a better BER performance. When the seeding light locates close to one of the free-running longitudinal modes, i.e., the wavelength offset is smaller than 0.2 nm or larger than 0.4 nm, the SMSR becomes smaller and the BER performance is degraded.

The power penalties of the upstream signal at BER of 10^{-4} as a function of wavelength offset are measured with best and worst polarization alignment, respectively. As illustrated in Fig. 5.9, the best receiver sensitivity is obtained when the wavelength offset is 0.21 nm whereas the largest sensitivity penalty is observed at a wavelength offset of 0.52 nm. Nevertheless, the power penalties are less than 3.5 dB throughout the whole detuning range regardless of the polarization alignment. Note that the worst polarization alignment has a receiver sensitivity 2.1 dB poorer than the best polarization alignment. Therefore, the worst case (i.e., a wavelength offset of 0.52 nm with the worst polarization alignment) gives rise to a maximum power penalty of 5.6 dB, which still makes the uncooled operation of the FP-LD feasible since the upstream power margin at BER of 10^{-4} is more than 20 dB as discussed later.

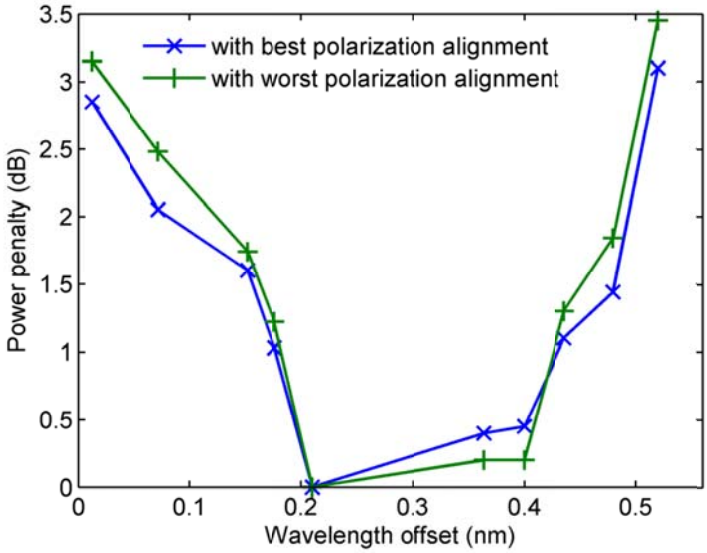

Fig. 5.9. Power penalty of the upstream signal at BER of 10^{-4} versus the wavelength offset.

5.3.3 Trade-off between downlink and uplink

In the proposed WDM-PON architecture, a trade-off exists between the downstream and the upstream receiver sensitivities. The crosstalk induced by the unsuppressed injected downstream data reduces the SNR of the upstream signal [85]. The power penalties of both the downstream and upstream (with best polarization alignment) receiver sensitivities at the BER of 10^{-9} with different downstream extinction ratios are measured and depicted in Fig. 5.10. For upstream measurement, the optical power of the depolarized seeding light is kept at -10 dBm and the wavelength offset is 0.21 nm.

Better downstream BER performance requires higher downstream ER whereas the power penalty for the upstream increases with the downstream ER. In our experiment, when the ER of the downstream signal is about 6 dB, an error floor at ~10^{-9} is observed for the upstream signal; when the ER is increased to 10 dB, the FP-LD could not be injection-locked by the seeding light due to the inadequate seeding power during the

spaces (bit “0”s). Therefore, the ER of the downlink signal has to be sacrificed to constantly injection-lock the FP-LD and achieve error-free upstream transmission.

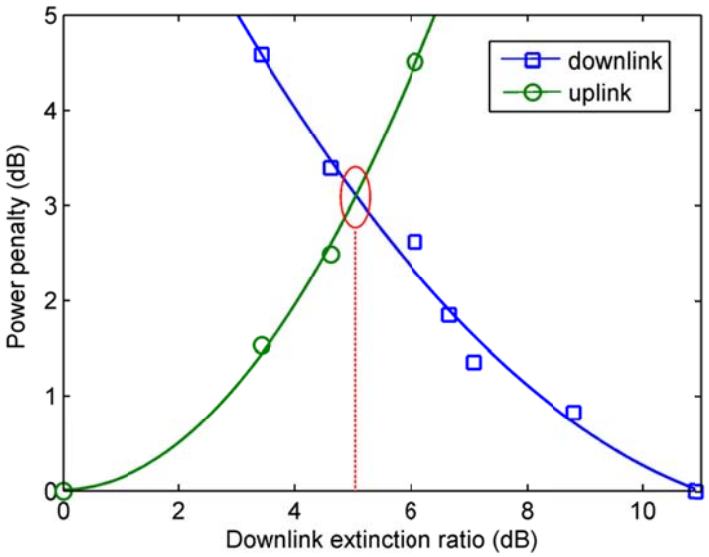

Fig. 5.10. Receiver power penalties at BER of 10^{-9} of the downstream and upstream signals with different downstream ERs.

Fig. 5.11 and Fig. 5.7 show the BER performance of the downstream and upstream signals, respectively, when the ER of the downstream signal is 5 dB, at which the power penalties of the downlink and uplink signal are both around 3 dB as shown in Fig. 5.10. The receiver sensitivities at the BER of 10^{-9} are -21.4 dBm for the downstream unicast signal and -21.5 dBm for the downstream broadcast signal. Compared to the back-to-back BER performance, the power penalty induced by 20-km SSMF transmission is measured to be 0.7 dB. By comparing the transmission performances of the downstream unicast signal with and without the broadcast service (i.e., cutting off the lower arm of the PBC in Fig. 5.3), the power penalty induced by polarization multiplexing is 0.2 dB.

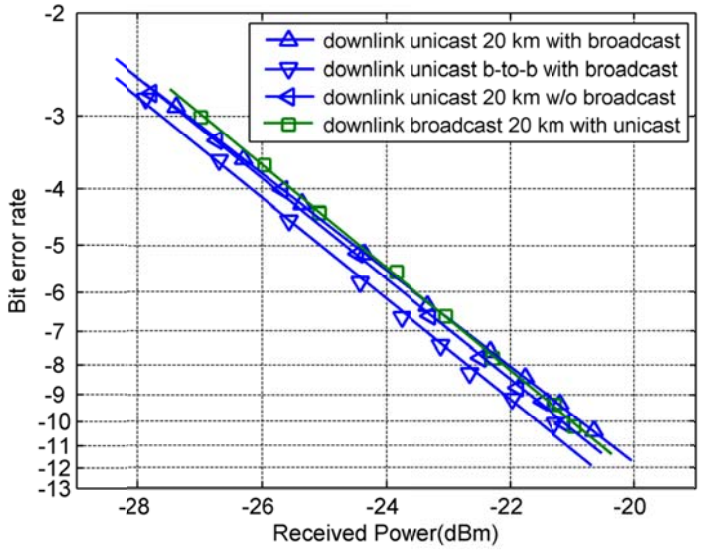

Fig. 5.11. BER performances of the downstream unicast and broadcast signals.

5.3.4 Effect of bit alignment

Lastly, the effects of the relative bit delay between the downstream unicast and broadcast data on the downstream and upstream performance are investigated. Since the power penalty of the downstream unicast signal induced by the polarization multiplexing technique is measured to be 0.2 dB, as long as the high polarization extinction ratio is satisfied when the downstream unicast and broadcast signals are polarization demultiplexed by a PBS, the crosstalk from the other polarization beam is insignificant regardless of the value of the relative bit delay. However, the relative bit delay affects how fast the seeding power fluctuates, which originates from the unsuppressed downlink modulation. Therefore, the upstream performance might be affected by the relative bit delay between the downstream unicast and broadcast data.

Fig. 5.12 shows the upstream receiver sensitivity (with best polarization alignment) at BER of 10^{-9} versus the relative bit delay. In this measurement, a tunable optical delay line is inserted between the 1-km SSMF and PC2 to adjust the relative bit delay. The

result shows that the upstream transmission performance is hardly influenced by the relative bit delay. Therefore, the proposed scheme is very robust against the bit alignment between the two downstream data.

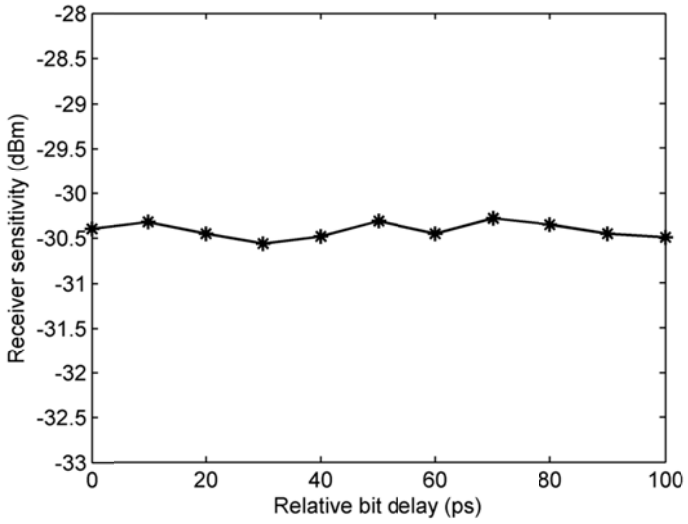

Fig. 5.12. Upstream receiver sensitivity at BER of 10^{-9} with best polarization alignment versus the relative bit delay.

5.3.5 Power budget

The power budget analysis for the proposed WDM-PON architecture is given in Table 5.1. For downlink, the receiver sensitivity of the unicast or broadcast signal is around -21 dBm but the required seeding power from the downstream unicast or broadcast signal is -13 dBm. Therefore, the downstream power budget is primarily limited by the minimum required seeding power of the FP-LD. The power of the downstream unicast or broadcast signal reaching the ONU should be at least -10 dBm to meet the power requirement of both the downstream detection and the external seeding for upstream remodulation simultaneously, considering the power loss induced by the 90/10 optical coupler, PC3 and PBS in the ONU. Thus, the minimum launch power of the downstream unicast or

broadcast signal from the OLT should be around -0.8 dBm considering the 9.2 dB link loss, including the wavelength multiplexer, the feeder fiber, and others.

For uplink, the launch power of injection-locked FP-LD is measured to be 2.4 dBm (with worst polarization alignment) and the link loss is around 16 dB. We could obtain 20.4-dB power margin for upstream transmission when the worst case of upstream BER performance at the FEC threshold (10^{-4}) is considered.

Table 5.1. Power budget analysis of the proposed WDM-PON scheme

<table>
<tr><th colspan="3">Downstream (unicast or broadcast signal)</th><th colspan="2">Upstream</th></tr>
<tr><td colspan="2">Minimum required power reaching ONU</td><td>-10 dBm</td><td rowspan="2">Receiver sensitivity
(worst case at BER of 10^{-4})</td><td rowspan="2">-34.0 dBm</td></tr>
<tr><td>Receiver sensitivity (-21 dBm)
90/10 coupler (10 dB)
PC & PBS (1 dB)</td><td>Seeding power per polarization (-13 dBm)
90/10 coupler (0.5 dB)</td></tr>
<tr><td colspan="2" rowspan="2">Total link loss
(excluding loss in OLT and ONU)</td><td rowspan="2">9.2 dB</td><td>FP-LD launch power
(worst case)</td><td>2.4 dBm</td></tr>
<tr><td>Total loss</td><td>16 dB</td></tr>
<tr><td colspan="2">Mux/Demux (in remote node)
Fiber
Connectors and others</td><td>4
4.2
1</td><td>Mux/DeMux
Fiber
Circulator
Connectors and others</td><td>4×2
4.2
0.6×3
2</td></tr>
<tr><td colspan="2">Minimum launch power of unicast or broadcast signal from the OLT</td><td>-0.8 dBm</td><td>Power Margin</td><td>20.4 dB</td></tr>
</table>

5.4 Summary

This chapter introduced a full-duplex WDM-PON architecture providing both unicast and broadcast services by employing polarization multiplexing technique. The downlink signals consisting of two uncorrelated, orthogonally polarized beams were used as the seeding light to injection-lock a polarization-sensitive FP-LD for upstream remodulation without any polarization control. Experimental demonstration of successful transmission of 10-Gb/s downstream unicast and broadcast signals with low ER as well as 2.5-Gb/s upstream signal with FEC confirmed the feasibility of the proposed architecture. Several technical issues including injection-locking polarization dependence, wavelength offset,

and performance tradeoff between downlink and uplink were investigated. The power budget might be constrained by the required seeding power of FP-LDs. This could be overcome by using an optical amplifier to amplify the downstream signals or improving the seeding efficiency of FP-LDs. It was also experimentally verified that the weak-resonant-cavity FP-LD possessed a wide injection-locking range which enabled uncooled operation of ONUs.

CHAPTER 6

A Broadcast-Capable WDM-PON Based on Offset Polarization Multiplexing with Improved Cost-Effectiveness

We have introduced a WDM-PON architecture providing broadcast overlay by exploiting polarization multiplexing technique in Chapter 5 [87]. In this WDM-PON architecture, the downlink unicast and broadcast data are carried by two orthogonally polarized optical beams from a single light source, respectively. Not only does this technique support broadcast services without allocating additional wavelength channels and using high-frequency SCM modulation, but it also depolarizes the seeding light which can constantly injection-lock the FP-LD in the ONU for upstream transmission. Therefore, the proposed scheme can be applied to low-cost polarization-sensitive colorless upstream optical transmitters. However, active polarization tracking is required to demultiplex the two polarization-multiplexed signals at each ONU, which may hinder the real deployment of such a system.

To eliminate the need for active polarization tracking, a new WDM-PON architecture in which offset polarization multiplexing is exploited to support broadcast capability has been proposed. This chapter gives a thorough introduction to the proposed scheme. The DPSK-formatted downstream unicast and broadcast signals whose wavelengths are slightly different from each other are combined through polarization multiplexing. At each ONU, the downstream DPSK-formatted unicast and broadcast

signals are demultiplexed and demodulated by two DPSK demodulators without any need of active polarization tracking. The scheme also completely depolarizes the seeding light for the upstream FP-LDs, which enables constant injection-locking of the polarization-sensitive FP-LDs.

Simultaneous transmissions of 10-Gb/s downstream unicast and broadcast DPSK signals as well as 2.5-Gb/s upstream OOK signal are experimentally demonstrated. The effects of Rayleigh backscattering, remodulation crosstalk, polarization fluctuation along the link, relative bit delay between the unicast and broadcast signals, frequency deviation of the downstream signals from the delay interferometer (DI), and imperfection of the DI on the transmission performances of the downstream and upstream signals are investigated in detail by both experiments and simulations.

6.1 Offset polarization multiplexing and demultiplexing

In the offset polarization multiplexing scheme, two DPSK-formatted optical signals separated by a frequency offset, f_{offset}, are polarization-multiplexed at the transmitter. At the receiver, they are demultiplexed and demodulated by two delay interferometers preceded by an optical coupler, without using any active polarization tracking and polarization beam splitters [192].

In DPSK reception, a sensitivity penalty arises when the laser frequency deviates from the DI frequency (i.e., the frequency at a transmission peak or transmission null). The frequency deviation (δf) between the input signal and the DI is related to the phase deviation through $\delta\phi=2\pi\cdot\delta f\cdot T_{DI}$, where T_{DI} is the time delay within the DI [193]. Penalty-free detection of DPSK signal is achieved when the phase deviation is a integer multiple

of π, whereas phase deviation of an odd multiple of π/2 completely closes eye opening of the detected signal, leading to infinite power penalty, as depicted in Fig. 6.1.

Therefore, if two offset polarization-multiplexed DPSK-formatted signals are separated by odd multiples of $1/(4T_{DI})$ in frequency (i.e., $f_{offset} = (2N\text{-}1)/(4T_{DI})$, where N is an integer) and one of the optical DPSK signals is aligned to a DI having a FSR of $1/T_{DI}$, then this optical DPSK signal can be demodulated by the DI with zero power penalty induced by frequency deviation, whereas the other optical DPSK signal, whose phase deviation from the DI equals to an odd multiples of π/2, would experience infinite power penalty and a complete eye closure is observed at the DI output consequently.

As illustrated in Fig. 6.1, the optical signal with phase deviation of zero (represented by the solid arrow) can be detected with minimum crosstalk from the other optical signal located $1/(4T_{DI})$ away (represented by the dot-dashed arrow). It is noted that the orthogonality between the two optical signals resulted from the polarization multiplexing technique helps to make the crosstalk added *in power* rather than *in E-field*. This substantially reduces the deleterious effects of crosstalk. For the detection of the other optical signal, we need another DI which is aligned to this optical signal with a zero phase deviation.

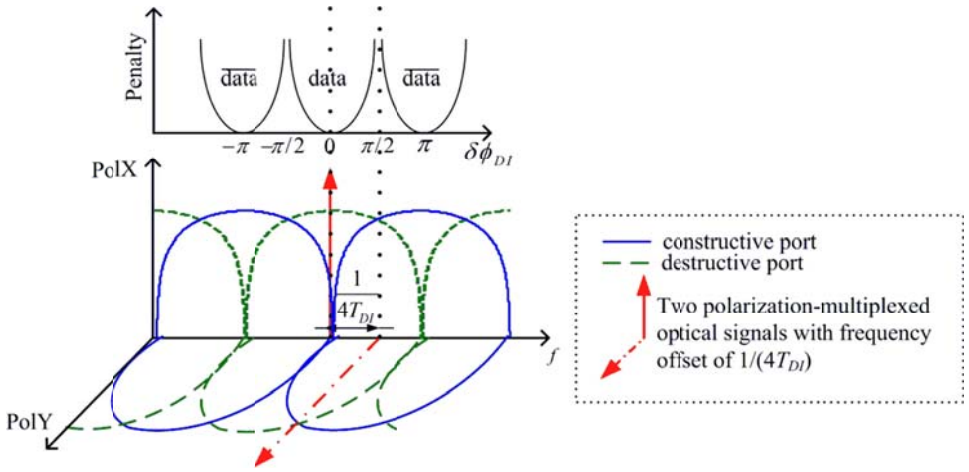

Fig. 6.1. Operation principle of demultiplexing/demodulation of the offset polarization-multiplexed DPSK signals. In this figure, the x-polarized signal is to be detected and thus the y-polarized signal becomes crosstalk to the x-polarized signal. To detect the y-polarized signal, we need another DI whose peak or null is aligned to the center wavelength of the y-polarized signal.

6.2 Proposed WDM-PON architecture

The schematic of the proposed WDM-PON architecture using offset polarization multiplexing is shown in Fig. 6.2. In the OLT, two DFB lasers separated by odd multiples of $1/(4T_{DI})$ in frequency are assigned to deliver the unicast and broadcast services, respectively, for each ONU. Each downstream unicast carrier is encoded with the unicast data in DPSK format through a dedicated MZM. After that, they are combined by a wavelength multiplexer. The downstream broadcast carriers are first combined by another wavelength multiplexer and then modulated with a common MZM driven by the broadcast data in DPSK format simultaneously. The downstream unicast signals are polarization-multiplexed with the broadcast signals using a polarization beam combiner.

The offset polarization-multiplexed signals are transmitted through a feeder fiber to the RN where they are wavelength-demultiplexed by an AWG. At each ONU, a portion of the downstream signals is divided into two equal parts for respective downstream unicast and broadcast detections. The other portion is injected into a FP-LD to enable the

upstream transmission. The upstream signal is wavelength-multiplexed at the RN and transmitted back to the OLT through the same feeder fiber and detected by the upstream receivers at the OLT.

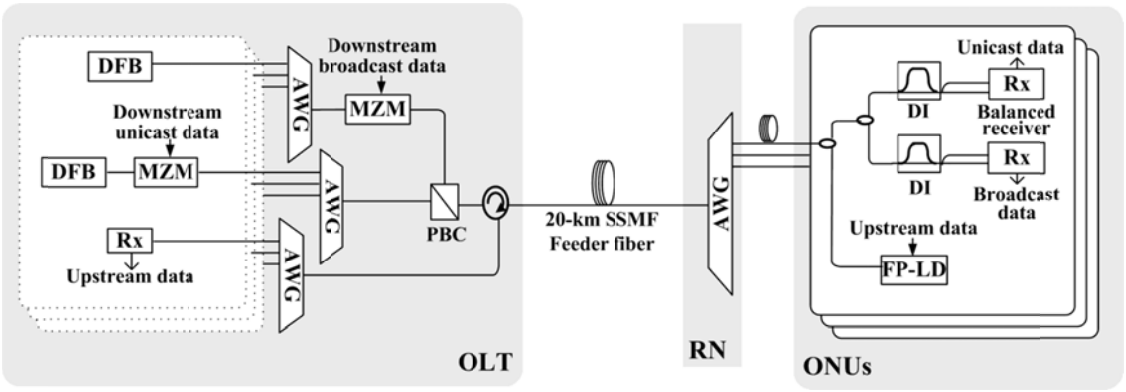

Fig. 6.2. Schematic of the proposed WDM-PON architecture using offset polarization multiplexing.

In the proposed broadcast-enabled WDM-PON architecture shown in Fig. 6.2, two sets of DFB lasers separated by f_{offset} are employed for unicast and broadcast deliveries, respectively. An alternative approach, which can reduce the complexity and implementation cost, is to simultaneously generate the broadcast carriers by frequency-shifting a portion of each of the unicast carriers by an amount of f_{offset} through subcarrier modulation using one optical single-sideband modulator (OSSBM) [194].

As shown in Fig. 6.3, the OSSBM is driven by an electrical sinusoidal signal with a frequency of f_{offset}, resulting in single-sideband carrier-suppressed signals whose frequencies differ from their respective original carriers by an amount of f_{offset}. These resultant single-sideband carrier-suppressed signals serving as the broadcast carriers are then fed into another MZM and modulated with broadcast data in DPSK format. In this way, only one set of DFB lasers are required in the OLT.

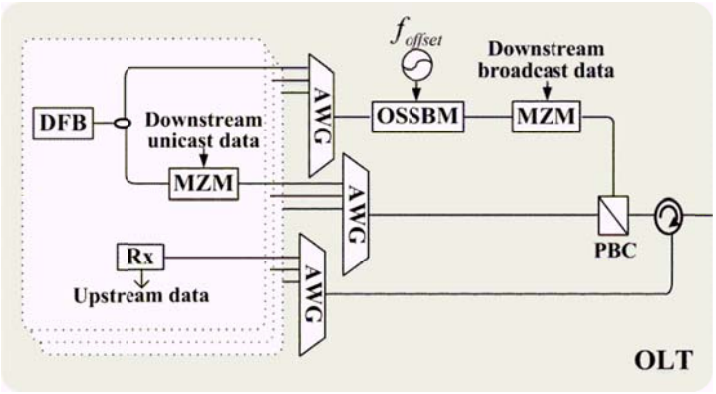

Fig. 6.3. An alternative structure of the OLT for the proposed WDM-PON scheme.

Two DIs in each ONU would increase the cost at customer premises. However, the additional cost incurred by two DIs in each ONU could be justified by the increased capacity brought by the proposed scheme. It doubles the spectral efficiency without doubling the line rate, or employing complicated higher-order modulation formats, or using active polarization tracking for polarization demultiplexing. It accommodates more end users than the scheme which assigns additional wavelengths to deliver broadcast services [110]. It eliminates the performance tradeoff between the downstream and upstream signals and the need of bit synchronization between the unicast and multicast data existed in the systems employing two orthogonal modulation formats [116]. Moreover, the DPSK receivers could be implemented in compact and cost-effective manners, e.g. using silicon semiconductor manufacturing technology [195, 196].

6.3 Experimental setup and transmission performance analyses

The experimental setup to demonstrate the proposed scheme and to characterize the transmission performances is depicted in Fig. 6.4. A DFB laser (LD1) and a tunable laser (LD2) are separately modulated through two MZMs. The frequency offset (f_{offset}) between the two lasers is set to be $(2N\text{-}1)/(4T_{DI})$, where T_{DI} = 100 ps in the experiment, by tuning

the wavelength of the tunable laser. The modulators are biased at their transmission nulls for phase modulation and driven by two 10-Gb/s 2^{31}-1 NRZ decorrelated pseudo-random binary sequences representing the downstream unicast and broadcast data, respectively. A differential encoder is not employed in the experiment since differentially coded PRBS is simply a time-delayed replica of the PRBS [193].

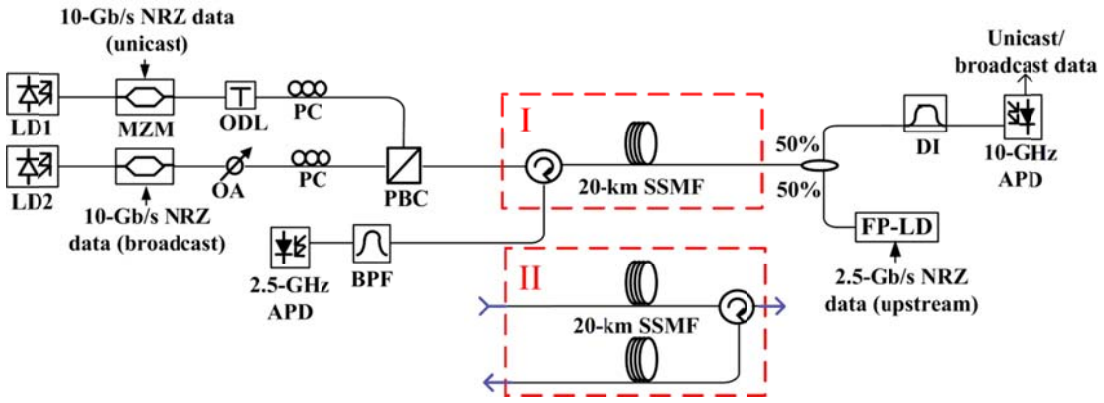

Fig. 6.4. Experimental setup in (I) single-feeder-fiber bidirectional configuration and (II) two-feeder-fiber unidirectional configuration (only used for investigating the RB-induced power penalty).

A tunable optical delay line is added to one of the signal paths before the PBC to study the effect of the relative bit delay between the two downstream data on the system performance. One PC is employed on each of the two PBC arms and it is adjusted to align the SOP of the optical signal to the principal axis of the PBC. As explained before, the reason for combining the downstream unicast and broadcast signals by a PBC instead of an optical coupler is that the orthogonality between the two signals is essential in this scheme to minimize the crosstalk from one another generated during demodulation. Meanwhile, the orthogonality could also minimize the DOP of the combined signal which would be utilized as the seeding light.

The powers of the two signals are equalized at the output of the PBC by a variable optical attenuator. It would balance the BER performance of the downstream unicast and broadcast signals and also help to minimize the DOP of the offset polarization-multiplexed downstream signals to facilitate the external seeding of the polarization-sensitive FP-LD used for upstream transmission.

The offset polarization-multiplexed downstream signals are transmitted through a 20-km SSMF. At the ONU, the downstream signals are divided into two portions by a 50/50 optical coupler, one for downstream detection and the other for upstream remodulation. The DPSK receiver is composed of a DI with a 10-GHz FSR and a10-Gb/s APD single-ended receiver. A single DPSK receiver is used to detect either the unicast or broadcast data. In a real implementation, two DPSK receivers are needed for each ONU to detect the unicast and broadcast signals simultaneously.

The other portion of the downstream signal is fed into a polarization-sensitive FP-LD which is directly-modulated by a 2.5-Gb/s NRZ PRBS with a pattern length of 2^{31}-1. The FP-LD is an uncooled device housed in a transistor-outlook-can package. The seeding power is -10 dBm and there is no polarization controller inserted between the optical coupler and the FP-LD. After injection, the upstream signal is transmitted back to the OLT through the same feeder fiber and detected by a 2.5-Gb/s APD receiver. An optical BPF having a 3-dB bandwidth of 40 GHz is utilized before the upstream receiver to emulate an AWG at the OLT.

6.3.1 Effect of the frequency offset

In our single-ended detection, we utilize the destructive port of the DI. This is because the return-to-zero-like waveform from the destructive port exhibits better receiver

sensitivity than the signal from the constructive port [197]. Fig. 6.5 shows the BER performance of the downstream unicast and broadcast signals.

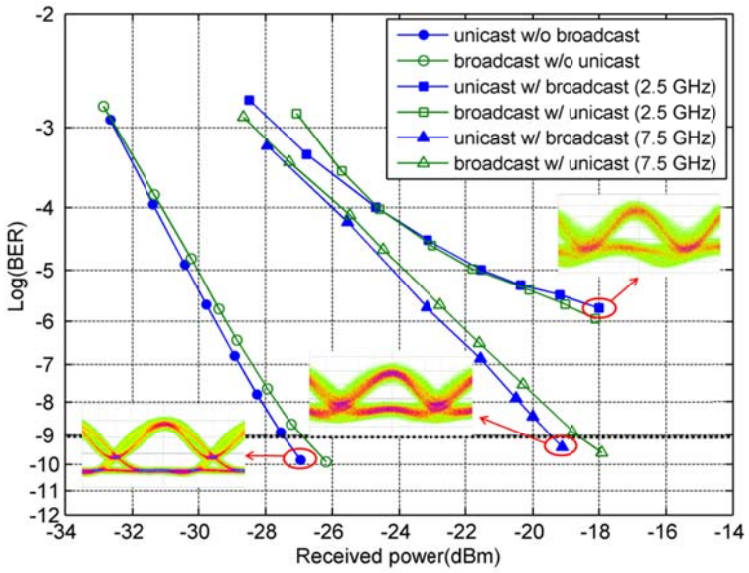

Fig. 6.5. BER performances of the downstream signals. The number inside the parenthesis in the legend indicates the frequency offset, f_{offset}.

When the broadcast service is disabled (i.e., LD2 is turned OFF), the receiver sensitivity of downstream unicast signal is measured to be -27.5 dBm at a BER of 10^{-9}; when the broadcast service is enabled and the frequency offset between the two downstream carriers is 2.5 GHz (= ¼ FSR of the DI), the BER performance of the unicast signal is degraded by the crosstalk from the broadcast signal and an error floor is observed at a BER of ~10^{-6}. Although error-free transmission could be achieved by adopting forward error correction, it raises the cost of both OLTs and ONUs.

To avoid the necessity of employing FEC, the frequency offset is increased to 7.5 GHz (= ¾ FSR of the DI), which helps to mitigate the crosstalk-induced performance degradation. During this measurement, the relative bit delay between the two downstream data is adjusted to achieve the best BER performance. In this case, we could achieve a

BER of less than 10^{-9} and the receiver sensitivities are measured to be -19.4 and -18.6 dBm for the downstream unicast and broadcast signals, respectively. The slight difference between the unicast and broadcast BER performance is mainly due to the different characteristics of the two Mach-Zehnder modulators used in the experiment.

A power penalty of ~8 dB is incurred in the presence of the offset polarization-multiplexed signals. Experiment and simulation results show the orthogonality between the unicast and broadcast signals is crucial for downstream detection. The eye opening of the detected unicast (broadcast) signal would be completely closed due to the crosstalk from the broadcast (unicast) signal if the two parallelly polarized downstream signals were combined by an optical coupler instead of a PBC.

It is interesting to note that further increasing the frequency offset will reduce the power penalty; however, it will lower the spectral efficiency. The downstream unicast and broadcast carriers for each ONU should be symmetric about the ITU grid frequency and stay within one DWDM channel. This avoids allocating additional wavelength channels for broadcast services in DWDM system with channel spacing of 50 GHz or even 25 GHz.

Fig. 6.6 shows the measured optical spectra of the offset polarization-multiplexed downstream signals with different frequency offsets. The resolution of the optical spectrum analyzer used in this measurement is 0.02 nm. The results clearly show that the signal linewidth increased with the frequency offset. Considering the tradeoff between the downstream performance and the spectral efficiency as well as the filtering effect of the AWG in the proposed architecture, we choose 7.5 GHz as the frequency offset between the two downstream signals in the following analyses.

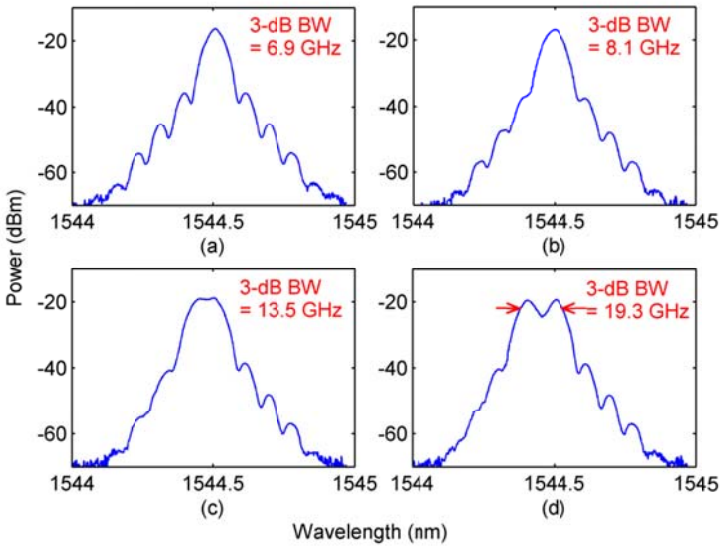

Fig. 6.6. Measured optical spectra of (a) a 10-Gb/s NRZ-DPSK signal, (b)-(d) the polarization-multiplexed 10-Gb/s NRZ-DPSK signals with frequency offset of 2.5, 7.5, and 12.5 GHz, respectively.

It is also worth noting that the receiver sensitivities of the downstream unicast (broadcast) signal can be improved if a balanced receiver is adopted since the broadcast (unicast) signal experiencing incoherent summation of two neighboring bits on both the constructive and destructive ports will be mostly canceled out by the balanced receiver.

6.3.2 Effect of Rayleigh backscattering and remodulation crosstalk

For uplink, polarization dependence of the FP-LD requires a depolarized seeding source if no polarization control is provided at the ONU. The polarization-multiplexed downstream signals with a frequency offset of 7.5 GHz naturally meet this requirement and are reused as the seeding light to injection-lock the FP-LD for upstream transmission. The DOP of the seeding source is measured to be 2~4%.

The depolarized seeding light also helps to reduce the RBS-induced crosstalk in the single-fiber loopback configured network since the beating between the signal and the RBS is polarization sensitive [198]. Furthermore, the linewidth of the seeding light is widened due to the frequency offset between the two polarization beams, as shown in Fig. 6.6. This also helps to reduce the RBS-induced penalty. As demonstrated in [81], the backreflection-induced penalty is reduced as the linewidth of the seeding light is increased. Therefore, the proposed scheme exhibits an improved robustness against the Rayleigh backscattering compared to the CW-injected FP-LDs.

The signal-to-backscattering-power ratio in our experimental demonstration is measured to be around 29.5 dB. The upstream BER performance is shown in Fig. 6.7. The receiver sensitivity at a BER of 10^{-9} is -30.5 dBm in the single-fiber loopback configuration and -31.7 dBm in the unidirectional configuration with two feeder fibers (refer to Fig. 6.4 for the experimental setup). Therefore, the power penalty induced by the RBS is 1.2 dB.

Another advantage of the seeding source composed of NRZ-DPSK signals is the relative constant intensity of phase modulation except for the transition-induced intensity dips from MZM-based DPSK transmitters when compared to OOK modulation [199].

There is no need to sacrifice the ER of the downstream signals to constantly injection-lock the FP-LD. The impact of the downstream modulation on the upstream performance is also investigated through BER measurement. As shown in Fig. 6.7, the receiver sensitivity of the upstream signal is -32.3 dBm when the downstream modulation is turned OFF but the seeding power is kept the same. Thus, the remodulation-induced power penalty is 1.8 dB. This should be ascribed to the transition-induced intensity dip of the downstream signals and can be reduced by using phase modulators for downstream DPSK modulation.

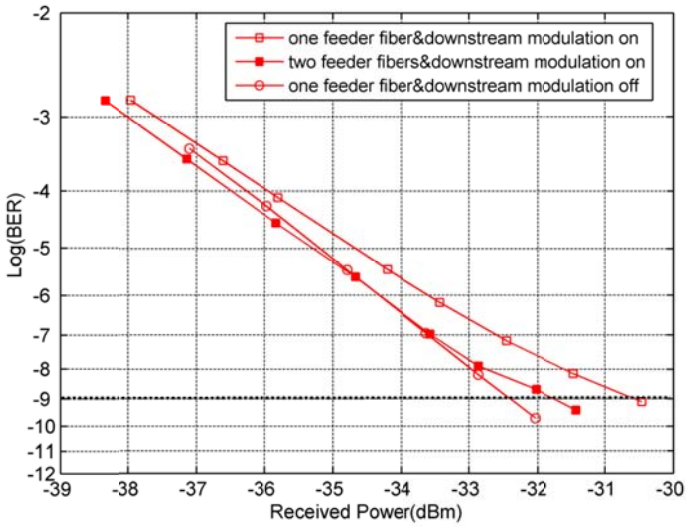

Fig. 6.7. BER performance of the upstream signal.

6.3.3 Analysis of polarization dependence and wavelength offset

To demonstrate that the seeding light in our scheme could constantly injection-lock the FP-LD without any polarization control, we deliberately add an electronically driven PC before the FP-LD. The seeding light is randomly rotated every ten seconds before being fed into the FP-LD and the upstream BER is recorded. Fig. 6.8 shows the measured BERs at a received optical power of -30.5 dBm. The results show a relative stable BER over 10

minutes. That is to say, the seeding light composed of two offset polarization-multiplexed signals can constantly injection-lock the FP-LD with no need of polarization control of the seeding light regardless of polarization perturbations.

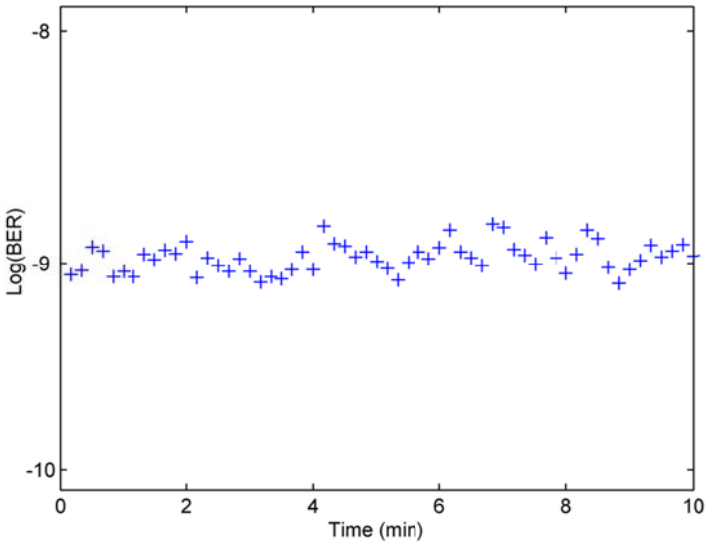

Fig. 6.8. Measured upstream BERs versus time when the seeding light is randomly rotated every ten seconds.

The weak-resonant-cavity FP-LD, whose front-facet and rear-facet reflectivities are 1% and 99% respectively, exhibits wider injection-locking range when compared to conventional FP-LDs. The BER performance of the upstream signal is measured when the wavelength offset, $\lambda_{down}-\lambda_{FP}$, where λ_{down} is the center wavelength of the offset polarization-multiplexed downstream signals and λ_{FP} is the wavelength of one of the longitudinal modes of the free-running FP-LD nearby λ_{down}, is tuned from 0 to 0.56 nm, which is the longitudinal mode spacing of the free-running FP-LD.

Fig. 6.9 shows a series of optical spectra of the injection-locked FP-LD with different wavelength offsets. Similar to Fig. 5.8 discussed before, the SMSR is reduced when the seeding light is located close to one of the free-running longitudinal modes and the resultant BER performance is degraded.

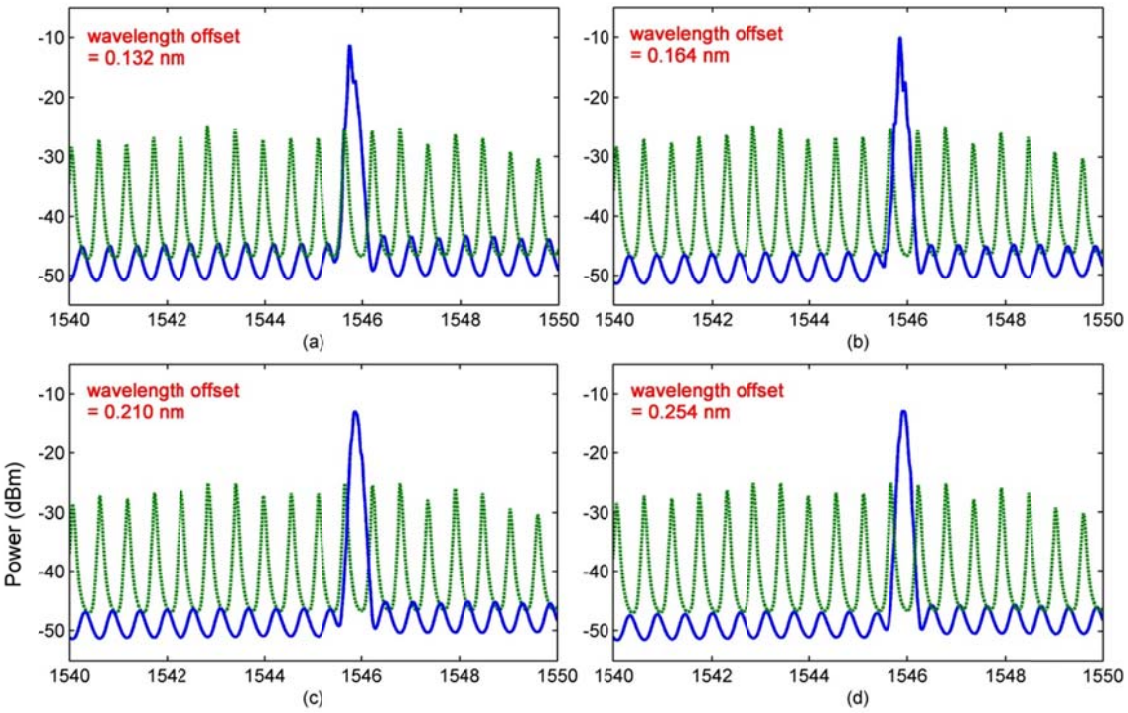

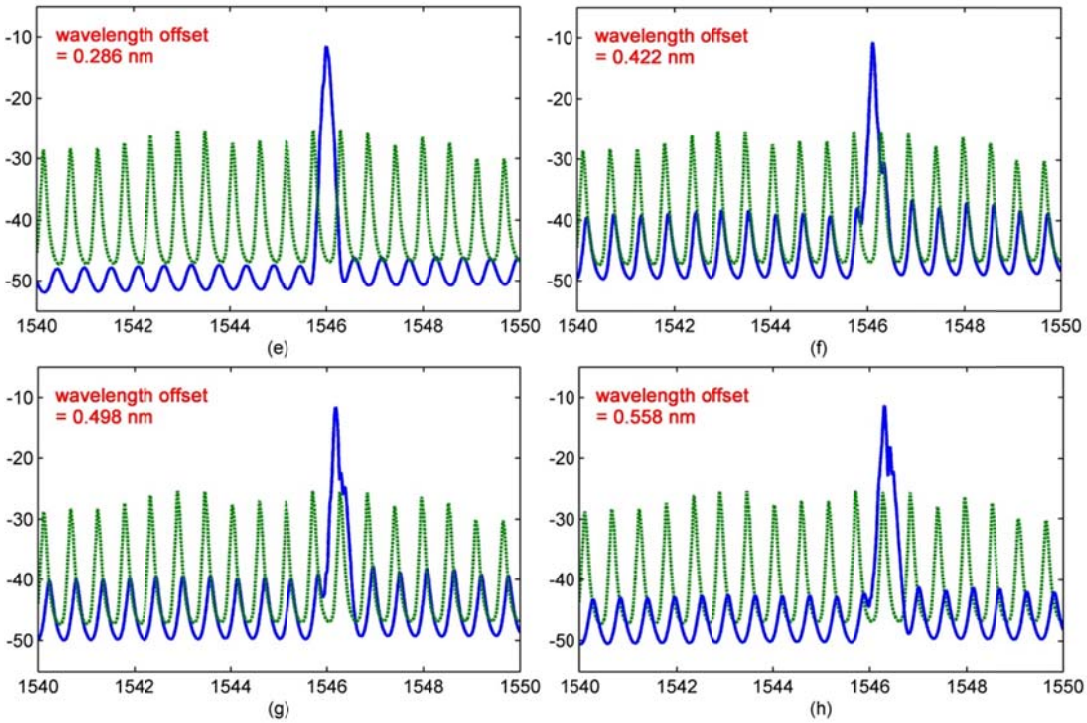

Fig. 6.9. The optical spectra of the injection-locked FP-LD with different wavelength offsets (dotted lines: free-running FP-LDs; solid lines: injection-locked FP-LDs).

The best receiver sensitivity of -30.5 dBm at a BER of 10^{-9} is obtained when the wavelength offset is 0.29 nm and this value is used as a reference in Fig. 6.10. The results show that a BER of $<10^{-9}$ is achieved over the wavelength offset ranged from 0.10 to 0.41 nm despite that maximum power penalty is 4.8 dB at the upper bound of this range.

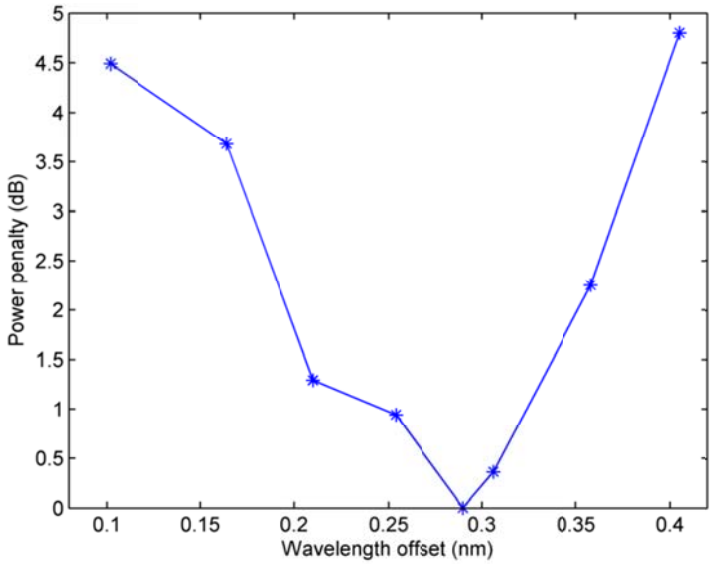

Fig. 6.10. Power penalties at BER of 10^{-9} of the upstream signal versus wavelength offset.

6.3.4 Power budget

For downlink, the seeding power for the FP-LD used in the experiment is kept at -10 dBm and the receiver sensitivity of the unicast or broadcast signal is about -19 dBm. Thus, the downstream power budget is primarily limited by the required seeding power of the FP-LD. The total link loss is 19 dB, including two AWGs (5.0 dB × 2), 20-km SSMF (4.0 dB), one 3-dB optical coupler, and other components (2.0 dB) such as PBC, circulator, and connectors. Thus, the launch power of the offset polarization-multiplexed downstream signals should be at least 9.0 dBm, i.e., 6.0 dBm from each polarization beam, to meet the power requirement of both downstream detection and upstream remodulation. For uplink, the launch power of the injection-locked FP-LD is measured to be 2.5 dBm. A power margin of 14.0 dB is obtained since the upstream receiver sensitivity is -30.5 dBm at a BER of 10^{-9}, as shown in Fig. 6.7.

6.4 Simulation results

The robustness of the proposed scheme against the relative bit delay between the two downstream data, the frequency deviation of the downstream signals from the DI, and the mismatched interferometer delay is investigated through simulation in which the downstream DPSK signals are detected by a balanced receiver. In the following analyses, the balanced receiver is tuned to detect one of the offset polarization-multiplexed signals, the unicast signal. Thus, the broadcast signal, which is 7.5 GHz away in frequency, is regarded as crosstalk. The same analyses and conclusions made in this section also apply to the detection of the broadcast signal. The simulation is implemented by the commercial software OptiSystem 9.0 [200].

6.4.1 Effect of the relative bit delay

Although the two offset polarization-multiplexed signals are independent and orthogonal to each other in polarization, the detection of one signal would still experience the crosstalk from the other signal. The crosstalk suppression of the DI could not be perfect throughout the entire bit duration and thus the relative bit delay between the unicast and broadcast data affects the transmission performance of the downstream unicast and broadcast signals.

By tuning the relative bit delay between the two signals, the peak of the crosstalk can be located to different positions of the eye diagram of the detected signal. The deleterious effect of the crosstalk becomes largest when the peak of the crosstalk falls on the sampling instance of the detected signal. Fig. 6.11 shows the receiver power penalty versus the relative bit delay between the two offset polarization-multiplexed signals.

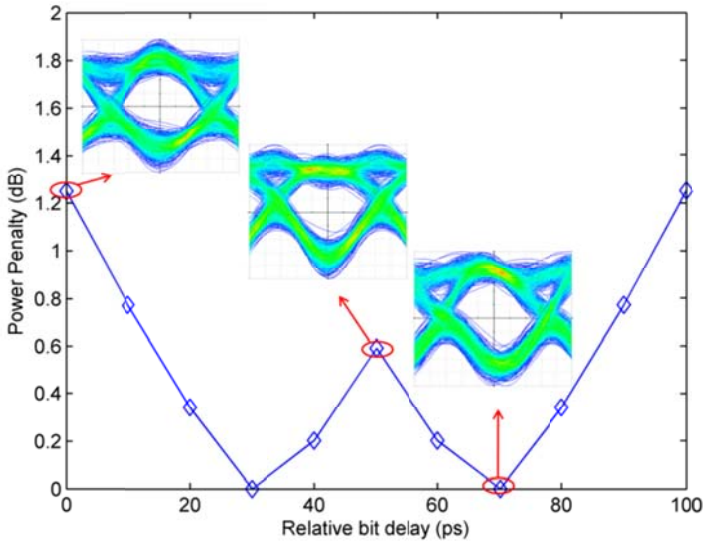

Fig. 6.11. Power penalty (at a BER of 10^{-9}) of the downstream unicast signal as a function of the relative bit delay between the unicast and broadcast data.

It shows that the relative bit delay has a marginal effect on the downstream performance. The penalties are always less than 1.3 dB, which can eliminate the necessity of controlling the relative bit delay. Nevertheless, the worst performance occurs when the two data are bit-aligned (i.e., delay = 0 or 100 ps). The best performance is obtained at the relative bit delays of 30 and 70 ps. At these bit delays, we have slightly better performance than when the two data are half-bit delayed. We ascribe this to the small asymmetry of signal eyes, which is caused by the electrical filter at the receiver. The corresponding eye diagrams with different relative bit delays are included in the inset in Fig. 6.11.

6.4.2 Effect of the frequency deviation

In DPSK reception, the deviation of the laser frequency from the DI leads to performance degradation [193]. The feasibility of the offset polarization multiplexing technique is based on this fact, as graphically illustrated by Fig. 6.1. However, due to the frequency

drift of both the laser sources and the DI, the unicast signal may not have an exact zero phase deviation with the DI in the unicast DPSK receiver and at the same time the broadcast signal may not have an exact phase deviation from the DI equaled to an odd multiples of π/2. Such misalignments are inevitable in real implementation and consequently induce power penalty.

Fig. 6.12 depicts the frequency deviation-induced power penalties. The dash curve represents the case when the unicast signal is exactly aligned to the penalty-free frequency (i.e. $\delta\phi = N\cdot\pi$) but the broadcast signal deviates from the infinite-penalty frequency (i.e. $\delta\phi = (2N-1)\cdot\pi/2$); the solid curve represents the case when the broadcast signal is exactly aligned to the infinite-penalty frequency but the unicast signal deviates from the penalty-free frequency.

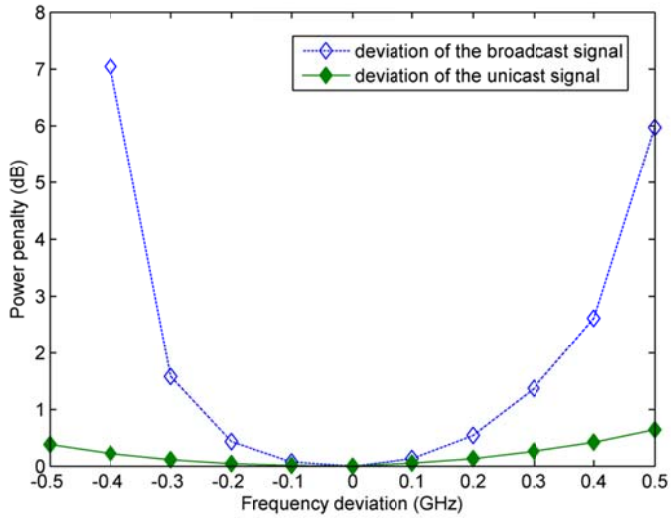

Fig. 6.12. Power penalty (at a BER of 10^{-9}) of the downstream unicast signal versus the frequency deviation of the downstream signals from the DI.

It shows that the performance of the unicast signal is much more sensitive to the deviation of the broadcast signal. For a penalty of less than 1.0 dB, the frequency deviation of the broadcast signal should be kept below 250 MHz. This frequency offset

tolerance could be achieved by using temperature-stabilized DIs. A feedback servo loop would be required to stabilize the DI and track the laser wavelength drift.

Another aspect closely related to the frequency deviation is the polarization dependence of the DI, which can be characterized by polarization-dependent wavelength shift (PDλ). PDλ is the wavelength shift of the DI wavelength response depending upon the state of polarization of the input signal. Although the offset polarization-multiplexed downstream signals may remain orthogonally polarized during transmission, the SOP of each signal is generally unknown and changes over time. Since no polarization control is provided at the receiver side in our scheme, the power penalty induced by polarization dependence of the DI is inevitable.

As discussed before, the deviation of the broadcast signal has a stronger effect on the detection of the unicast signal, so the worst performance of the unicast signal detection which could be caused by polarization dependence of the DI is that the broadcast signal deviates from the infinite-penalty frequency for an amount of PDλ. For a penalty of less than 1.0 dB, the polarization-dependent frequency shift of the DI should be kept below 250 MHz and therefore, the PDλ should be smaller than 2 picometers. Most commercially available 10-GHz DIs could satisfy this requirement [201, 202].

6.4.3 Effect of interferometer delay-to-bit rate mismatch

The mismatch between the interferometer delay and the data rate of the downstream signals would induce the receiver sensitivity degradation. The mismatch is denoted by the ratio between the interferometer delay and the data rate. As shown in Fig. 6.13, when the broadcast service is disabled (i.e., LD2 is turned OFF), a 5% mismatch leads to less than

0.1-dB power penalty. However, when the broadcast service is enabled, the power penalty induced by the interferometer delay-to-bit-rate mismatch increases dramatically.

In fact, the interferometer delay-to-bit-rate mismatch is closely related to the frequency deviation between the broadcast signal and the infinite-penalty frequency. A 5% mismatch could lead to a 375 MHz deviation of the broadcast signal at maximum, which would give rise to around 4.0-dB power penalty as shown in Fig. 6.12. To control the power penalty within 1.0 dB, the interferometer delay-to-bit-rate mismatch should stay within 3%. Imperfection in DI manufacturing may cause such a mismatch; however, the error of the interferometer delay of commercial DIs is usually smaller than 1% [201].

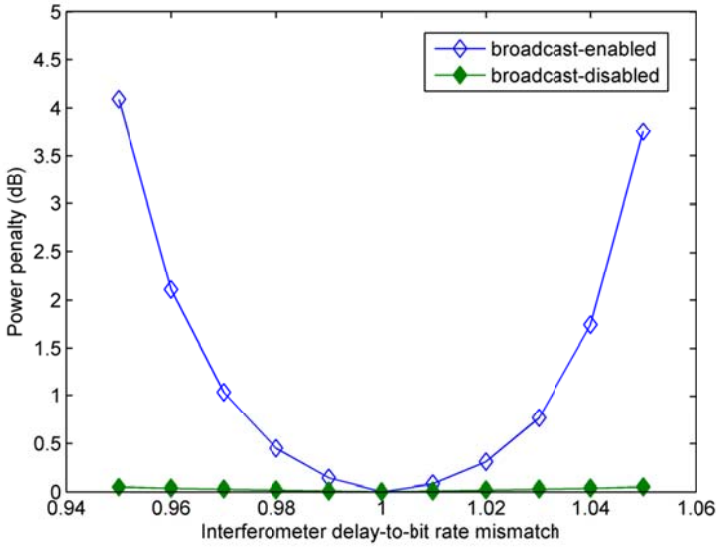

Fig. 6.13. Power penalty (at BER of 10^{-9}) of the downstream unicast signal versus the interferometer delay-to-bit-rate mismatch.

6.5 Comparison of broadcast/multicast-enabling schemes for WDM-PONs

Various schemes for enabling broadcast/multicast service in WDM-PON systems are listed in Table 6.1, including those introduced in Section 2.2 and the two schemes demonstrated and analyzed in Chapters 5 and 6. They are compared in terms of cost-effectiveness-the primary concern in WDM-PON technologies, spectral efficiency, operation complexity as well as the line-rate and modulation format transparency.

Table 6.1. Comparison of different schemes for enabling broadcast/multicast delivery over WDM-PON architectures

	Cost-effectiveness	Spectral efficiency	Operation complexity	Line-rate & modulation format transparency	References
Additional light sources	★★★★★ Additional light sources for broadcast service	★★ Low; dedicated wavelength channel for broadcast service	★★ Simple; assign different wavebands for unicast and broadcast	Yes	[110], [111], [113]
Subcarrier multiplexing	★★ High-speed modulators to generate subcarriers; devices to separate carriers and subcarriers in optical or electrical domain	★★★ Relative high; Unicast and broadcast confined in one wavelength channel but they occupy dedicated frequency bands	★★★★★ Two sets of feeder and distribution fibers needed to deliver carrier and subcarrier separately	Yes	[114], [115]
Orthogonal modulation	★★★★ Different receivers at each ONU for two orthogonal formats	★★★★★ High; unicast and broadcast occupy same frequency band	★★★★ Performance tradeoff between unicast and broadcast; accurate bit alignment might needed	No	[116], [117] [120]

Time-interleaving	★★★★ Devices for time control in OLT and ONUs	★★★★ High; unicast and broadcast occupy same frequency band	★★★★ Timing control needed in both OLT and ONUs	Yes	[121]
Polarization multiplexing	★★ Automatic polarization tracking needed at each ONU	★★★★★ High; unicast and broadcast occupy same frequency band	★★★ Automatic polarization tracking needed to demultiplex unicast and broadcast signals	Yes	[87]
Offset polarization multiplexing	★★★ Two DPSK receivers needed at each ONU	★★★★ High; unicast and broadcast occupy same frequency band	★★★★ Wavelength alignment between signals and DPSK receivers needed	No	[203]
★★★★★indicates the highest grade of cost-effectiveness, spectral efficiency and operation complexity.					

6.6 Summary

In this chapter, a WDM-PON system with a downstream broadcast overlay using the offset polarization multiplexing technique was introduced. The downstream DPSK-formatted unicast and broadcast signals, which were separated by a quarter or three quarters of the data rate in frequency, were polarization-multiplexed at the transmitter. The offset polarization-multiplexed signals were demultiplexed and demodulated by a pair of delay interferometers without any polarization tracking at the receiver.

The offset polarization-multiplexed downstream signals were also exploited to facilitate the constant injection-locking of polarization-sensitive Fabry-Perot laser diodes for upstream transmission. Therefore, no polarization control or tracking was needed for both downstream and upstream transmissions. Based on the proposed scheme, bidirectional transmissions of 10-Gb/s unicast and 10-Gb/s broadcast signals for downlink and 2.5-Gb/s signal for uplink were successfully demonstrated.

The experimental results and simulation studies showed that the proposed scheme was very robust against the polarization fluctuation on the link and the relative bit delay between the downstream unicast and broadcast signals. The simulation study also revealed that the downstream performance was sensitive to the frequency deviation of the downstream signals from the DI. However, the frequency deviation could be controlled within an acceptable range with commercially available DIs and wavelength-stabilized laser sources. A feedback servo loop would be needed to stabilize the DIs and track the laser wavelength drift at the ONU.

Due to the device and equipment constraint, investigation on transmission performance of multiple wavelength channels and the effect of interchannel crosstalk cannot be conducted. However, such studies have been reported by other research works which employ the injection-locked FP-LDs as the colorless transmitters. In [204], it is demonstrated that colorless operation by an injection-locked FP-LD could be achieved over the wavelength range of 1530-1560 nm, which implies 32 channels can be accommodated in the WDM-PON system based on injection-locked FP-LDs. A 3-channel and 12-channel WDM transmission using injection-locked FP-LDs are studied in [205, 206]. Both of them have shown a negligible crosstalk induced by WDM transmission. Therefore, it can be concluded that the power penalty induced by interchannel crosstalk in WDM transmission systems is negligible thanks to the channel isolation of standard wavelength multiplexer/demultiplexer.

CHAPTER 7

Conclusions and Future Work

7.1 Conclusions

Wavelength-division-multiplexed passive optical network has been considered as a promising technology for access networks to meet the ever-increasing bandwidth demand. However, mass deployment of WDM-PONs is hindered by the higher installation and maintenance cost compared to the TDM-based technologies. It will take time for WDM-PONs to mature and progress down the cost curve. The time will come when the access network needs to support high-capacity symmetric traffic and cost reduction enables WDM-PONs to become commercially viable in the cost-sensitive access network market. While this dissertation is devoted to developing and investigating enabling techniques for cost-effective and viable WDM-PON systems, two major research aspects in WDM-PON technologies are addressed, including1) implementation of cost-effective colorless ONUs and 2) delivery of broadcast service over WDM-PON architectures.

In Chapter 3, in-depth analyses of directly modulated self-seeded RSOAs which are used as the colorless light sources at ONUs in a WDM-PON system are carried out. The impact of various system parameters on the transmission performance is investigated. Because of the inevitable remodulation crosstalk existing in the self-seeding operation, the signal extinction ratio of the self-seeded RSOA should be carefully adjusted to

optimize the transmission performance. Since low cavity loss (or high seeding power) is desirable, a RSOA with high gain, high saturated output power, and low PDG is preferred for the self-seeding application. It also shows that self-seeded RSOAs favor a flat-top instead of Gaussian-shaped filter (i.e., the AWG) located within the self-seeding cavity. The system transmission performance is robust against the phase perturbation but degraded by extending the length of the self-seeding cavity. Based on the characterization results, a cost-effective bidirectional 5/1.25-Gb/s WDM-PON based on self-seeded RSOAs for downlink and remote-seeded RSOAs for uplink is demonstrated. Despite the RSOA has a limited E/O bandwidth < 1 GHz, the data rate of the self-seeded RSOA is enhanced to 5 Gb/s by increasing the seeding power and employing offline electronic equalization. The study provides a better understanding of the mechanism of the directly modulated self-seeded RSOAs and also guidance on designing the WDM-PON systems using the self-seeded RSOAs.

In Chapter 4, another type of prevalent colorless light sources, FP-LDs, for WDM-PON systems is investigated in detail. The injection-locking of a FP-LD is theoretically analyzed and simulated. Some basic properties of FP-LDs including frequency response and polarization dependency are experimentally characterized. Based on the fact that the RIN of a spectrum-sliced ASE could be suppressed by being injected into a FP-LD, a multimode-injected FP-LD is proposed where the FP-LD acts as a common noise suppressor for multiple injected ASE spectrum slices. Simulation results show that the receiver sensitivities at a BER of 10^{-9} are improved by 3.6 dB and 3.9 dB, respectively, when the spectrum-sliced multimode-injected FP-LD is employed as an optical carrier

and a remote seeding light source for carrier-distributed WDM-PONs, compared to a spectrum-sliced ASE source.

Chapters 5 and 6 discuss two feasible techniques to enable broadcast service delivery over WDM-PON architectures. In Chapter 5, polarization multiplexing technique is exploited to achieve simultaneous delivery of downstream unicast and broadcast signals without allocating additional wavelength channels and using high-frequency SCM modulation. The downstream signals consisting of two uncorrelated, orthogonally polarized beams are used as the seeding light to injection-lock a polarization-sensitive FP-LD for upstream remodulation without any polarization control. Experimental demonstration of successful transmission of 10-Gb/s downstream unicast and broadcast signals with low ER as well as 2.5-Gb/s upstream signal with FEC confirmed the feasibility of the proposed architecture. Several technical issues including injection-locking polarization dependence, wavelength offset, and performance tradeoff between downlink and uplink are investigated. It is demonstrated that the weak-resonant-cavity FP-LD possesses a wide injection-locking range which could enable uncooled operation of ONUs. For practical implementations, active polarization tracking is required to demultiplex the downstream unicast and broadcast signals at each ONU. Therefore, mass deployment of the proposed WDM-PON would count on cost-effective automatic polarization demultiplexing techniques.

Chapter 6 introduces another broadcast-capable WDM-PON system developed based on the method discussed in Chapter 5. It not only preserves the advantages of the former scheme but also improves the cost-efficiency by eliminating the need of automatic polarization tracking at ONUs. This broadcast-capable WDM-PON system utilizes offset

polarization multiplexing technique. The offset polarization-multiplexed downstream unicast and broadcast DPSK signals are demultiplexed and demodulated by a pair of delay interferometers without resorting to polarization tracking. The offset polarization-multiplexed downstream signals also facilitate the constant injection-locking of polarization-sensitive Fabry-Perot laser diodes for upstream transmission. Moreover, the constant intensity of the downstream DPSK signals avoids the performance trade-off between downlink and uplink in a wavelength-remodulated WDM-PON system. Bidirectional transmissions of 10-Gb/s unicast and 10-Gb/s broadcast signals for downlink and 2.5-Gb/s signal for uplink are successfully demonstrated. The proposed scheme is very robust against the polarization fluctuation on the link and the relative bit delay between the downstream unicast and broadcast signals. However, the downstream performance is sensitive to the frequency deviation of the downstream signals from the DI.

7.2 Future work

Self-seeding of RSOAs is an attractive solution for colorless operation of ONUs in WDM-PON systems but it is less explored compared to external-seeding of RSOAs. Similar to an external-seeded RSOA, the data rate of a directly modulated self-seeded RSOA is primarily limited by the modulation bandwidth of the RSOA itself. Therefore, the techniques used to achieve high-speed operation of external-seeded RSOAs, e.g. electronic equalization, detuned optical filtering, and bandwidth-efficient modulation format, might be also applicable to enhance the data rate of self-seeded RSOAs. Unlike external-seeded RSOAs, self-seeded RSOAs inevitably suffer from remodulation crosstalk. The output of a self-seeded RSOA has a low degree of coherence. These

characteristics also limit the bit rate supported by self-seeded RSOAs. Special techniques should be developed to suppress the remodulation crosstalk and improve the degree of coherence. All in all, high-speed operation of self-seeded RSOAs is a research direction worthy of further exploration.

With the deepening penetration of DSP into conventional optical communication, complex spectrally-efficient modulation formats such as M-ary PSK and quadrature amplitude modulation (QAM) have been introduced into PON applications. Moreover, optical orthogonal frequency division multiplexing (OFDM), due to its high spectral efficiency and adaptability to various advanced modulation formats, is considered as a powerful technique to achieve high capacity symmetric WDM-PONs in which the upstream transmission rate is limited by the modulation bandwidth of the colorless light sources, i.e., RSOAs and FP-LDs. Optical coherent detection has also been applied to PON applications to enable supporting of advanced modulation formats. In short, symmetric high-speed operation of WDM-PONs with cost-effective bandwidth-limited colorless light sources is a promising research topic.

Another significant research aspect is to establish models for analyzing the economic feasibility of implementing WDM-PON systems in areas with different density of population. With the availability of various WDM-PON technologies in future, the model could help to determine which specific WDM-PON system including the colorless light sources, downstream and upstream data rate and transmission reach should be implemented according to the bandwidth demand and geographic distribution of end users. It is also worthwhile to develop reliable techniques to reduce the energy consumption of the WDM-PON system, especially ONUs for end users. For example, the

ONUs could be switched to sleep mode automatically when there is data to transmit or receive and be recovered to active mode without losing data when there is a transmission request.

After more than ten years' extensive studies on WDM-PON technologies, almost every technical issue in WDM-PON systems has been or is being addressed. WDM-PON has become a ready-to-use technology which would be possibly deployed massively in the next ten or twenty years. While preparing for real implementation, efforts should be made to tailor the characteristics of devices, especially colorless light sources, to meet the exact requirements and needs in the future WDM-PON systems.

Bibliography

[1] Banerjee, "Wavelength-division-multiplexed passive optical network (WDM-PON) technologies for broadband access: a review," *J. Opt. Networking*, vol. 4, pp. 737-758, Nov. 2005.

[2] T. Koonen, "Fiber to the home/fiber to the premises: what, where, and when?" *Proc. IEEE*, vol. 94, pp. 911-934, May 2006.

[3] J.-P. Faure, B. Lavigne, C. Bresson, O. Bertran-Pardo, A. C. Colomer, and R. Canto, "40G and 100G deployment on 10G infrastructure: market overview and trends, coherent versus conventional technology," presented at the *Optical Fiber Communication Conference*, San Diego, CA, 2010, paper OThE3.

[4] *Technology Future INC.*, [Online]. Available: http://www.tfi.com/index.html

[5] K. Grobe, M. Roppelt, A. Autenrieth, J.-P. Elbers, and M. Eiselt, "Cost and energy consumption analysis of advanced WDM-PONs," *IEEE Commun. Mag.*, pp. 25-32, Feb. 2011.

[6] K. Grobe and J.-P. Elbers, "PON in adolescence: from TDMA to WDM-PON," *IEEE Commun. Mag.*, pp. 26-34, Jan. 2008.

[7] E. Trojer, S. Dahlfort, D. Hood and H. Mickelsson, "Current and next-generation PONs: A technical overview of present and future technology," *Ericsson Review*, No. 2, pp. 64-69, May 2008.

[8] K. Iwatsuki and J.-I. Kani, "Applications and technical issues of wavelength-division multiplexing passive optical networks with colorless optical network units," *J. Opt. Commun. Netw.*, vol. 1, pp. 17-24, Sep. 2009.

[9] J.-P. Elbers, "Optical access solutions beyond 10G-EPON/XG-PON," presented at the *Optical Fiber Communication Conference*, San Diego, CA, 2010, paper OTuO1.

[10] ITU-T G.983.1: Broadband optical access systems based on passive optical networks, [Online]. Available : www.itu.int/rec/T-REC-G.983.1-200501-I/en

[11] IEEE 802.3ah-2004, [Online]. Available : http://standards.ieee.org/findstds/standard/802.3ah-2004.html

[12] ITU-T G.984.1: Gigabit-capable passive optical networks (GPON): General characteristics, [Online]. Available : http://www.itu.int/rec/T-REC-G.984.1-200803-I/en

[13] IEEE 802.3av-2009, [Online]. Available : http://standards.ieee.org/findstds/standard/802.3av-2009.html

[14] ITU-T G.987: 10-Gigabit-capable passive optical network (XG-PON) systems: Definitions, abbreviations and acronym, [Online]. Available : http://www.itu.int/rec/T-REC-G.987-201206-I/en

[15] E. Harstead, "Future bandwidth demand favors TDM PON, not WDM PON," presented at the *Optical Fiber Communication Conference*, Los Angeles, CA, 2011, paper NTuB7.

[16] C-H. Lee, W. V. Sorin, and B. Y. Kim, "Fiber to the home using a PON infrastructure," *IEEE J. of Lightwave Technol.*, vol. 24, pp. 4568–4583, Dec. 2006.

[17] C.-H. Lee, S.-M. Lee, K.-M. Choi, J.-H. Moon, Si.-G. Mun, and K.-T. Jeong et al, "WDM-PON experiences in Korea," *J. Opt. Networking*, vol. 6, pp. 451-464, May 2007.
[18] B. Kim and B.-W. Kim, "WDM-PON development and deployment as a present optical access solution," presented at the *Optical Fiber Communication Conference*, San Diego, CA, 2009, paper OThP5.
[19] M. Maier, "WDM passive optical networks and beyond: the road ahead," *J. Opt. Commun. Netw*., vol. 1, pp. C1-C16, Sep. 2009.
[20] G. Das, B. Lannoo, A. Dixit, D. Colle, M. Pickavet, and P. Demeester, "Flexible hybrid WDM/TDM PON architectures using wavelength selective switches," *Optical Switching and Networking*, vol. 9, pp. 156-169, Apr. 2012.
[21] A. Dixit, B. Lannoo, D. Colle, M. Pickavet, and P. Demeester, "Wavelength switched hybrid TDMA/WDM (TWDM) PON: a flexible next-generation optical access solution," presented at the 14th *International Conference on Transparent Optical Networks*, Coventry, England, 2012
[22] Statistics from the Web of Knowledge, [Online]. Available: http://thomsonreuters.com/web-of-knowledge/
[23] N. J. Frigo, P. P. Iannone, P. D. Magill, T. E. Darcie, M. M. Downs, B. N. Desai et al, "A wavelength-division multiplexed passive optical network with cost-shared components," *IEEE Photon. Technol. Lett.*, vol. 6, pp. 1365-1367, Nov. 1994.
[24] Y. C. Chung, "Challenges toward practical WDM PON," presented at *Opto-Electronics and Communications Conference*, Hong Kong, China, 2009, paper 6C4-1-1.
[25] WDM-PON standards: playing the long game, [Online]. Available: http://blog.advaoptical.com/wdm-pon-standards-playing-the-long-game/
[26] L. W. Zhou, C. M. Machuca, R. Zhao, and K. Grunert, "Migration towards fibre to the home: key cost factors," presented at *Communications and Photonics Conference and Exhibition*, Shanghai, China, 2010.
[27] A. Banerjee, Y. Park, F. Clarke, H. Song, S. Yang, G. Kramer, K. Kim, and B. Mukherjee, "Wavelength-division-multiplexed passive optical network (WDM-PON) technologies for broadband access: a review," *J. of Opt. Netw.*, vol. 4, pp. 737-758, Nov. 2005
[28] K. H. Han, E. S. Son, H. Y. Choi, K. W. Lim, and Y. C. Chung, "Bidirectional WDMPON using light-emitting diodes spectrum-sliced with cyclic arrayed-waveguide grating," *IEEE Photon. Technol. Lett.*, vol. 16, pp. 2380-2382, 2004.
[29] J. H. Lee, C. H. Kim, Y. G. Han, and S. B. Lee, "Broadband, high power, erbium fibre ASE-based CW supercontinuum source for spectrm-sliced WDM PON applications" *Electron. Lett.*, vol. 42, No. 9, Apr. 2006.
[30] J. S. Lee, Y. C. Chung, and D. J. DiGiovanni, "Spectrum-sliced fiber amplifier light source for multichannel WDM applications," *IEEE Photon. Technol. Lett.*, vol. 5, pp.1458-1461, Dec. 1993.
[31] Y. J. Wen, X. Cheng, Z. Xu, Y. Wang, and J. Shankar, "Light sources for WDM passive optical networks," presented at *Joint International Conference on Optical Internet and Australian Conference on Optical Fibre Technology*, Melbourne, Australia, 2007.

[32] H. Suzuki, H. Nakamura, J. Kani, and K. Iwatsuki, "A carrier-distributed wide-area WDM-based passive optical network (WDM-PON) accommodating 10 gigabit Ethernet-based VPN services," presented at *European Conference of Communications*, Stockholm, Sweden, 2004, paper Tu4.6.3.

[33] K. Asaka, Y. Suzaki, S. Kondo, Y.Noguchi, H. Okamoto, R. Iga, and S. Oku, "Lossless Electroabsorption modulator monolithically integrated with a semiconductor optical amplifier and a passive waveguide, " *IEEE Photon. Technol. Lett.*, vol.15, pp.679-681, May 2003.

[34] F. Y. Shih, C. H. Yeh, C. W. Chow, C. H. Wang, and S. Chi, "Utilization of self-injection Fabry-Perot laser diode for long-reach WDM-PON," *Opt. Fiber Technol.*, vol. 16, pp. 46-49, Oct. 2009.

[35] E. Wong, K. L. Lee and T. B. Anderson, "Directly modulated self-seeding RSOAs as colorless transmitters in WDM-PONs," *IEEE J. of Lightwave Technol.*, vol. 25, pp. 67-74, Jan. 2007.

[36] O. Couderc, "WDM-PON technology: how it can facilitate the last mile," presented at *Trans-European Research and Education Networking Association*, Amsterdam, Netherland, 2008.

[37] N. Cheng and F. Effenberger, "WDM-PON: system and technologies," presented at *European Conference of Communications*, Turino, Italy, 2010.

[38] Transmode White Paper "WDM-PON: a key component in next generation access," [Online]. Available: www.transmode.com/en/resource/whitepapers

[39] R. D. Feldman, E. E. Harstead, S. Jiang, T. H. Wood, and M. Zirngibl, "An evaluation of architecture incorporating wavelength division multiplexing for broad-band fiber access," *IEEE J. of Lightwave Technol.*, vol. 16, pp. 1546-1559, Sep. 1998.

[40] H. Y. Rhy and G. Y. Yi, "Current status of WDM-PON system development and standardization," presented at the *Opto-Electronics and Communications Conference*, Busan, Korea, 2012, paper 3A1-5.

[41] S. L. Woodward, P. P Iannone, K. C. Reichmann, and N. J. Frigo, "A spectrally sliced PON employing Fabry-Perot lasers," *IEEE Photon. Technol. Lett.*, vol.10, pp.1337-1339, Sep. 1998.

[42] D. K. Jung, S. K. Shin, C.-H. Lee, and Y. C. Chung, "Wavelength-division-multiplexed passive optical network based on spectrum-slicing techniques," *IEEE Photon. Technol. Lett.*, vol.10, pp.1334-1336, Sep. 1998.

[43] Z. Al-Qazwini and H. Kim, "Ultranarrow spectrum-sliced incoherent light source for 10-Gb/s WDM PON," *IEEE J. of Lightwave Technol.*, vol. 30, pp. 3157-3163, Oct. 2012.

[44] G. de Valicourt, D. Make, C. Fortin, A. Enard, F. Van Dijk, and R. Brenot, "10 Gbit/s modulation of reflective SOA without any electronic processing," presented at the *Optical Fiber Communication Conference*, Los Angeles, CA, 2011, paper OThT2.

[45] G. de Valicourt, F. Pommereau, F. Poingt, M. Lamponi, G. H. Duan, P. Chanclou, M. A. Violas, and R. Brenot, "Chirp reduction in directly modulated multi-electrode RSOA devices in passive optical networks," *IEEE Photon. Technol. Lett.*, vol.22, pp.1425-1427, Oct. 2010.

[46] K. Y. Cho, B. S. Choi, Y. Takushima, and Y. C. Chung, "25.78-Gb/s operation of RSOA for next-generation optical access networks," *IEEE Photon. Technol. Lett.*, vol.23, pp.495-497, Apr. 2011.
[47] L. Marazzi, P. Parolari, M. Brunero, A. Gatto, M. Martinelli, R. Brenot, S. Barbet, P. Galli, and G. Gavioli, "Up to 10.7-Gb/s high-PDG RSOA-based colorless transmitter for WDM networks," *IEEE Photon. Technol. Lett.*, vol.25, pp.637-640, Apr. 2013.
[48] K. Y. Cho, Y. Takushima and Y. C. Chung, "10-Gb/s operation of RSOA for WDM-PON," *IEEE Photonics Technol. Lett.*, vol. 20, pp. 1533-1535, Sep. 2008.
[49] K. Y. Cho, B. S. Choi, Y. Takushima, and Y. C. Chung, "25.78-Gb/s operation of RSOA for next-generation optical access networks," *IEEE Photon. Technol. Lett.*, vol. 23, pp.495-497, Apr. 2011.
[50] Q. Guo and A. V. Tran, "20-Gb/s single-feeder WDM-PON using partial-response maximum likelihood equalizer," *IEEE Photon. Technol. Lett.*, vol. 23, pp.1802-1804, Dec. 2011.
[51] I. Cano, M. Omella, J. Prat, and P. Poggiolini, "Colorless 10Gb/s extended reach WDM PON with low BW RSOA using MLSE," presented at the *Optical Fiber Communication Conference*, San Diego, CA, 2010, paper OWG2.
[52] M. Omella, V. Polo, J. Lazaro, B. Schrenk, and J. Prat, "10 Gb/s RSOA transmission by direct duobinary modulation," presented at *European Conference of Communications*, Brussels, Belgium, 2008, paper Tu.3.E.4.
[53] M. Omella, I. Papagiannakis, B. Schrenk, D. Klonidis, J. A. Lazaro, A. N. Birbas, J. Kikidis, J. Prat and I. Tomkos, "10 Gb/s full-duplex bidirectional transmission with RSOA-based ONU using detuned optical filtering and decision feedback equalization," *Opt. Express*, vol. 17, pp. 5008-5013, Feb. 2009.
[54] I. Papagiannakis ,M. Omella, D. Klonidis, A. N. Birbas, J. Kikidis, I. Tomkos, and J. Prat, "Investigation of 10-Gb/s RSOA-based upstream transmission in WDM-PONs utilizing optical filtering and electronic equalization," *IEEE Photon. Technol. Lett.*, vol. 20, pp.2168-2170, Dec. 2008.
[55] Q. Guo, A. V, Tran, and C.-J. Chae, "20 Gb/s WDM-PON system with 1 GHz RSOA using partial response equalization and optical filter detuning," presented at the *Optical Fiber Communication Conference*, Los Angeles, CA, 2011, paper NTuB5.
[56] M. Presi, A. Chiuchiarelli, R. Corsini, P. Choudury, F. Bottoni, L. Giorgi, and E. Ciaramella, "Enhanced 10 Gb/s operations of directly modulated reflective semiconductor optical amplifiers without electronic equalization," *Opt. Express*, vol. 20, pp. 507–512, Dec. 2012.
[57] H. Kim, "10-Gb/s operation of RSOA using a delay interferometer," *IEEE Photon. Technol. Lett.*, vol. 22, pp. 1379-1381, Sep. 2010.
[58] H. Kim, "Transmission of 10-Gb/s directly modulated RSOA signals in single-fiber loopback WDM PONs," *IEEE Photon. Technol. Lett.*, vol. 23, pp. 965-967, Jul. 2011.
[59] H. Kim, "A dual-detector optical receiver for WDM PON utilizing directly modulated RSOAs and delay interferometer," *IEEE Photon. Technol. Lett.*, vol. 23, pp. 1733-1735, Nov. 2011.

[60] K. Y. Cho, Y. Takushima, and Y. C. Chung, "Demonstration of 11-Gb/s, 20-km reach WDM PON using directly-modulated RSOA with 4-ary PAM signals," presented at the *Optical Fiber Communication Conference*, San Diego, CA, 2010, paper OWG1.

[61] K. Y. Cho, U.H. Hong, A. Agata, T. Sano, Y. Horiuchi, H. Tanaka, M. Suzuki, and Y. C. Chung, "10-Gb/s. 80-km reach RSOA-based WDM PON employing QPSK signal and self-homodyne receiver," presented at the *Optical Fiber Communication Conference*, San Diego, CA, 2012, paper OW1B.1.

[62] H. K. Shim, K. Y. Cho, U. H. Hong, and Y. C. Chung, "Demonstration of 40-Gb/s QPSK upstream transmission in long-reach RSOA-based coherent WDM PON using Offset PDM technique," presented at the *Optical Fiber Communication Conference*, Anaheim, CA, 2013, paper OW1A.6.

[63] T. Sano, A. Agata, and K. Nishimura, "10.5 Gbit/s 8-PSK signal generated by directly modulating RSOA with instantaneous injection/depletion currents," presented at the *Optical Fiber Communication Conference*, Anaheim, CA, 2013, paper OW1A.2.

[64] M. Presi, G. Cossu, A. Chiuchiarelli, F. Bottoni, R. Corsini, P. Choudhury, L. Giorgi, and E. Ciaramella, "25 Gb/s operation of 1-GHz bandwidth R-SOA by using DMT and optical equalization," presented at the *Optical Fiber Communication Conference*, Anaheim, CA, 2013, paper OW1A.7.

[65] M. Fujiwara, J. Kani, H. Suzuki, and K. Iwatsuki, "Impact of backreflection on upstream transmission in WDM single-fiber loopback access networks," *IEEE J. of Lightwave Technol.*, vol. 24, pp. 740-746, Feb. 2006.

[66] Y. S. Jang, C.-H. Lee, and Y. C. Chung, "Effects of crosstalk in WDM systems using spectrum-sliced light sources," *IEEE Photon. Technol. Lett.*, vol. 11, pp. 715-717, Jun. 1999.

[67] P. J. Urban, A. M. J. Koonen, G. D. Khoe, and H. de Waardt, "Interferometric crosstalk reduction in an RSOA-based WDM passive optical network," *IEEE J. of Lightwave Technol.*, vol. 27, pp. 4943-4953, Nov. 2009.

[68] J. A. Lazaro, C. Arellano, V. Polo, and J. Prat, "Rayleigh scattering reduction by means of optical frequency dithering in passive optical networks with remotely seeded ONUs," *IEEE Photon. Technol. Lett.*, vol. 19, pp. 64-66, Jan. 2007.

[69] P. J. Urban, A. M. J. Koonen, G. D. Khoe, and H. de Waardt, "Mitigation of reflection-induced crosstalk in a WDM access network," presented at the *Optical Fiber Communication Conference*, San Diego, CA, 2008, paper OThT3.

[70] M. Presi, A. Chiuchiarelli, R. Corsini, P. Choudhury, G. Constestabile, and E. Ciaramella, "Single feeder bidirectional WDM-PON with enhanced resilience to Rayleigh-Backscatteing," presented at the *Optical Fiber Communication Conference*, San Diego, CA, 2010, paper OThG2.

[71] Q. Guo and A. V. Tran, "Mitigation of Rayleigh noise and dispersion in REAM-based WDM-PON using spectrum-shaping codes," *Opt. Express*, vol. 20, pp. 452-461, Dec. 2012.

[72] A. Chowdhury, H.-C. Chien, M.-F. Huang, J. Yu, and G.-K. Chang, "Rayleigh backscattering noise-eliminated 115-km long-reach bidirectional centralized WDM-PON with 10-Gb/s DPSK downstream and remodulated 2.5-Gb/s OCS-

SCM upstream signal," *IEEE Photon. Technol. Lett.*, vol. 20, pp. 2081-2083, Dec. 2008.
[73] C. W. Chow, C. H. Yeh, L. Xu, and H. K. Tsang, "Rayleigh backscattering mitigation using wavelength splitting for heterogeneous optical wired and wireless access," *IEEE Photon. Technol. Lett.*, vol. 22, pp. 1294-1296, Sep. 2010.
[74] H. D. Kim, S.-G. Kang, and C.-H. Lee, "A low-cost WDM source with an ASE injected Fabry-Perot semiconductor laser," *IEEE Photon. Technol. Lett.*, vol. 12, pp. 1067-1069, Aug. 2000.
[75] X. F. Cheng, Y. J. Wen, Y. Dong, Z. W. Xu, S. Xu, Y. X. Wang and C. Lu, "Optimization of spectrum-sliced ASE source for injection-locking a Fabry-Perot laser diode," *IEEE Photonics Technol. Lett.*, vol. 18, pp. 1961-1963, September 2006.
[76] C. H. Kim, J. H. Lee, D. K. Jung, Y.-G. Han, and S. B. Lee, "Performance comparison of directly-modulated, wavelength-locked Fabry-Perot laser diode and EAM-modulated, spectrum-sliced ASE source for 1.25 Gb/s WDM-PON," presented at the *Optical Fiber Communication Conference*, Anaheim, CA, 2007, paper JWA82.
[77] J. H. Lee, C. H. Kim, Y.-G. Han and S. B. Lee, "WDM-based passive optical network upstream transmission at 1.25 Gb/s using Fabry-Perot laser diodes injected with spectrum-sliced, depolarized, continuous-wave supercontinuum source," *IEEE Photonics Technol. Lett.*, vol. 18, pp. 2108-2110, Oct. 2006.
[78] H. Kim, "An ASE-injected FP-LD-based return-to-zero transmitter for long reach WDM-PONs," presented at the *Optical Fiber Communication Conference*, San Diego, CA, 2010, paper OWG6.
[79] J. S. Jeong and C.-H. Lee, "Optical noise suppression techniques for wavelength-locked Fabry-Perot laser diode," presented at the *Asia-Pacific Conference on Communications*, Shanghai, China, 2009.
[80] Z. Xu, Y. J. Wen, W.-D. Zhong, C.-J. Chae, X.-F. Cheng, Y. Wang, C. Lu and J. Shankar, "High-speed WDM-PON using CW injection-locked Fabry-Perot laser diodes," *Opt. Express*, vol. 15, pp. 2953-2962, Mar. 2007.
[81] D. Heo, D.-J. Shin, I.-K. Yun, J.-S. Lee, J. Jeong and J. Lee, "BLS polarization-induced performance degradation in WDM-PON systems based on wavelength-locked FP-LDs," *Opt. Commun.*, vol. 283, pp. 258-261, Oct. 2009.
[82] H.-C. Kwon, W.-S. Jang, and S.-K. Han, "WDM-PON downstream optical link using wavelength-locked FP-LD by spectrally-sliced FP-LD," *IEICE Trans. Commun.*, Vol. E88-B, pp. 384-387, Jan. 2005.
[83] F. Xiong, W.-D. Zhong, and H. Kim, "Multimode-injection-locked Fabry-Perot laser diode as remote seeding light for WDM-PONs," presented at *Photonics Global Conference*, Singapore, 2010, paper conf10a657.
[84] J.-H. Moon, K.-M. Choi, S.-G. Mun, and C.-H. Lee, "Effects of back-reflection in WDM-PONs based on seed light injection," *IEEE Photonics Technol. Lett.*, vol. 19, pp. 2045-2047, Dec. 2007.
[85] Y.-H. Lin, C.-J. Lin, G.-C. Lin, and G.-R. Lin, "Saturated signal-to-noise ratio of up-stream WRC-FPLD transmitter injection-locked by down-stream data erased ASE carrier," *Opt. Express*, vol. 19, pp. 4067-4075, Feb. 2011.

[86] G.-R. Lin, H.-L. Wang, G.-C. Lin, Y.-H. Huang, Y.-H. Lin, and T.-K. Cheng, "Comparison on injection-locked Fabry-Perot laser diode with front-facet reflectivity of 1% and 30% for optical data transmission in WDM-PON system," *IEEE J. of Lightwave Technol.*, vol. 27, pp. 2779-2785, Jul. 2009.

[87] F. Xiong, W.-D. Zhong, and H. Kim, "A broadcast-capable WDM-PON based on polarization-sensitive weak-resonant-cavity Fabry-Perot laser diodes," *IEEE J. of Lightwave Technol.*, vol. 30, pp. 355-361, Feb. 2012.

[88] H. Yoo, H. J. Lee, Y. D. Jeong and Y. H. Won, "All-optical wavelength conversion at 10 Gbit's using absorption modulation in a Fabry-Perot laser diode with a CW holding beam," *Microwave Opt. Technol. Lett*., vol. 47, no. 5, pp. 508–511, Dec. 2005.

[89] A. Shen, D. Make, F. Poingt, L. Legouezigou, F. Pommereau, "Polarisation insensitive injection locked Fabry-Perot lasers diodes for 2.5 Gb/s WDM access applications" presented at the *European Conference of Communications*, Brussels, Belgium, 2008, paper Th.3.D.1.

[90] L.Y. Chan, C.K. Chan, D.T.K Tong, E Tong and L.K. Chen, "Upstream traffic transmitter using injection-locked Fabry-Perot laser diode as modulator for WDM access networks," *IEE Electron. Lett.*, vol. 38, pp. 43-44, Jan. 2002.

[91] W. Lee, M. Y. Park, S. H. Cho, J. H. Lee, C. Y. Kim, G. Jeong, and B. Y. Kim, "Bidirectional WDM-PON based on gain-saturated reflective semiconductor optical amplifiers," *IEEE Photonics Technol. Lett.*, vol. 17, pp. 2460–2462, Nov. 2005.

[92] G-W. Lu, N. Deng, C-K. Chan, and L-K Chen, "Use of downstream inverse-RZ signal for upstream data remodulation in a WDM passive optical network," presented at *Optical Fiber Communication Conference*, Anaheim, CA, 2005, paper OFI8.

[93] S. Y. Kim, S. B. Jun, Y. Takushima, E. S. Son, and Y. C. Chung, "Enhanced performance of RSOA-based WDM PON by using Manchester coding," *J. of Opt. Networking,* vol. 6, pp. 624-630, Jun. 2007.

[94] S. K. Metya, V. Janyani, D. Bansal, and S. G. Modani, "Miller coding-based wavelength remodulation for optical access network," *IEEE Photonics Technol. Lett.*, vol. 24, pp. 1715-1717, Oct. 2012.

[95] Q. Guo and A. V. Tran, "Level coding technique for a wavelength-division-multiplexed optical access system using a remodulation scheme," *Optics Lett.*, vol. 37, pp. 4137-4139, Oct. 2012.

[96] W. Hung, C.-K. Chan, L.-K. Chen and F. Tong, "An optical network unit for WDM access networks with downstream DPSK and upstream remodulated OOK data using injection-locked FP laser," *IEEE Photonics Technol. Lett.*, vol. 15, pp. 1476–1478, Oct. 2003.

[97] M. Attygalle, T. Anderson, D. Hewitt, and A. Nirmalathas, "WDM passive optical network with subcarrier transmission and baseband detection scheme for laser-free optical network units," *IEEE Photonics Technol. Lett.*, vol. 18, pp. 1279-1281, Jun. 2006.

[98] M. Attygalle, N. Nadarajah, and A. Nirmalathas, "Wavelength reused upstream transmission scheme for WDM passive optical networks," *IEEE Electron. Lett.*, vol. 41, pp. 1025-1027, Sep. 2005.

[99] B. Schrenk, J. A. Lazaro, and J. Prat, "Employing feed-forward downstream cancellation in optical network unit for 2.5G/1.25G RSOA-based and 10G/10G REAM-based passive optical networks for efficient wavelength reuse," presented at *International Conference on Transparent Optical Networks*, Azores, Portugal, 2009, paper Th.B3.4.
[100] S. Yamashita, K. Hsu, and T. Murakami, "High-performance single-frequency fibre Fabry-Perot laser (FFPL) with self-injection locking," *IEEE Electron. Lett.*, vol. 35, pp. 1952-1954, Oct. 1999.
[101] C. H. Yeh, F. Y. Shih, C. H. Wang, C. W. Chow, and S. Chi, "Cost-effective wavelength-tunable fiber laser using self-seeding Fabry-Perot laser diode," *Opt. Express*, vol. 16, pp. 435-439, Jan. 2008.
[102] H. Wu, N. H. Zhu, J. W. Man, and H. Q. Yuan, "Continuously wavelength-tunable laser source using a self-injected Fabry-Perot laser diode," *IEEE Photonics Technol. Lett.*, vol. 23, pp. 332-334, Mar. 2011.
[103] M. Presi, A. Chiuchiarelli, and E. Ciaramella, "Polarization independent self-seeding of Fabry-Perot laser diodes for WDM-PONs," presented at the *Optical Fiber Communication Conference*, Los Angeles, CA, 2012, paper OW1B.5.
[104] M. Presi, A. Chiuchiarelli, R. Corsini and E. Ciaramella, "Uncooled and polarization independent self-seeded Fabry-Perot lasers for WDM-PONs," *IEEE Photonics Technol. Lett.*, vol. 24, pp. 1523-1526, Sep. 2012.
[105] M. Presi and E. Ciaramella, "Stable self-seeding of R-SOAs for WDM-PONs," presented at the *Optical Fiber Communication Conference*, Los Angeles, CA, 2011, paper OMP4.
[106] L. Marazzi, P. Parolari, R. Brenot, G. de Valicourt, and M. Martinelli, "Network-embedded self-tuning cavity for WDM-PON transmitter," *Opt. Express*, vol. 20, pp. 3781–3786, Feb. 2012.
[107] L. Yi, Z. Li, Y. Dong, S. Xiao, J. Chen, and W. Hu, "Upstream capacity upgrade in TDM-PON using RSOA based tunable fiber ring laser," *Opt. Express*, vol. 20, pp. 10416-10425, Apr. 2012.
[108] L. Marazzi, P. Parolari, M. Brunero, R. Brenot, S. Barbet, and M. Martinelli, "Remotely-pumped network-embedded self-tuning transmitter for 80-Gb/s conventional hybrid TDM/WDM PON with 256-split," *Opt. Express*, vol. 21, pp. 4376-4381, Feb. 2013.
[109] J. Xu, Y. Zhang, L.-K. Chen and C.-K. Chan, "A delay-based multicast overlay scheme for WDM passive optical networks with 10-Gb/s symmetric two-way traffics," *IEEE J. of Lightwave Technol*, vol. 28, pp. 2660-2666, Sep. 2010.
[110] J.-H. Moon, K.-M. Choi, and C.-H. Lee, "Overlay of broadcasting signal in a WDM-PON," presented at the *Optical Fiber Communication Conference*, Anaheim, CA, 2006, paper OThK8.
[111] H.-K. Lee, S.-G. Mun, J.-H. Moon, and C.-H. Lee, "Broadcast signal transmission for WDM-PON with ASE injection to an FP-LD," presented at *Conference on Lasers and Electro-Optics*, Baltimore, MD, 2009, paper CTuJ2.
[112] S.-H. Yoo, J.-Y. Kim, B.-I. Seo, and C.-H. Lee, "Noise-suppressed mutually injected Fabry-Perot laser diode for 10-Gb/s broadcast signal transmission in WDM passive optical networks," *Opt. Express*, vol. 21, pp. 6538-6546, Mar. 2013.

[113] F. Zhang, W.-D. Zhong, Z. Xu, T. H. Cheng, C. Michie, and I. Andonovic, "A broadcast/multicast-capable carrier-reuse WDM-PON" *IEEE J. of Lightwave Technol*, vol. 29, pp. 2276-2284, Aug. 2011.
[114] M. Khanal, C. J. Chae, and R. S. Tucker, "Selective broadcasting of digital video signals over a WDM passive optical network, *IEEE Photon. Technol. Lett.*, vol. 17, pp. 1992–1994, Sep. 2005.
[115] Y. Tian, Q. J. Chang, and Y. K. Su, "A WDM passive optical network enabling multicasting with color-free ONUs," *Opt. Exp.*, vol. 16, pp. 10434–10439, Jul. 2008.
[116] Y. Zhang, N. Deng, C.-K. Chan, and L.-K. Chen, "A multicast WDM-PON architecture using DPSK/NRZ orthogonal modulation, *IEEE Photon. Technol. Lett.*, vol. 20, pp. 1479–1481, Sep. 2008.
[117] N. Deng, C.-K. Chan, L.-K. Chen, and C. L. Lin, "A WDM passive optical network with centralized light sources and multicast overlay," *IEEE Photon. Technol. Lett.*, vol. 20, pp. 114–116, Jan. 2008.
[118] F. Zhang, S. Fu, J, Wu, K. Xu, J. Lin, and P. Shum, "A wavelength-division-multiplexed passive optical network with simultaneous centralized light source and broadcast capability," *IEEE Photon Journal*, vol. 2, pp. 445–453, Jun. 2010.
[119] X. Xin, B. Liu, L. Zhang, and J. Yu, "40-Gb/s FSK modulated WDM-PON with variable-rate multicast overlay," *Opt. Express*, vol. 19, pp. 12515-12523, Jun. 2011.
[120] B. Liu, X. Xin, L. Zhang, J. Yu, and Q. Zhang "A WDM-OFDM-PON architecture with centralized Lightwave and PolSK-modulated multicast overlay," *Opt. Express*, vol. 18, pp. 2137-2143, Jan. 2010.
[121] J. Xu, Z. Liu, L.-K. Chen, and C.-K. Chan, "Time-interleaved phase remodulation to enable broadcast transmission in bidirectional WDM-PONs without additional light sources," presented at the *Optical Fiber Communication Conference*, Los Angeles, CA, 2011, paper OThK4.
[122] K. Lee, S. B. Lee, P. Ghelfi, A. T. Nguyen, L. Poti, and G. Prati, "Multicasting in WDM-PON using cross-gain modulation in semiconductor optical amplifier," presented at the *European Conference of Communications,* Torino, Italy, 2010, paper Mo.1.B.6.
[123] X. B. Yu, J. B. Jensen, D. Zibar, C, Peucheret and I. T. Monroy, "Converged wireless and wireline access system based on optical phase modulation for both radio-over-fiber and baseband signals," *IEEE J. of Lightwave Technol.,* vol. 20, pp. 1814–1816, Oct. 2008.
[124] A. Chowdhury, H.-C. Chien, J. Yu and G.-K. Chang, "A novel 50-GHz spaced DWDM 60-GHz millimeter-wave radio-over-fiber systems using optical interleaver," presented at the *Optical Fiber Communication Conference*, San Diego, CA, 2009, paper OTuB1.
[125] G. H. Smith, D. Novak, and Z. Ahmed, "Overcoming chromatic-dispersion effects in fiber-wireless systems incorporating external modulators," *IEEE Trans. Microwave Theory Tech*. vol. 45, pp. 1410-1415, Aug. 1997.
[126] H.-C. Chien, A. Chowdhury, Y.-T. Hsueh, Z. Jia, S.-H. Fan, J. Yu and G.-K. Chang, "A novel 60-GHz millimeter-wave over fiber with independent 10-Gbps wired and wireless services on a single wavelength using PolMUX and wavelength-reuse

techniques," presented at the *Optical Fiber Communication Conference*, San Diego, CA, 2009, paper OTuB7.
[127] B. Leesti, A. J. Zilkie, J. S. Aitchison, M. Mojahedi, R. H. Wang, T. J. Rotter, C. Yang, A. Stintz, and K. J.Malloy, "Broad-band wavelength up-conversion of picosecond pulses via four-wave mixing in a quantum dash waveguide," *IEEE Photon. Technol. Lett.*, vol. 17, no. 5, pp. 1046–1048, May 2005.
[128] Y.-K. Seo, C.-S. Choi, and W.-Y. Choi, "All-optical signal up-conversion for radio-on-fiber applications using cross-gain modulation in semiconductor optical amplifiers," *IEEE Photon. Technol. Lett.*, vol. 14, no. 10, pp. 1448–1450, Oct. 2002.
[129] J. Yu, M. Huang, Z. Jia, A. Chowdhury and G.-K. Chang, "All-optical up-conversion for 30x7.5Gb/s WDM signals in a 60 GHz ROF system," presented at the *Optical Fiber Communication Conference*, San Diego, CA, 2009, paper OTuB4.
[130] S. Fu, W.-D. Zhong, P. Shum, Y. J. Wen and M. Tang, "Simultaneous multichannel photonic up-conversion based on nonlinear polarization rotation of an SOA for radio-over-fiber systems," *IEEE Photon. Technol. Lett.*, vol. 21, pp. 563–565, May 2009.
[131] M. Ogusu, K. Inagaki and Y. Mizuguchi, "60 GHz millimeter-wave source using two-mode injection-locked of a Fabry-Perot slave laser," *IEEE Microwave and Wireless Components Lett.*, vol. 11, pp. 101–103, Mar. 2001.
[132] M.-K. Hong, Y.-Y. Won, S.-K. Han, "Gigabit optical access link for simultaneous wired and wireless signal transmission based on dual parallel injection-locked Fabry-Pérot laser diodes," *J. Lightw. Technol.*, vol. 26, pp. 2725–2731, Aug. 2008.
[133] L. Noel, D. Wake, D. G. Moodie, D. D. Marcenac, L. D. Westbrook, and D. Nesset, "Novel techniques for high-capacity 60-GHz fiber-radio transmission systems," *IEEE Trans. Microw. Theory Tech.*, vol. 45, pp. 1416–1423, Aug. 1997.
[134] D. P. Shea and J. E. Mitchell, "Long-reach optical access technologies," *IEEE Network*, vol. 21, pp. 5-11, Sep./Oct., 2007.
[135] J. M. Oh, S. G. Koo, D. Lee and S.-J. Park, "Enhancement of the performance of a reflective SOA-based hybrid WDM/TDM PON system with a remotely pumped erbium-doped fiber amplifier," *J. Lightw. Technol.*, vol. 26, pp. 144–149, Jan. 2008.
[136] J. B. Jensen, I. T. Monroy, R. Kjaer and P. Jeppesen, "Reflective SOA re-modulated 20 Gbit/s RZ-DQPSK over distributed Raman amplified 80 km long reach PON link," *Opt. Express*, vol. 15, pp. 5376–5381, Apr. 2007.
[137] S. P. Jung, Y. Takushima, and Y. C. Chung, "Generation of 5-Gbps QPSK signal using directly modulated RSOA for 100-km coherent WDM-PON," presented at the *Optical Fiber Communication Conference*, Los Angeles, CA, 2011, paper OTuB3.
[138] M. Presi, R. Proietti, K. Prince, G. Contestabile and E. Ciaramella, "A 80 km reach fully passive WDM-PON based on reflective ONUs," *Opt. Express*, vol. 16, pp. 19043–19048, Nov. 2008.
[139] R. Glatty, P. Guignard, and P. Chanclou, "Fair resource distribution within the flexible WDMA/TDMA optical access network based on GPON infrastructure," *J. Opt. Commun. Netw.*, vol. 1, pp. A17-A24, Jul. 2009.
[140] T.-J. C, C.-K. Chan, L.-K. Chen and F. Tong, "A self-protected architecture for wavelength-division-multiplexed passive optical networks," *IEEE Photonics Technol. Lett.*, vol. 15, pp. 1660–1662, Nov. 2003.

[141] C. H. Yeh, C. W. Chow, C. H. Wang, F. Y. Shih, H. C. Chien and S. Chi, "A self-protected colorless WDM-PON with 2.5 Gb/s upstream signal based on RSOA," *Opt. Express*, vol. 16, pp. 12296–12301, Aug. 2008.
[142] X. Sun, C.-K. Chan and L. K. Chen, "A survivable WDM-PON architecture with centralized alternate-path protection switching for traffic restoration," *IEEE Photonics Technol. Lett.*, vol. 18, pp. 631–633, Feb. 2006.
[143] C. H. Yeh, C. W. Chow, F. Y. Shih, Y. F. Wu and S. Chi, "An optical switch-based self-restored WDM-PON architecture against fiber faults," presented at *Communications and Photonics Conference and Exhibition*, Shanghai, China, 2010.
[144] C. K. Chan, L.-K. Chen, and C. Lin, "Novel network architectures for survivable WDM passive optical networks," presented at *European Conference of Communications,* Brussels, Belgium, 2008, paper Th. 1.F.6.
[145] K. Lee, S.-G. Mun, C.-H. Lee and S. B. Lee, "Reliable wavelength-division-multiplexed passive optical network using novel protection scheme," *IEEE Photonics Technol. Lett.*, vol. 20, pp. 679–681, May 2008.
[146] C. H. Yeh, C. W. Chow, S. P. Huang, J. Y. Sung, Y. L. Liu, and C. L. Pan, "Ring-based WDM access network providing both Rayleigh backscattering noise mitigation and fiber-fault protection," *IEEE J. Lightw. Technol.*, vol. 30, pp. 3211–3218, Oct. 2012.
[147] P. Leisching and M. Pickavet, "Energy footprint of ICT: Forecasts and network solutions," presented at the *Optical Fiber Communication Conference*, San Diego, CA, Mar. 2009.
[148] P. Chowdhury, M. Tornatore, S. Sarkar and B. Mukherjee, "Building a green wireless-optical broadband access network (WOBAN)," *J. of Lightwave Technol*, vol. 28, pp. 2217–2227, Aug. 2010.
[149] K.-H. Tse, W. Jia and C.-K. Chan, "A cost-effective pilot-tone-based monitoring technique for power saving in RSOA-based WDM-PON," presented at the *Optical Fiber Communication Conference*, Los Angeles, CA, 2011, paper OThB6.
[150] T. Uchikata and A. Tajima, "A novel power saving scheme for WDM-PON with centralized light sources," presented at *OptoElectronics and Communications Conference (OECC)*, Hong Kong, China, 2009.
[151] M. Zhu, W.-D. Zhu, Z. Zhang, and F. Luan, "An efficient energy-saving scheme incorporating dozing and sleep modes for CLS-based WDM-PONs with colorless ONUs," *Opt. Express*, vol. 20, pp. 29931–29939, Dec. 2012.
[152] Y. Ma, D. Liu, J. Yu, and X. Wang, "System evaluation of economic 16/32chs 1.25Gbps WDM-PON with self-seeded RSOA," *Opt. Express*, vol. 20, pp. 22523–22530, Sep. 2012.
[153] B. W. Kim, M. Y. Park, W.-R. Lee, T. Y. Kim, "Reflective semiconductor optical amplifier (RSOA), RSOA module having the same, and passive optical network using the same," U.S. Patent 8,125,707 B2, Feb. 28, 2012.
[154] C. Michie, T. Kelly, and I. Andonovic, "Reflective semiconductor optical amplifiers in passive optical networks," presented at the *Opto-Electronics and Communications Conference*, Hong Kong, China, 2009.
[155] M. Martinelli, L. Marazzi, P. Parolari, M. Brunero, and G. Gavioli, "Polarization in retracing circuits for WDM-PON," *IEEE Photonics Technol. Lett.*, vol. 24, pp. 1191-1193, Jul. 2012.

[156] *Finisar WaveShaper*, [Online]. Available: http://www.finisar.com/products/optical-instrumentation/WaveShaper-4000S
[157] G. P. Agrawal and N. A. Olsson, "Self-phase modulation and spectral broadening of optical pulses in semiconductor laser amplifiers," *IEEE J. Quantum Electron*., vol. 25, pp. 2297–2306, Nov. 1989.
[158] Maxim, "Spectral content of NRZ test patterns," [Online]. Available: http://pdfserv.maximintegrated.com/en/an/AN3455.pdf
[159] Agilent White Paper, "Equalization: the correction and analysis of degraded signals," [Online]. Available: www.cp.literature.agilent.com
[160] W. Rosenkranz and C. Xia, "Electrical equalization for advanced optical communication systems," *Int. J. Electron. Commun.*, vol. 51, pp. 1-8, Mar. 2007.
[161] T. Mizuochi, K. Kubo, M. Akita, M. Imai, S. Kurahashi, N. Takemura, *et al*, "Transparent multiplexer featuring super FEC for optical transport networking," presented at the *SubOptic*, Kyoto, Japan, 2001, Paper P.4.2.3.
[162] U. R. Duarte, R. S. Penze, F. R. Pereira, F. F. Padela, J. B. Rosolem, and M. A. Romero, "Combined self-seeding and carrier remodulation scheme for WDM-PON," *IEEE J. Lightwave Technol*., vol. 31, pp. 1323-1330, Apr. 2013.
[163] J. H. Lee, S.-H. Cho, Y. S. Jang, and S.-S. Lee, "Enhancement of power budget in RSOA based-loopback type WDM-PON by using cascade RSOAs," presented at the *International Conference on Transparent Optical Network*, Munich, Germany, 2010, Paper Tu.B1.5.
[164] Y.-H. Lin, T.-K. Cheng, H.-L. Wang, G.-C. Lin, and G.-R. Lin, "Effect of AWG channel bandwidth on BER of injection-locked RSOA based ONU in WDM-PON system," presented at the *International Conference on Photonics in Switching*, Sappora, Japan, 2008.
[165] R. Lang, "Injection locking properties of a semiconductor laser," *IEEE J. Quantum Electron.*, vol. QE-18, pp. 976-83, Jun. 1982.
[166] F. Mogensen, H. Olesen, and G. Jacobsen, "Locking conditions and stability properties for a semiconductor laser with external light injection," *IEEE J. Quantum Electron.*, vol. QE-21, pp. 784-93, Jul. 1985.
[167] T. B. Simpson, J. M. Liu, and A. Gavrielides, "Bandwidth enhancement and broadband noise reduction in injection-locked semiconductor lasers," *IEEE Photonics Technol. Lett.*, vol. 7, pp. 709-711, Jul. 1995.
[168] J. H. Seo, Y. K. Seo, and W. Y. Choi, "Nonlinear distortion suppression in directly modulated DFB lasers by sidemode optical injection," *Proc. IEEE MTT-S Int. Microw. Symp. Dig.*, vol. 1, pp. 555-558, Jun. 2001.
[169] E. K. Lau, H.-K. Sung, and M. C. Wu, "Frequency response enhancement of optical injection-locked lasers," *IEEE J. Quantum Electron.*, vol. 44, pp. 90-99, Jan. 2008.
[170] E. K. Lau, "High-speed modulation of optical injection-locked semiconductor lasers", Ph.D. dissertation, Dept. Elect. Eng. & Computer Science, Univ. of California, Berkeley, 2006.
[171] K.-Y. Park, S.-G. Mun, K.-M. Choi, and C.-H. Lee, "A theoretical model of a wavelength-locked Fabry-Perot laser diode to the externally injected narrow-band ASE," *IEEE Photonics Technol. Lett.*, vol. 17, pp. 1797-1799, Sep. 2005.

[172] G. P. Agrawal and N. K. Dutta, *Semiconductor Lasers*. Van Nostrand Reinhold, New York, 1993, pp. 231-258.
[173] L. V. T. Nguyen, "Mode-partition noise in semiconductor lasers," [Online]. Available: www.dsto.defence.gov.au/publications/2482/DSTO-RR-0244.pdf
[174] H. F. Chen, J. M. Liu and T. B. Simpson, "Response characteristics of direct current modulation on a bandwidth-enhanced semiconductor laser under strong injection locking," *Opt. Commun*, vol. 173, pp. 349-355, Jan. 2010.
[175] A. Murakami, K. Kawashima and K. Atsuki, "Cavity resonance shift and bandwidth enhancement in semiconductor lasers with strong light injection," *J. of Quantum Electron.*, vol. 39, pp. 1196-1204, Oct. 2003.
[176] N. Kashima, "Dynamic properties of FP-LD transmitters using side-mode injection locking for LANs and WDM-PONs," *J. of Lightwave Technol*, vol. 24, pp. 3045-3058, Aug. 2006.
[177] M. M. Krstic and D. M. Gvozdic, "Side-mode-suppression-ratio of injection-locked Fabry-Perot lasers," *ACTA Physica Polonica A*, vol. 116, pp. 664-667, Oct. 2009.
[178] J. M. Liu, H. F. Chen, X. J. Meng and T. B. Simpson, "Modulation bandwidth, noise, and stability of a semiconductor laser subject to strong injection locking," *IEEE Photon. Technol. Lett.*, vol. 9, pp. 1325-1327, Oct. 1997.
[179] H. Kim, S. Kim, S. Hwang and Y. Oh, "Impact of dispersion, PDM and PDL on the performance of spectrum-sliced incoherent light sources using gain-saturated semiconductor optical amplifier," *J. of Lightwave Technol*, vol. 24, pp. 775-785, Feb. 2006.
[180] A. D. McCoy, P. Horak, B. C. Thomsen, M. Ibsen and D. J. Richardson, "Noise suppression of incoherent light using a gain-saturated SOA: implications for spectrum-sliced WDM systems," *J. of Lightwave Technol*, vol. 23, pp. 2399-2409, Aug. 2005.
[181] V. Curri, P. Poggiolini, A. Carena, and F. Forghieri, "Performance analysis of coherent 222-Gb/s NRZ PM-16QAM WDM system over long-haul links," *IEEE Photonics Technol. Lett.*, vol. 22, pp. 266-268, Mar. 2010.
[182] J. Q. Li, K. Xu, Y. J. Wen, S. N. Fu, M. Tang, P. Shum, J. Wu, and J. T. Lin, "Experimental demonstration of polarization multiplexing for simultaneously providing broadband wireless and wired access," *Opt. Commun.*, vol. 281, pp. 2806-2810, Jan. 2008.
[183] Z. Wang and C. Xie, "Automatic optical polarization demultiplexing for polarization division multiplexing signals," *Opt. Express*, vol. 17, pp. 3183-3189, Mar. 2009.
[184] X. Steve Yao, L.-S. Yan, B. Zhang, A. E. Willner, and J. Jiang, "All-optic scheme for automatic polarization division demultiplexing," *Opt. Express*, vol. 15, pp. 7407-7414, Jun. 2007.
[185] General Photonics PolaRITEIII, [Online]. Available: http://www.generalphotonics.com/pdf/PolaRITE%20III.pdf .
[186] E. Bradley, E. Miles, B. Loginov, and N. Vu, "Polarization control with piezoelectric and LiNbO3 Transducers," *Fiber and Integrated Optics*, vol. 21, pp. 75-104, Feb. 2002.

[187] K. Ogaki, M. Nakada, and Y. Nagao, "Fluctuation differences in the principal states of polarization in aerial and buried cables," presented at the *Optical Fiber Communication Conference*, Atlanta, Georgia, 2003, paper MF13.
[188] D. S. Waddy, P. Lu, L. Chen, and X. Bao, "Fast state of polarization changes in aerial fiber under different climatic conditions," *IEEE Photonics Technol. Lett.*, vol. 13, pp. 1035-1037, Sep. 2001.
[189] X. S. Yao and D. Bar, "Optical communications based on optical polarization multiplexing and demultiplexing," U.S. Patent 7,343,100 B2, March 11, 2008.
[190] Paul K. J. Park, S. B. Jun, H. Kim, D. K. Jung, W. R. Lee, and Y. C. Chung, "Reduction of polarization-induced performance degradation in WDM-PON utilizing MQW-SLD-based broadband source," *Opt. Express*, vol. 15, pp. 14228-14233, Oct. 2007.
[191] Y.-S. Liao, Y.-C. Chi, H.-C. Kuo, and G.-R. Lin, "Pulsating master and injected slave weak-resonant-cavity laser diodes based quasi-color-free 2.5 Gb/s RZ DWDM-PON," presented at the *Optical Fiber Communication Conference*, Los Angeles, CA, 2011, paper JWA67.
[192] H. Zhang, J.-X. Cai, C. R. Davidson, B. Anderson, O. Sinkin, M. Nissov, and A. N. Pilipetskii, "Offset PDM RZ-DPSK for 40 Gb/s long-haul transmission," presented at the *Optical Fiber Communication Conference*, San Diego, CA, 2009, paper OThR2.
[193] H. Kim and P. J. Winzer, "Robustness to laser frequency offset in direct-detection DPSK and DQPSK systems," *IEEE J. Lightwave Technol.*, vol. 21, pp. 1887-1891, Sep. 2003.
[194] K. Higuma, S. Oikawa, Y. Hashimoto, H. Nagata, and M. Izutsu, "X-cut lithium niobate optical single-sideband modulator," *Electron. Lett*., vol. 37, pp. 515-516, Apr. 2001.
[195] K. Voigt, L. Zimmermann, G. Winzer, M. Schnarrenberger, T. Mitze, J. Bruns, and K. Petermann, "Silicon-on-insulator (SOI) delay-line interferometer with low polarization-dependent wavelength shift," presented at the *European Conference of Optical Communication*, Copenhagen, Denmark, 2007, paper ThC2.
[196] G. Unterborsch, M. Kroh, J. Honecker, A. G. Steffan, G. Tsianos, H.-G. Bach, *et. al.*, "Hybrid flip-chip integration of a 40 Gb/s DPSK receiver comprising a balanced photodetector on a DLI-SOI board," presented at the *European Conference of Optical Communication*, Brussels, Belgium, 2008, paper P.2.04.
[197] P. J. Winzer and J. Leuthold, "Return-to-zero modulator using a single NRZ drive signal and an optical delay interferometer," *IEEE Photonics Technol. Lett.*, vol. 13, pp. 1298-1300, Dec. 2001.
[198] M. O. van Deventer, "Polarization properties of rayleigh backscattering in single-mode fibers," *IEEE J. Lightwave Technol*., vol. 11, pp. 1895-1899, Dec.1993.
[199] A. H. Gnauck and P. J. Winzer, "Optical phase-shift-keyed transmission," *IEEE J. Lightwave Technol*., vol. 23, pp. 115-130, Jan. 2005.
[200] *OptiSystem 9.0*, [Online]. Available: http://www.optiwave.com/products/system_features.html
[201] Optoplex DPSK demodulator, [Online]. Available: http://www.optoplex.com/DPSK_Demodulator.htm.

[202] Avensys Tech, [Online]. Available: http://www.avensystech.com/AvensysTech/Products.php?locale=en&Line_no=13&sub_category_id=155&cat_category_id=138.
[203] F. Xiong, W.-D. Zhong, and H. Kim, "A broadcast-capable WDM passive optical network using offset polarization multiplexing," *IEEE J. of Lightwave Technol.*, vol. 30, pp. 2329-2336, Jul. 2012.
[204] H.-K.Lee, H.-S.Cho, J.-Y.Kim, and C.-H. Lee, "A WDM-PON with an 80 Gb/s capacity based on wavelength-locked Fabry-Perot laser diode," *Opt. Express*, vol. 18, pp. 18077-18085, Aug. 2010.
[205] K.-M.Choi and C.-H. Lee, "Broadband light source using mutually injected Fabry-Perot laser diode for WDM-PON," *IEEE Photon. Technol. Lett.*, vol. 17, pp. 2529-2531, Dec. 2005.
[206] S.-M.Lee, K.-M.Choi, S.-G.Mun, J.-H.Moon, and C.-H. Lee, "Dense WDM-PON based on wavelength locked Fabry-Perot lasers," presented at the *Optical Fiber Communication Conference*, Anaheim, California, 2005, paper JWA.

Author's Publications

Journal publications

[1] **F. Xiong**, W.-D. Zhong, M. Zhu, H. Kim, Z. Xu, and D. Liu, "Characterization of directly modulated self-seeded reflective semiconductor optical amplifiers utilized as colorless transmitters in WDM-PONs," *IEEE J. Lightwave Technol.*, vol. 31, pp. 1727-1733, Jun. 2013. *(Chapter 3)*

[2] **F. Xiong**, W.-D. Zhong, and H. Kim, "A broadcast-capable WDM passive optical network using offset polarization multiplexing," *IEEE J. Lightwave Technol.*, vol. 30, pp. 2329-2336, Jul. 2012.*(Chapter 6)*

[3] **F. Xiong**, W.-D. Zhong, and H. Kim, "A broadcast-capable WDM-PON based on polarization-sensitive weak-resonant-cavity Fabry-Perot laser diodes," *IEEE J. Lightwave Technol*., vol. 30, pp. 355-361, Feb. 2012.*(Chapter 5)*

Conference publications

[1] **F. Xiong** and W.-D. Zhong, "Performance of self-seeded RSOAs in WDM-PONs," presented at the *Conference on Lasers and Electro-Optics*, San Jose, CA, 2013, paper CTu3L.2.

[2] **F. Xiong**, W.-D. Zhong, and H. Kim, "A broadcast-overlaid full-duplex WDM-PON based on offset polarization multiplexing," presented at the *OptoElectronic and Communication Conference*, Busan, Korea, 2012, paper 6A1-3.

[3] **F. Xiong**, W.-D. Zhong, and H. Kim, "A WDM-PON enabling broadcast service based on polarization multiplexing," presented at the *Quantum Electronics Conference & Lasers and Electro-Optics*, Sydney, Australia, 2011, paper 3440-CT-4.

[4] **F. Xiong**, W.-D. Zhong, and H. Kim, "Multimode-injection-locked Fabry-Perot laser diode as remote seeding light for WDM-PONs," presented at *Photonics Global Conference*, Singapore, 2010, paper conf10a657.